



PLATFORM FOR OPERATION  
OF DISTRIBUTION NETWORKS



**Platone**

PLATform for Operation of distribution NEtworks



**D4.2 v1.0**

**State estimation tool**



The project PLATform for Operation of distribution NEtworks (Platone) receives funding from the European Union's Horizon 2020 research and innovation programme under Grant Agreement no 864300.

<b>Project name</b>	<b>Platone</b>
<b>Contractual delivery date:</b>	30.11.2020
<b>Actual delivery date:</b>	30.11.2020
<b>Main responsible:</b>	Themistoklis Xygkis, NTUA
<b>Work package:</b>	WP4 – Greek Demo (Mesogeia)
<b>Security:</b>	P
<b>Nature:</b>	R
<b>Version:</b>	V1.0
<b>Total number of pages:</b>	75

### Abstract

The deliverable D4.2 “State estimation tool” elaborates on the development and testing of a state estimator based on the current metering infrastructure of the Greek demo site as well as considering its upgrade via the installation of phasor measurement units. The objective of the state estimation procedure is to find the most likely operating state of a power grid, which is determined via a set of state variables, based on a set of real-time, available measurements obtained throughout the grid. This report provides the essential theoretical background of power system state estimation, a detailed description of the developed algorithms and extensive simulations on the test network. The related results indicate that the proposed state estimation tool performs efficiently within the framework of Use Cases UC-GR-01 and UC-GR-02, exhibiting fast convergence rates to solution and delivering highly accurate estimates of the grid state considering installed phasor measurement units. Hence, the establishment of the state estimation tool at central management level for real-time monitoring and operation planning purposes is well regarded.

### Keyword list

Accuracy, data integration, load estimation, measurements, missing data, state, observability, PMU, pseudo-measurements, SCADA, smart meters, state estimation, weighted least squares.

### Disclaimer

All information provided reflects the status of the Platone project at the time of writing and may be subject to change. All information reflects only the author’s view and the Innovation and Networks Executive Agency (INEA) is not responsible for any use that may be made of the information contained in this deliverable.

---

## Executive Summary

The state estimation (SE) tool comprises the cornerstone for the development of the Greek demo. It is the core computational procedure for real-time monitoring and the key-enabler for the operation of the advanced distribution applications that will be created within the Platone project. Given that the operational state of a power grid cannot be directly obtained from the available measurements due to metering or telecommunication errors, missing data or lack of synchronization, the SE filters the input streams of electrical measurements with a view to attaining the most precise image of the grid state in real-time conditions. This report provides the essential background regarding SE, and, then, describes and demonstrates the development of a SE tool which will support the monitoring for the Greek demo site by estimating the most likely, real-time grid state. In addition, the accumulated state estimates can be used to build a valuable data repository for operation planning purposes, encompassing the smart use of distributed energy resources (DER) and the provision of ancillary services.

SE is a mathematical method used for the estimation of the current operational status of a power grid based on a specified set of measurements and known grid topology. The grid state is defined by a set of state variables, usually the voltage magnitudes and angles of all network buses, whose calculation secures that all the other grid variables (mainly referring to active/reactive power flows and injections) can be evaluated from them. The state variables are computed based on the physical laws directing the operation of power networks, which are used to formulate measurement functions mapping the state variables to the available electrical measured quantities. In this way, the so-called SE problem is expressed as an optimization task whose proper solving yields the estimated grid state.

The SE tool of the current study is founded upon the well-established weighted least squares (WLS) optimization model, which aims at the minimization of an objective function equal to the weighted sum of squares of measurement residuals. An iterative solution algorithm is used for the WLS-based model and provides the most probable real-time grid state. The SE tool is applied to a high voltage/medium voltage (HV/MV) primary substation of Mesogeia area in Attica region, covering MV feeders incident to the HV/MV substation, and, as a result, only the MV level state variables are calculated. Finally, it is assumed that the SE tool will be installed at the central management level, that is, the distribution system operator technical platform (DSOTP).

The SE tool is developed and implemented in such a way that it meets the requirements and performance criteria, i.e., key performance indicators (KPIs) of Use Cases UC-GR-01 and UC-GR-02. The two Use Cases have been defined taking into account the required capabilities for a distribution state estimation (DSE) functionality, the inherent characteristics and particularities of distribution networks and the metering infrastructure of the Mesogeia pilot site, before and after the potential installation of phasor measurement units (PMUs).

The Use Case UC-GR-01 has been designed in order to investigate the capability of the SE tool to achieve observability for the Mesogeia pilot site based on its pre-existing metering infrastructure, namely the supervisory control and data acquisition (SCADA) system of the HV/MV substation, the smart meters (SMs) at DER, MV and low voltage (LV) consumers. In addition, pseudo-measurements for load buses where no metering devices are installed – originating from short-term load forecasting (LF) or load estimation (LE), are used. The final goal is to accurately estimate the actual operational grid state. In essence, the WLS based SE tool performs data filtering and cleansing, i.e., improves confidence in actual measurement data and pseudo-measurements via suppression of metering errors, identification of bad data and reconciliation of inconsistent data, in order to attain the most likely, real-time grid state under various network operating scenarios. Various challenges and issues, typically hindering the application of DSE mainly related to lack of instrumentation, delays in measurement availability, increased use of pseudo-measurements, and grid structure, commonly consisting of long radial feeders with heterogeneous lines and cables, are also addressed by the SE tool. The performance criteria adopted examine the efficacy of the SE tool in terms of accuracy and convergence rate to solution.

The Use Case UC-GR-02 follows as an extension to the abovementioned accomplishments, since the objective is the smooth integration of PMU data into the SE tool in case that the pre-existing metering equipment at Mesogeia pilot site is upgraded via placement of PMUs. The installation of PMUs at selected buses is sure to enhance the information content of the available measurement set, offering abundant synchronized data of bus voltage and line current phasors. Yet, their proper utilization is a complicated task since algorithmic and technical issues are raised. The SE tool provides solutions to

these problems, thus, ensuring that the PMU data will be smoothly incorporated into the pre-existing measurement set. The same performance criteria as the ones in UC-GR-01 are adopted and, expectedly, lead to improved accuracy and convergence of the SE tool due to the fertile use of highly accurate and synchronized PMU data.

Through extensive simulations on actual measurement data from the Mesogeia pilot site, it is demonstrated that the developed SE tool can operate based on the pre-existing measurement infrastructure of the Mesogeia pilot site with limited accuracy in terms of states estimates and very good convergence rates. Considering the scenario of PMU installation, the simulations showed that the SE tool fulfils the highest quality standards with regard to the accuracy of state estimates and the efficiency of the solution algorithm, in order to support real-time monitoring and operation planning services. The abovementioned challenges and issues raised during the implementation of DSE are successfully dealt with. In conclusion, the SE tool is regarded as a reliable and efficient module for the development of the DSOTP for the Greek demo and, ultimately, reinforces the Platone architecture by providing efficient solutions and valuable feedback concerning manifold aspects of DSE.

## Authors and Reviewers

Main responsible		
Partner	Name	E-mail
<b>NTUA</b>		
	Themistoklis Xygkis Panagiotis Padiaditis	txygkis@power.ece.ntua.gr
Author(s)/contributor(s)		
Partner	Name	
<b>HEDNO</b>		
	Stavroula Tzioka Eleni Daridou	
Reviewer(s)		
Partner	Name	
<b>ENG</b>		
	Ferdinando Bosco	ferdinando.bosco@eng.it
<b>ACEA</b>		
	Simone Minniti	Simone.Minniti@aceaenergia.it
Approver(s)		
Partner	Name	
<b>RWTH</b>		
	Padraic McKeever	

## Table of Contents

<b>1</b>	<b>Introduction .....</b>	<b>8</b>
1.1	Task 4.2.....	8
1.2	Objectives of the Work Reported in this Deliverable .....	8
1.3	Outline of the Deliverable .....	9
1.4	How to Read this Document.....	9
<b>2</b>	<b>Distribution state estimation: current situation, challenges and trends.....</b>	<b>10</b>
2.1	Current situation .....	10
2.2	Challenges and impediments .....	11
2.3	Current trends and goals .....	13
2.4	Distribution state estimation within Platone.....	15
<b>3</b>	<b>Design and development of the SE tool .....</b>	<b>16</b>
3.1	Introduction .....	16
3.2	Requirements and specifications.....	18
3.2.1	Choice of DSE method.....	19
3.2.2	The observability issue.....	19
3.2.3	Availability of PMU data .....	20
3.3	Design of the SE tool.....	20
3.4	WLS based modelling of the DSE problem .....	21
3.4.1	Assumptions .....	21
3.4.2	Problem formulation .....	21
3.4.3	Solution algorithm.....	22
3.4.4	Insight into the WLS model .....	23
3.5	Generation of pseudo-measurements.....	23
3.5.1	Short term load forecasting .....	23
3.5.2	Load allocation .....	24
3.6	Integration of PMU data.....	25
<b>4</b>	<b>Simulations studies of the SE tool .....</b>	<b>27</b>
4.1	The test network of the Mesogeia site.....	27
4.2	Description of the UCs.....	28
4.3	Description of simulations.....	29
4.3.1	Simulation framework for UC-GR-01.....	29
4.3.2	Simulation framework for UC-GR-02.....	32
4.4	Simulation studies .....	33
4.4.1	Results for UC-GR-01 .....	33
4.4.2	Results for UC-GR-02 .....	41
<b>5</b>	<b>Conclusion.....</b>	<b>45</b>
<b>6</b>	<b>List of Tables .....</b>	<b>46</b>

---

<b>7</b>	<b>List of Figures</b> .....	<b>47</b>
<b>8</b>	<b>List of References</b> .....	<b>48</b>
<b>9</b>	<b>List of Abbreviations</b> .....	<b>51</b>
<b>Annex A</b>	<b>Data of the Mesogeia pilot site</b> .....	<b>52</b>
<b>Annex B</b>	<b>Measurement model</b> .....	<b>71</b>
	B.1 Functions and partial derivatives of conventional measurements.....	71
	B.2 Functions and partial derivatives of measurements from PMUs.....	74

## 1 Introduction

The project “PLATform for Operation of distribution Networks – Platone - aims to develop an architecture for testing and implementing a data acquisitions system based on a two-layer approach (an access layer for customers and a Distribution System Operator (DSO) observability layer) that will allow greater stakeholder involvement and will enable an efficient and smart network management. The tools used for this purpose will be based on platforms able to receive data from different sources, such as weather forecasting systems or distributed smart devices spread all over the urban area. These platforms, by talking to each other and exchanging data, will allow collecting and elaborating information useful for DSOs, Transmission System Operators (TSOs), customers and Aggregators. In particular, the DSO will invest in a standard, open, non-discriminating, economic dispute settlement blockchain-based infrastructure, to give to both the customers and to the aggregator the possibility to more easily become flexibility market players. This solution will see the DSO evolve into a new form: a market enabler for end users and a smarter observer of the distribution network. By defining this innovative two-layer architecture, Platone removes technical barriers to the achievement of a carbon-free society by 2050 [1], creating the ecosystem for new market mechanisms for a rapid roll out among DSOs and for a large involvement of customers in the active management of grids and in the flexibility markets. The Platone platform will be tested in three European trials in Greece, Germany and Italy and within the Distributed Energy Management Initiative (DEMI) in Canada. The Platone consortium aims to go for a commercial exploitation of the results after the project is finished. Within the H2020 programme “A single, smart European electricity grid” Platone addresses the topic “Flexibility and retail market options for the distribution grid”.

Acknowledging the significance of distribution state estimation (DSE) in real-time monitoring and operation of modern distribution networks, the Greek demo has been designed in such a manner that the state estimation (SE) tool is constructed as an enabling function of the distribution system operator technical platform (DSOTP). The SE tool not only captures the operating state of a distribution grid in real-time conditions, but also allows and assists the implementation of functionalities for advanced management and control which leverage archived data of state estimates in order to perform operational control of distributed energy resources (DER), to manage flexible loads, and to provide services for frequency control. The SE tool is founded upon the weighted least squares (WLS) method and is primarily designed based on the pre-existing metering infrastructure, pertaining to supervisory control and data acquisition (SCADA) system and smart meters (SMs). Several challenges and typical issues regarding real-world application of DSE have been taken into account and properly confronted. Moreover, the availability of data obtained from phasor measurement units (PMUs), whose installation is scheduled to take place at the Greek pilot site within Platone framework, is also considered. Since phasor measurements need special treatment, the SE tool is properly adjusted to fuse PMU data into the set of pre-existing measurements. In this way, the SE tool will be able to leverage real-time measurements from PMUs when they become available. With a view to addressing the aforementioned aspects, a solid framework for the design, implementation and testing of the SE tool, is conceptualized and established through two benchmark Use Cases which study grid observability, load estimation (LE), missing data, data integration and reconciliation within the DSE environment, and set the necessary key performance indicators (KPIs) and related threshold values in terms of accuracy and convergence rate to solution. The demonstration of the performance of the SE tool within the framework of the Use Cases showcases how the Hellenic Electricity Distribution Network Operator (HEDNO) and, indeed, the Platone project itself can take advantage of it and streamline its operation.

### 1.1 Task 4.2

The Task 4.2 deals with the development of a SE tool in the context of the Greek demo. The SE tool is based on a WLS model, which is a well-established method for DSE purposes, and tested on the Mesogeia pilot site. LE techniques are deployed for observability achievement and a rigorous study for proper integration of PMU data is conducted. All related work, that is, designing, implementing and testing of the proposed SE tool, is organized via two benchmark Use Cases.

### 1.2 Objectives of the Work Reported in this Deliverable

The objective of the work reported in this deliverable is to document, describe and demonstrate the development of a SE tool which will support real-time monitoring and operation planning for the pilot site

of Mesogeia of the Greek demo. The proposed SE tool was configured to meet the requirements elaborated in the Use Cases and comply with the quality standards set by the KPIs.

### 1.3 Outline of the Deliverable

Following this introductory first chapter, Chapter 2 introduces the reader to the current situation regarding DSE worldwide, focusing on the advancements due to the transition towards smart grid solutions, the main challenges and issues related to DSE implementation, as well as some examples of real-world examples of DSE application. Chapter 3 provides the fundamental background of WLS-based DSE and, then, describes thoroughly the complete methodology behind the design and implementation of the proposed SE tool, in compliance with the specifications for the two benchmark Use Cases. Chapter 4 is dedicated to the testing of the SE tool via extensive simulations on the Mesogeia pilot site. The related results are presented in two separate sections, one per Use Case, and evaluated based on the defined KPIs. Finally, the conclusions of the deliverable are stated in Chapter 5.

### 1.4 How to Read this Document

The essential mathematical background and methodology for the WLS based SE tool are presented in the present report, so no prior knowledge on the DSE problem is required for comprehension of the work and evaluation of the outcomes.

The report is closely linked to D4.1 [2], which provides a detailed description of the Greek demo, its Use Cases and the related KPIs, and D1.2 [3], which elaborates on calculation methodology, data collection and baseline details for all Demos' KPIs and defines Project KPIs. All information content with regard to Use Cases and KPIs of all Demos are, also, available in the online repository GitHub [4].

---

## 2 Distribution state estimation: current situation, challenges and trends

### 2.1 Current situation

Power system SE has been the core computational procedure for real-time situation awareness and monitoring in power transmission systems worldwide for the last 5 decades, comprising a constituent part of power control centres [5], [6]. In essence, SE is a data processing algorithm for converting redundant measurement data, network parameters and other available information into an estimate of the state of an electric power network [7]. The SE algorithm estimates the grid state runs with rates which ranges between one and a few minutes depending on the available metering infrastructure of the network. The WLS method has been indisputably the most widespread model for the formulation and solving of the SE problem [7], with only slight alterations over the years.

Despite the consolidation of the SE procedure in transmission systems, its application to real-world distribution grids is currently the exception rather than the rule<sup>1</sup>. DSE has been undergoing constant progress since the middle of 1990s as a result of remarkable academic research and targeted field testing conducted by scientific institutes and DSOs, globally [8], [9]. Nonetheless, the DSOs lacked motivation for the upgrade of metering and telecommunication infrastructure, similar to the one installed in transmission systems, in order to implement viable DSE functions. The cost for instrumenting complex distribution grids with countless points of interest, e.g. medium to low voltage (MV/LV) transformers was prohibitive, thus, the number of available measurements to be processed by DSE was considerably low [6]. Thus, grid observability was unattainable and automatic control was supported only in high to medium voltage (HV/MV) substations thanks to SCADA systems and related remote terminal units (RTUs). In most cases, these limited distribution management system (DMS) capabilities sufficed for the operation of passive grids, that is, to accept bulk power from transmission systems and distribute it to consumers [10]. A typical DMS operates the network in a routine manner, by maintaining flows within bounds to protect equipment and disconnecting parts of it in case of breached operation constraints, usually automatically [11]. Only MV lines of increased interest, due to their criticality for grid operation or vulnerability to overloads, are monitored in real time for purposes of automated control. Under these circumstances, a considerable part of power distribution tasks, like interrupting the power to loads, parameter checking on regular basis, fault diagnosis etc., relies on manual labor and low-level automation.

The required incentives for the DSOs occurred over the past decade. The requirements for real-time and control of distribution grids have grown due to a gradual shift towards more active operational behaviour [12], [13]; passive load consumers are replaced by flexible customers, increasing DER units inject power to be distributed and, as a consequence, one-way power flows from HV/MV substations to load buses have been transformed into bidirectional power exchange from and towards the transmission system. Hence, the need for DSE has been intensified, while capturing a rapidly changing grid state, which exhibits active, dynamic characteristics, rendered the implementation of DSE solutions a rather challenging task. Moreover, the escalated demand for high quality services on behalf of consumers, DER owners and, lately, the players of liberalised energy markets (providers, aggregators etc.) render the application of sophisticated solutions for local and coordinated control of voltage, flows and fault levels, a necessity. As expected, these requirements have triggered large-scale investments in telecommunications and instrumentation [8]–[10]. Smart metering systems, remote-controlled switching equipment, bidirectional telecommunication channels, data centres, and advanced software for DMS are the main components of the ongoing development of contemporary distribution networks in order to rise up to the quality standards of envisioned smart grid capabilities.

These advances are timely due to the concurrent ascent of DSE, which is now regarded by DSOs and utilities as a prerequisite for real-time monitoring of grid state with high update rates and to reliably carry out laborious control and planning tasks in the increasingly dynamic environment of active distribution networks [8], [9], [14]. The essential technical means for commercial implementation of DSE is spatially dispersed measurement devices with remote access capability, reliable telecommunication links, and data concentrators, which are becoming more and more available day by day. One-way automated

---

<sup>1</sup> In this report, the terms “network” and “grid” are used interchangeably with the same meaning.

meter reading (AMR) systems have been the first generation of metering technology enabling the on-demand reading of consumption records, alarms, and status from customers' premises remotely [10], [15]. This data is collected and delivered to DMS mostly on a daily basis or less (e.g. every 12 hours) for billing purposes. State-of-the-art advanced metering infrastructure (AMI) systems have followed as a more mature technology supporting two-way communication channels for measurement, command and control services [10], [15]. SMs, intelligent electronic devices (IEDs) and, lately, PMUs are the backbone of AMI systems delivering measurements throughout the grid, from end users and MV/LV transformers to HV/MV substations and adjacent feeders. Near real-time data availability to DMS is achievable, for example, every 15 minutes. As perceived, the contribution of AMR and AMI to the pre-existing poor measurement sets obtained from SCADA system is a game changer, since it substantially boosts the measurement redundancy needed for DSE purposes [8], [9].

Taking into account the provided outline of the current condition in distribution networks, it is undeniable that the passive – “business as usual” – approach of DSOs is obsolete and fails to settle the emerging complex interactions within modern energy markets and to support highly efficient and profitable energy management policies. The application of new approaches and solutions aligning with the active nature of future distribution networks is facilitated by the modernization of power distribution equipment. Although the majority of power distribution grids is still characterized by deficiencies in terms of instrumentation, significant infrastructural changes have already been realized. In the foreseeable future, AMI and AMR systems are anticipated to further expand and serve an even larger number of DSOs and utilities. Approximately 65 million smart meters had been installed in the USA until 2015, whereas, according to European Commission, member states have committed to deploy 200 million SMs by 2020 [15]. In Greece, a large-scale project for the installation of 170 thousand smart meters is currently in progress under the guidance of HEDNO. As a consequence, the implementation of viable DSE solutions for real-world power distribution is getting more and more realizable. As a matter of fact, major electric energy firms have already developed DSE based software programs aiming at their commercial/industrial use by DSOs and utilities for real monitoring and control [8], [9].

## 2.2 Challenges and impediments

As already discussed, the most challenging problem for the implementation of DSE has been the inadequate number of sensors installed throughout distribution networks. To get insight into the origin of the problem, the term “observability” needs to be introduced [16]. In control theory, a system is said to be observable if it is possible to infer its state based upon a set of outputs. As regards power systems, this set of outputs identifies with the available set of real-time measurement data and, of course, the inference about the network observability is obtained via the DSE procedure. The number and location of measurements, as well as the type of measured quantities, determine the observability status of a network. Insufficient instrumentation of a distribution network directly affects its observability: the available dataset is deficient in terms of the quantity of measurement points, thus, the mathematical problem of DSE is underdetermined and cannot be solved, leading to an unobservable grid status [16].

Keeping in mind that the DSE problem is solved only if measurement redundancy is secured, i.e., the available measured data outnumber the number of variables that define the grid state, the usage of pseudo-measurements has been an unavoidable practice [8], [9], [14]. A pseudo-measurement is an estimated value of an injection – obtained either from load forecasting (LF)/ LE methods or generation schedules – which is used as a substitute for unmeasured or missing ones in order to achieve observability [16]. Given the limited real-time availability of actual measurements in typical distribution grids, a large number of pseudo-measurements is needed for observability purposes. Indeed, the DSE problem can then be solved, yet, this overuse of estimated, and not actually measured, data harms the accuracy of the state estimates [11]. The advent of AMR and AMI systems is beneficial to DSE implementation in both quantitative and qualitative manner. On one hand, more actual measurements will be available in real time, mitigating the use of pseudo-measurements (this advancement is mostly achieved via AMI systems); on the other, the abundant amount of historical load data can be leveraged by LE/LF methods for generation of increased quality pseudo-measurements.

Another issue related to instrumentation is the heterogeneity of the dataset provided as input to the DSE procedure [8], [14], [17]. This impediment originates from two main characteristics of DSE implementation:

1. the combined use of actual, pseudo- and virtual measurements, for example, power values from zero injection buses, and
2. the integration of different metering technologies and devices, namely SCADA, AMR, AMI and, recently, PMUs.

The abovementioned features induce the co-existence of intensely diverse measurements in terms of accuracy and temporal availability, into the same dataset. Needless to say, the capacity of telecommunications and related limitations, which influence the accuracy and rate of data exchange, are also considered.

In respect to accuracy, it is obvious that actually measured data, e.g. from RTUs, are more precise than pseudo-measurements which are estimates or forecasts of injections, often severely erroneous. Furthermore, virtual measurements, which represent perfect information on certain aspects of grid configuration and operation (for example, a zero power flow through an open switching device), even though not actually measured, are deemed as error-free data for DSE, thus, the most accurate of all [6]. These three basic levels of accuracy exhibit large variation increasing the risk of the occurrence of computational problems for the DSE solution algorithm. The problem exacerbates considering that each metering technology have its own accuracy standards. Additionally, telecommunication apparatus and links introduce errors into measured data. For example, recorded data obtained from SMs at LV consumers are associated with far higher uncertainties than the ones from PMUs. As a consequence, tuning of measurement weights, i.e., the preprocessing stage dealing with the calibration of weighting factors depending on accuracy per individual measurement, gets a rather laborious task with a high degree of complexity [11].

In view of time availability, one should discriminate between recording (or sampling) rates of metering devices and the update rate of measurements in DMS centres, a parameter determined by telecommunication capabilities. Considering the first parameter, regular SCADA measurements and recordings from state-of-the-art sensors such as IEDs provide quite accurate snapshots captured with latencies up to one minute. Synchronized data from PMUs have even faster sampling rates, in the order of milliseconds. On the contrary, the respective time windows for SMs are, usually, 15 minutes and, not rarely, come up to 1 hour. These discrepancies create a framework of two time scales for the execution of the DSE procedure [17], even if the time delays in data delivery to DMS centres were negligible. This statement is far from realistic, though, taking into account the actual refreshing rates in DMS centres.

Telemetered data from RTUs can be available in (near) real-time conditions, as well as PMU data. The same holds true for measurements from major DER units which are periodically transmitted to DMS centres. The lack of synchronization between SCADA and PMU data varies within a range of minutes and, thus, is easily manageable. Yet, the time lags for the delivery of AMI/AMR data pertaining to active/reactive load consumptions, in most cases, exceed 12 hours. Related update rates on daily or, even, weekly basis (for AMR systems), have been reported [18]. These major delays stem from limited telecommunication capacity given the complex grid structure with a huge number of nodes. Adverse effects on reliability in data transmissions also emerge, augmenting the risk for missing measured values. Hence, since real telemetry with adequate synchronization is currently unattainable for these data, the latter cannot be directly exploited for DSE purposes when delivered to DMS centres [8], [14]. To this end, preprocessing stages, mainly referring to the application of LE/LF methods to delayed load data, are implemented with a view to estimating the real-time loading conditions and, thus, providing pseudo-measurements to the DSE algorithm [19]. Evidently, time lags in data availability have a major impact on their accuracy. Delayed measurements are penalized with lower weighting factors, whereas pseudo-measurements, which are, essentially, estimates based on previous day or historic load recordings, are considered by far the less precise data.

In conclusion, the integration of heterogeneous measurements into mixed datasets is a matter of major importance, requiring careful design and delicate techniques for data handling in order to circumvent practical barriers caused by time skewness among measurements, to avoid algorithmic problems and achieve high performance within the DSE framework.

Beyond instrumentation and communication issues, there are distinct, intrinsic characteristics of distribution grids, mostly owing to their configuration, which hinder the performance of DSE solution algorithm. More specifically, the following features have been documented [6], [6], [20]:

- The combination of long distribution feeders with heterogeneous lines and cables, in a radial topology may be detrimental to DSE solution. Such configurations often yield poor conditioned matrices during the problem solving.
- The large number of buses increase grid complexity, thus, leading to long calculation times.
- The occurrence of high ratios of line resistance  $R$  to reactance  $X$ , not rarely well above unity, render the simplified models applied to transmission SE unsuitable for DSE purposes, since active and reactive power measurements cannot be decoupled.
- The presence of current magnitude measurements, which is rather frequent for practical reasons (e.g. monitoring of feeder overloads), introduces an additional degree of complexity to DSE due to strong nonlinearity of their measurement functions and incompliance with the decoupling principle.
- The substantial amount of injection measurements, mostly referring to pseudo-measurements, is also deemed as a source of ill conditioning.

In addition to the forenamed features, the unbalanced loading conditions at distribution level also complicates the formulation of the DSE problem. Yet, given that, usually, electrical measurands are not available separately, on each phase and, for most cases, a three-phase analysis at MV level is not required, a single-phase equivalent network model with assumed balanced operation is considered.

Last but not least, fusing conventional with PMU measurements, an upcoming need due to penetration of PMU technology in distribution grids, introduces new challenges in the solution scheme of the DSE problem due to the inclusion of current phasor measurements and their large weighting factors [14], [20]. The term “conventional” refers to measurements from SCADA, SMs or other devices which, contrarily to time-stamped PMU data based on the universal clock of the global positioning system (GPS), are not synchronized on a common time reference. Additionally, conventional datasets do not include measured phase angles (voltage/current).

Summing up, despite the infrastructural advancements that help DSOs to tackle the observability problem, the design and implementation of a DSE procedure still face various challenges and impediments. Heterogeneity of measurement data, communication bottlenecks, complex network configuration and overuse of pseudo-measurements are the main barriers to the development of high performance DSE solutions, bringing on time-skewed measurements, poor numerical stability, increased computational burdens, and low quality state estimates. The cautious study and proper treatment of these issues is a matter of vital importance.

### 2.3 Current trends and goals

The intermediate step towards the gradual development of smart grid functionalities in the foreseeable future, is the expansion of DMS and, subsequently, DSE-based monitoring and control throughout distribution networks. This expansion is conceptualized both as an extension of geographical coverage and as a growth of capabilities. Evidently, pre-existing DMS, serving typical distribution grids, need to be transformed into or replaced by advanced DMS, as envisaged within the framework of smart grids [21]. The installation or upgrade of DMS software/hardware, instrumentation, protection and operation equipment as well as telecommunications at power distribution level, invokes an unprecedented amount of investments and workload. Considering that these advancements can realistically be accomplished through a step-by-step process with incremental progress and different implementation rates per country or geographical region [10], DSOs and utilities are oriented towards localized DMS solutions [17], applied to: strategically selected portions of extended distribution networks, isolated electrical grids (e.g. island systems) and the so-called “microgrids”, i.e., decentralized energy entities capable of operating either in interconnected or in islanded mode. Clearly, distribution grids hosting significant DER units or potentially flexible loads, thus, exhibiting inherently active behavior, are among the most favorable sites.

The advantages of such implementation strategies are manifold. Budget needs are significantly restrained and the installation of AMI systems is facilitated due to reduced points of interest. In addition, the real-time operation of DSE and advanced DMS functions at regional level entails a manageable computational burden and telecommunication capacity compared to large-scale systems. Long-term planning purposes are also served, since future DMS is conceived to operate in a hierarchical manner embracing management subsystems, which will be able to collect data at faster rates than achieved in a centralized mode of operation and support local data storage and preprocessing tasks. To this end, hierarchical schemes of DSE, that is, multi-area SE with distributed/parallel architecture, are considered

as the only viable solution in order to exploit the ubiquitous sources of information and manage the vast amount of obtained data in real-time conditions [22]. Indisputably, DSOs and utilities can leverage the scalability of pre-existing, regional DMS with a view to integrating them into a unified operational framework where the already mature concept of multi-area DSE will be serviceable.

Another trend of the methodologies that DSOs develop for advanced DMS refers to the deployment of data analytics for DSE purposes and other functions [20]. Given a challenging information environment heavily loaded by large volumes of data to be handled, with more dynamic and heterogeneous characteristics, a broad range of algorithms based on data science can be applied to convert unrefined data into structured information and knowledge [23]. The most common algorithms can be classified into data analytics, machine learning, data mining or artificial intelligence. As regards DSE, novel techniques need to be introduced aiming at the extraction of relevant state information from raw measurements. Several disciplines stemming from data science have already been applied to LE/LF methods and techniques for topology identification [14], i.e., determination of current network configuration (or model) with up-to-date states of all switching devices. The basic idea behind these applications is the development of training-based models by exploring the periodic pattern of distribution network operation, based on the wealth of historical load data, network parameters and estimated system states. It is noted that data driven approaches for the formulation of the DSE problem itself is, also, a forthcoming advancement that is currently under academic investigation.

As far as instrumentation is concerned, at MV level, there is a prevailing movement towards the conversion of distribution automation equipment into units capable of fusing both actuator and sensor functions [17]. Remotely operated intermediate switching devices for fault detection, isolation and restoration, mainly pertaining to feeder protection relays, can be upgraded into true RTUs. The investment needed for such small-scale solutions is low and most vendors growingly support this service for their products. An excellent example of this trend is the deployment of pre-existing overcurrent relays for synchronized metering, which amounts to their upgrade into PMUs. In fact, there are remarkable research and commercial efforts for the development of a smaller and less expensive PMU form factor designed for distribution grids, called a  $\mu$ PMU (micro-PMU), which will be the catalyst for the introduction of the technology at distribution sector [11]. It should be noted, though, that cutting-edge multi-functional devices are often preferable to separate dedicated PMUs, as long as the former provide a comprehensive combination of protection, fault-locating features, monitoring, and control, without compromising the accuracy criteria set for phasor measurements. Summing up, the main global tendencies are to upgrade, wherever possible, MV equipment, to invest on multi-functional and interoperable devices and, of course, to pioneer synchronized sensing, either via stand-alone PMUs or as integrated capability of distribution equipment units.

At this point, the latest advances regarding the growing footprint of DSE in functions and applications of advanced DMS, are worth to be mentioned [8], [9], [11], [13], [14], [21]. As stated above, real-time monitoring is the main service provided by DSE. In addition to the estimation of the operation status of a network, the DSE procedure is beneficial to DSO and utility because it improves the level of confidence in network data obtained during its operation: measurements, forecasts, grid model and parameters. The output of DSE is a filtered, rigid dataset ready to use from DMS applications for real-time operation and control. A great variety of such DMS functions are highly dependent upon DSE, such as Volt/VAR control, fault location, network reconfiguration, and service restoration. The contribution of DSE to advanced DMS tasks will also be valuable, including islanding microgrids, TSO-DSO coordination and cybersecurity, i.e., protecting the vital automation and monitoring infrastructure against cyber intrusion and related malicious attacks. Furthermore, the DSE based operation of real-time markets is on the focus of relevant scientific research aiming to use the estimated grid state as basis for determination of locational market prices taking into account any constraint violations.

Finally, the offline applications of advanced DMS are also expected to leverage the increasing data repositories, describing historical measurements, states and parameters, for purposes of operation planning [8], [11], [21]. Generally, in active distribution grids, it is complicated to foresee the impact of grid control and to carry out highly accurate planning studies. The provision of improved information to DSOs is sure to boost their awareness of system trends, thus, resulting in an understanding of future values based on the historical outputs of DSE. DER scheduling, demand response programming, offline contingency analysis, optimal power flow analysis, scheduling of condition-based maintenance, load forecasting, as well as billing inference are among the tasks whose execution and validation can be supported by DSE results. Besides, an overview of the existing literature indicates that quite a few day-

ahead planning methodologies for optimized dispatch of DER units, Volt/VAr control and integration of demand side response, are based on an interaction with the DSE procedure.

In Figure 1 [24], the indicative time frames of the basic components of an energy management system, are displayed. Given the introduction of PMU technology as well as real-time functions for decision making into distribution level, these update and execution rates are also valid for DMS. As perceived, the placement of PMUs adds a new dimension to the time scale of monitoring and control services. It is noted that the contingency analysis can also work as an online DMS tool.

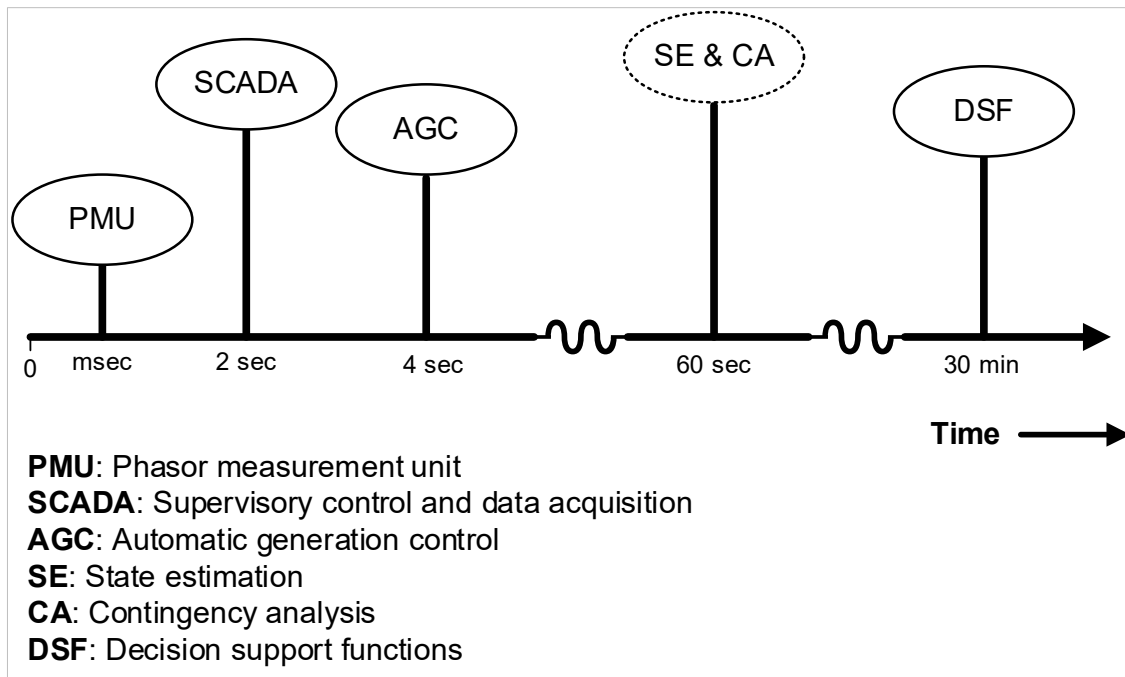


Figure 1: Time frames of components in energy management systems [24].

## 2.4 Distribution state estimation within Platone

As mentioned in subchapter 2.1, DSOs gradually go away from the traditional passive operation of the distribution networks to adopt a more complex and efficient use of them by investing in cutting-edge solutions for DMS software, metering technology and electrical equipment. The Greek DSO, HEDNO, following this worldwide trend and having recognised the importance and the multiple capabilities of DSE analysed in subchapter 2.3, chose to use in Platone the SE tool developed by the NTUA. The SE tool is the core computational procedure for real-time monitoring in the Greek demo, as well as a valuable data repository, for not only operation planning purposes of HEDNO, but also other flexibility services developed in the project.

The SE tool, which is a component of the DSOTP that will be created for the Greek demo within Platone, successfully filters the measurement data throughout the grid, characterized by limited availability, heterogeneity, errors, lack of synchronization, and missing values, in order to provide the its optimal – closest to reality – state in real time. Especially after integrating the data coming from the PMUs that are planned to be installed in selected nodes of the Mesogeia pilot site within the project's duration, the SE tool will be able to produce highly accurate state estimates, which the algorithms that are developed in parallel for the Greek demo can benefit from. The new services which will be shaped within Platone, aiming at optimal dispatch of DER and innovative management of flexible loads, will effectively necessitate the grid state estimation as an input. Finally, even after the project's lifetime, the SE tool remains a powerful module of the DSOTP and the Platone architecture as a whole for additional future requirements and applications as per HEDNO's needs.

### 3 Design and development of the SE tool

#### 3.1 Introduction

A power system state estimator – built to operate either at power transmission or distribution level – is a composite real-time tool of power control centres, which constitutes the solver of the SE problem for the network being monitored [5], [6]. It consists of the SE procedure itself and the following four modules which cope with individual subproblems in a sequential manner and co-operate through data exchange [6]:

1. *Topology processor*: extracts the current network model based on any available information about the statuses of the switching devices.
2. *Observability analysis*: decides whether the SE problem can be solved for the full network model based on the available set of measurements or not, and identifies the observable islands of the network, if any exist, for the latter case.
3. *State estimation*: calculates the optimal estimate of the network state, which comprises the voltage magnitudes and angles of all network buses, based on the obtained network model and the available measurement data, and also provides estimations for all measured quantities.
4. *Bad data processing*: discovers grossly erroneous measurements and rejects them, provided that the level of measurement redundancy is high enough.
5. *Parameter and structural error processing*: provides estimates of network parameters, detects errors in the network model and identifies incorrect statuses of switching devices in case that there an adequate level of measurement redundancy.

In Figure 2, the flowchart of a typical scheme of a state estimator is described. As observed, the SE module is the core procedure of the flowchart since it communicates with the other modules exchanging data and information.

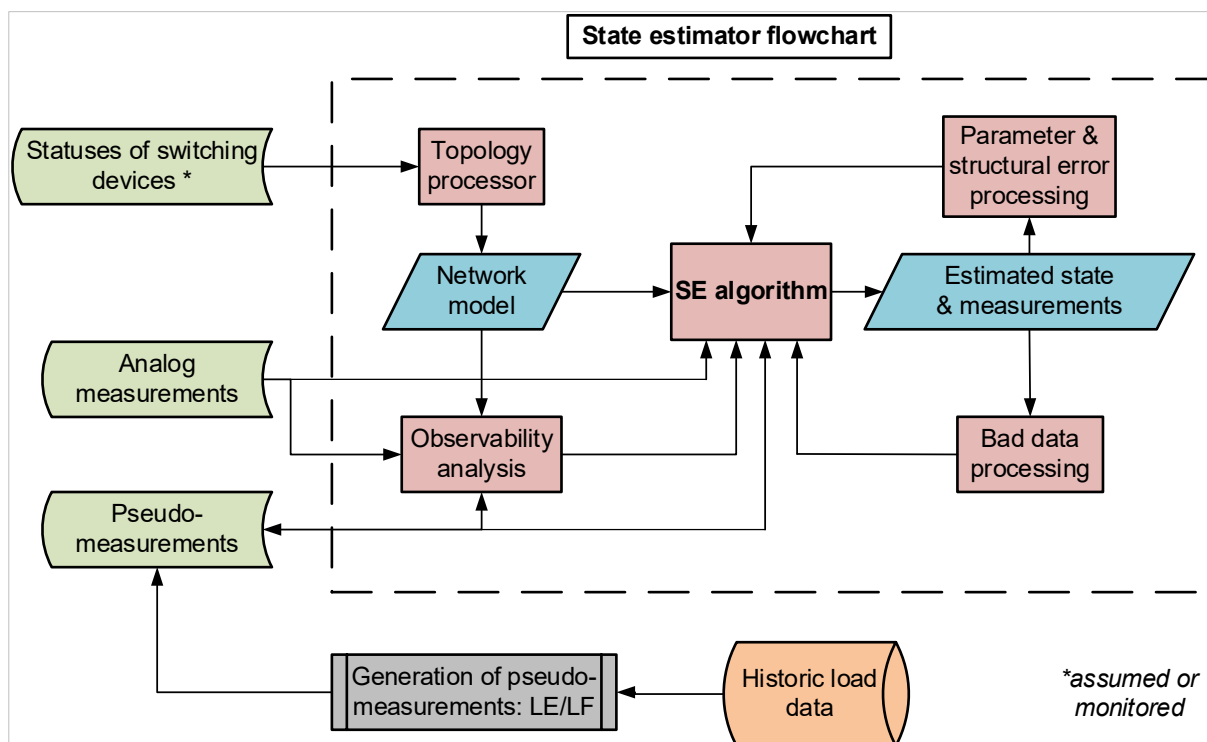


Figure 2: Typical structure of a state estimator.

The analog measurements pertain to the following electrical quantities:

- Bus voltage magnitudes or, in case of installed PMUs, bus voltage phasors (magnitudes and angles).
- Branch current magnitudes or, in case of installed PMUs, branch current phasors (magnitudes and angles).

- Active/reactive power flows through branches.
- Active/reactive power injections at buses.

The statuses of switching equipment are considered as digital measurements since they get discrete values, that is, 1 for closed state or 0, instead. Pseudo-measurements refer to estimated power injections at selected buses, as described in Chapter 1, and their generation relies on an external LE/LF procedure which exploits a database of past load consumptions. Summing up, the dataset inputted into the SE algorithm is composed of the available analog measurements, the pseudo-measurements generated for observability achievement and the obtained network model via the topology processing.

To get a deeper insight into the interaction between the individual modules, it is clarified that the observability analysis is a prerequisite for the execution of the SE algorithm, since it examines if the necessary conditions for problem solving are fulfilled [16]. Moreover, the topology processor is often incorporated into the SE procedure, thus, both analog and digital measurements are co-processed. Not rarely at distribution level, the network model is configured considering the normal statuses of the switching devices [6]. Besides, the modules for processing bad data, parameter and structural errors are built to assess the output of the SE algorithm and provide the proper feedback to it, if any related problems are identified. Finally, it is noted that there is a bidirectional interplay between the SE module and the “pool” of pseudo-measurements; in case that observability is not achieved or measurement redundancy has to be boosted, additional pseudo-measurements are introduced into the SE algorithm.

The SE procedure improves the confidence in the full dataset mentioned above, by performing data cleansing, and estimates the most probable operation point of the distribution grid [6], [11]. It is highly important to mention that all measurement data are introduced into the SE algorithm together with their corresponding accuracy metrics (e.g. standard deviations). As a result, thanks to its capability to suppress measurement errors, the SE procedure also provides estimated values for all measured quantities. Hence, the overall output is composed of the estimated state variables, i.e., the complex voltages for all network buses, and related measures for quantifying their uncertainty, as well as the estimates of available measurements. This output is characterized by minimized errors with regard to the grid state and the available measurement data and, thus, describes the closer to reality behavior of the grid in real-time conditions.

Before moving to the description of the proposed SE tool, a brief overview of the problem formulations and solution algorithm for DSE purposes is considered useful [8], [9], [14]. Since the SE tool is dedicated to distribution grids, it is noted that, hereinafter, the term DSE will be used instead of general purpose SE. During the 30 years of academic research for efficient DSE, several related methods have been proposed and tested on standard systems of the Institute of Electrical and Electronics Engineers (IEEE) or actual distribution networks, whereas a limited number of real-world DSE applications have been successfully carried out for purposes of field testing [8], [25], [26]. The proposed methods are classified into two basic categories based on whether the electrical measurands and the state variables are modelled as functions of time or not. The former category pertains to dynamic models, whereas the latter refers to static modelling. The static approach has originally been proposed by the prominent works of Schweppe [7] as a suitable solution for the treatment of snapshots of measurements, i.e., the meters are assumed to be read at the same instant of time and the measured data are fed into the SE algorithm as one vector, and prevailed owing to its simplified mathematical structure.

As regards static approaches, the WLS based formulation of the DSE problem is the most popular choice compared to other applicable mathematical models [8]. The WLS based methods are classified into two subcategories depending on the determination of state variables; either bus voltages or branch currents can be used in order to describe the grid state. Both approaches yield comparable results in terms of accuracy [27]. The most widespread solution scheme adopted for the nonlinear WLS model considering bus voltages is the iterative algorithm of Newton-Raphson, also known as Newton’s method [7]. Contrarily, for the WLS models considering branch currents, the solution schemes are mostly based on an iterative procedure which exploits the radial topology of distribution grids, the so-called forward/backward sweep [28], [29]. Few variations of the original WLS formulation and the proposed solution schemes can also be found in the related literature, whereas several methodologies have been proposed in order to enhance the robustness of the WLS model, that is, to boost their insensitivity to outliers [30], [31]. Apart from WLS based methods, a few static approaches rely on load adjustment [32], [33], that is, determining the load values, power or current, throughout the network so that they are compliant to the few, available actual measurements. Their solution is derived via iterative schemes,

ranging from forward/backward sweep to load flow algorithms. Finally, the deployment of Bayesian networks for the formulation of the DSE task is a novel, rather promising advancement [34], [35].

With respect to dynamic modelling, the related works are limited and have been published during the last decade. In general, the dynamic behavior of the grid is described by means of state transition models and the DSE problem is formulated based on Kalman filtering techniques [36], [37]. These works are related to forecasting aided SE methods [38], which leverage measured data in consecutive time samples in order to forecast future values (states variables and measurements) and, subsequently, to refine state estimates. The lack of such methods devoted to the DSE problem, is noteworthy, yet, anticipated since the update rates of measurements at distribution level are diverse, thus, constructing fast, consecutive snapshots of measured data is difficult.

### 3.2 Requirements and specifications

The design of the SE tool should meet certain requirements which are determined based on the challenges for DSE implementation, as elaborated in subchapter 2.1, and the characteristics of the pilot site of Mesogeia of the Greek demo. With a view to systematizing their description, the requirements are individually considered from the technical and the algorithmic points of view. The former consideration deals with the monitoring needs, availability of measurement data and infrastructural issues and, whereas the latter with the computational tasks assigned to the DSE algorithm and the required performance features.

From the technical standpoint, the SE tool will be based at the top of the system architecture and operate at central management level, that is, the DSOTP of the Greek demo. The monitoring requirements refer to the whole pilot site of Mesogeia, which comprises selected distribution feeders originating from the primary HV/MV substation and serving MV and LV customers (consumers and DER). As a result, the SE tool will provide DSE services at the functional level of the HV/MV substation and only state variables at the MV level will be estimated.

All the information available for the network is required to be processed in order to derive consistent and precise state estimates. The following information will be inputted as a unified dataset into the SE tool: network parameters and configuration (topology), analogue measurements, including actual (telemetered) measurements subject to errors (due to metering uncertainties, transmission noise and distortion etc.) and virtual measurements assumed to contain no errors, as well as pseudo-measurements subject to errors (due to limited accuracy of LE/LF methods). Every single value of the aforementioned dataset will be accompanied by its individual accuracy metric.

Given the pre-existing metering infrastructure, the SE tool will be provided with the following types of measurements, which are listed based on their source:

- SCADA/RTUs
  - Voltage magnitude at the HV/MV substation, identified with the slack bus of the network
  - Active/reactive power flows or current magnitudes at the top of the distribution feeders
- AMR system
  - Active and reactive power injections – loads and generations – from MV customers.
- LE method
  - Estimates of power injections – loads – for all buses which are not supported by the AMR system.

In addition, virtual measurements are also available pertaining to active/reactive power injections from buses without loads or DER, commonly named as zero injection buses.

Taking into account a potential upgrade of the infrastructure described above, synchronized measurements will be exploitable as well, referring to:

- PMUs
  - Voltage phasors at selected buses where PMUs are installed
  - Current flow phasors through branches incident to the PMU equipped buses.

The measured data from SCADA and AMR systems both have a 15-min temporal resolution, yet, they are not synchronized based on a common reference clock. As far as their update rates are concerned, SCADA measurements are available in (near) real time to the DMS centre of HEDNO, thus, the DSOTP can also have this capability. On the contrary, AMR data are transmitted to the telemetry centre of HEDNO on a daily basis, as a result there is a 24-hour delay in their delivery. This fact ensures that the SE tool can, at least, have recorded active and reactive power injections from the previous day of all the customers supported by the AMR system. Based on these measurements, a set of pseudo-measurements is required to be generated and used in order to make the network fully observable and guarantee an adequate degree of redundancy for running the DSE algorithm. Finally, the placement of PMUs will furnish real-time phasor measurements synchronized by the GPS signal.

In view of the algorithmic part, the SE tool is principally required to secure the observability status of the distribution grid at Mesogeia site by determining the quantity and positioning of pseudo-measurements, based on an established method for observability analysis. Furthermore, after the installation of PMUs, it is necessary that the PMU data are integrated into the set of pre-existing, conventional measurements in a smooth and fertile manner. In any case, the core of the SE tool, that is, the DSE algorithm is expected to attain a high accuracy level, exhibit fast convergence to the optimal solution and to maintain its performance in the face of uncertainties and errors.

Based on the requirements elaborated above, the specifications of the proposed SE tool are provided in the sequel.

### 3.2.1 Choice of DSE method

Taking into account the introduction of the current chapter, the WLS model is most preferable solution among the eligible methodologies for the formulation of the DSE problem. The reasons for this selection are manifold:

- Given the relatively slow update rates of the snapshots of measurements available as well as the increased number of pseudo-measurements needed for observability achievement, the dynamic modelling is an inappropriate approach for the Mesogeia pilot site.
- Among static modelling methodologies, load adjustment techniques are originally oriented to the treatment of a limited number of measurements, so, an increased level of measurement availability cannot be fully exploited. On the other hand, the deployment of Bayesian networks is a promising practice for DSE purposes, yet, still under development.
- WLS based schemes have been acknowledged as the most suitable solvers for the DSE problem compared to other optimization based approaches applied to power systems, in general [39].
- Since reliable detection of violations of permissible voltage limits is needed for the operation of advanced algorithms for smart use of DER and flexible loads, which are also developed within the framework of the Greek demo, bus voltages are considered as the state variables for the WLS based DSE.

### 3.2.2 The observability issue

In order to determine the observability status of the grid, a numerical method for observability analysis, is used [5]. It is based on the application of matrix algebra to the WLS model and is discussed in subchapter 3.4.4. As stated above, the usage of pseudo-measurements for observability achievement is required. The combination of the WLS model with LE/LF techniques is a well-established, overall scheme for dealing with the DSE problem [18], [19], [40]–[43].

In respect to MV customers served by the AMR system, special treatment is required because measured power injections from the previous day are available for solving the DSE problem in real time. For example, a short term LF method can be deployed for estimating the corresponding loads for the current day based on the data from the previous day. An available real-time information, such as temperature or day type, can be leveraged in order to enhance the accuracy of the load estimates. As a result, estimated power injections for the corresponding MV substations, can be introduced into the DSE algorithm.

With regard to LV customers with no AMR equipment installed, there are no exploitable load data for DSE purposes. Instead of this, historical loading values at MV/LV transformer level are available. The

application of load allocation (LA) techniques, that is, the allotment of power flow measured at the top of a feeder among the set of MV/LV transformer buses connected to it, by using appropriate ratios, can be based on the aforesaid historical data. In this way, estimated power injections for all MV/LV substations can also be available for processing by the DSE algorithm.

Overall, this mixed set of pseudo-measurements can ensure the grid observability. Their temporal resolution cannot be less than 15 minutes. Due to their different sources, their accuracy levels are distinct, thus, the tuning of the related weighting factors should be carried out meticulously.

### 3.2.3 Availability of PMU data

Since refreshing rates for PMU data are, by far, the fastest compared to other data types, their introduction into the SE tool is not anticipated to raise difficulties in order to build snapshots of measurements. Due to their high temporal resolution, a common time window between them and SCADA measurements can effectively be decided so that the time skewness of the resulting mixed set is small. Contrariwise, from a computational point of view, there are challenging issues, as elaborated in subchapter 2.2. Their high accuracy compared to the corresponding value for pseudo-measurements, results in sizeable variations between their weighting factors, thus, leading to ill-conditioning matrices during problem solving. Hence, in case of PMU availability, all weighting factors should be revised. Finally, fusing the PMU data with pre-existing measurements needs careful planning regarding the mathematical expression of the measurement functions for current phasors. Concluding, all the forenamed subtle tasks should be considered.

## 3.3 Design of the SE tool

The SE tool is designed to run at pre-defined time intervals, for example on an hourly basis or every 15 minutes. Given that the available measurements from the AMR system are delivered to HEDNO database with a 24-hour delay, accurate load models are critical for the reliable operation of the DSE algorithm. LE and LF techniques are used for identification of load models and estimation of real-time load consumption at network buses, using standard available measurement data, historical load data and general information about demand composition. Additionally, since the same delays exist with regard to measured generation of DER units, an estimation technique for real-time DER generation is applied.

The generation of pseudo-measurements for the distribution feeders of the Mesogeia site is organized as follows:

- For load buses supported by the AMR system, which pertain exclusively to MV consumers, a short term LF method is deployed for the estimation of load consumptions (active and reactive) on an hourly basis for the current day based on the measured load data from the previous day as well as real-time information, e.g. weather data.
- For buses hosting DER units, also supported by the AMR system, the observation of the weather conditions in real time can lead to satisfactory estimates of their generation. In case of photovoltaic (PV) units, power generation during hours of sunshine can be approximated via the measured values for the corresponding hours from the previous day. Of course, real-time information about the connection status per individual PV unit is also taken into account.
- For unmeasured load buses, historical samples of loading conditions for MV/LV transformers obtained for different seasons, days and hours, are leveraged for purposes of load modelling. Typical load profiles are generated and, subsequently, used for real-time LA based on the actual SCADA measurements from the HV/MV substation and the AMR based pseudo-measurements.

In case of PMUs installation, synchronized phasor measurements can also be introduced into the aforementioned procedure and enhance the quality of the LA.

With respect to the identification of the grid topology, there is no availability of digital measurements, which means that the statuses of the switching devices are not recorded. Hence, the network model is obtained based on the assumption that all switching devices are at their normal operational state. This model is introduced into the DSE algorithm.

Figure 3 illustrates the flowchart of the SE tool wherein the flowchart for the generation of pseudo-measurements is also detailed.

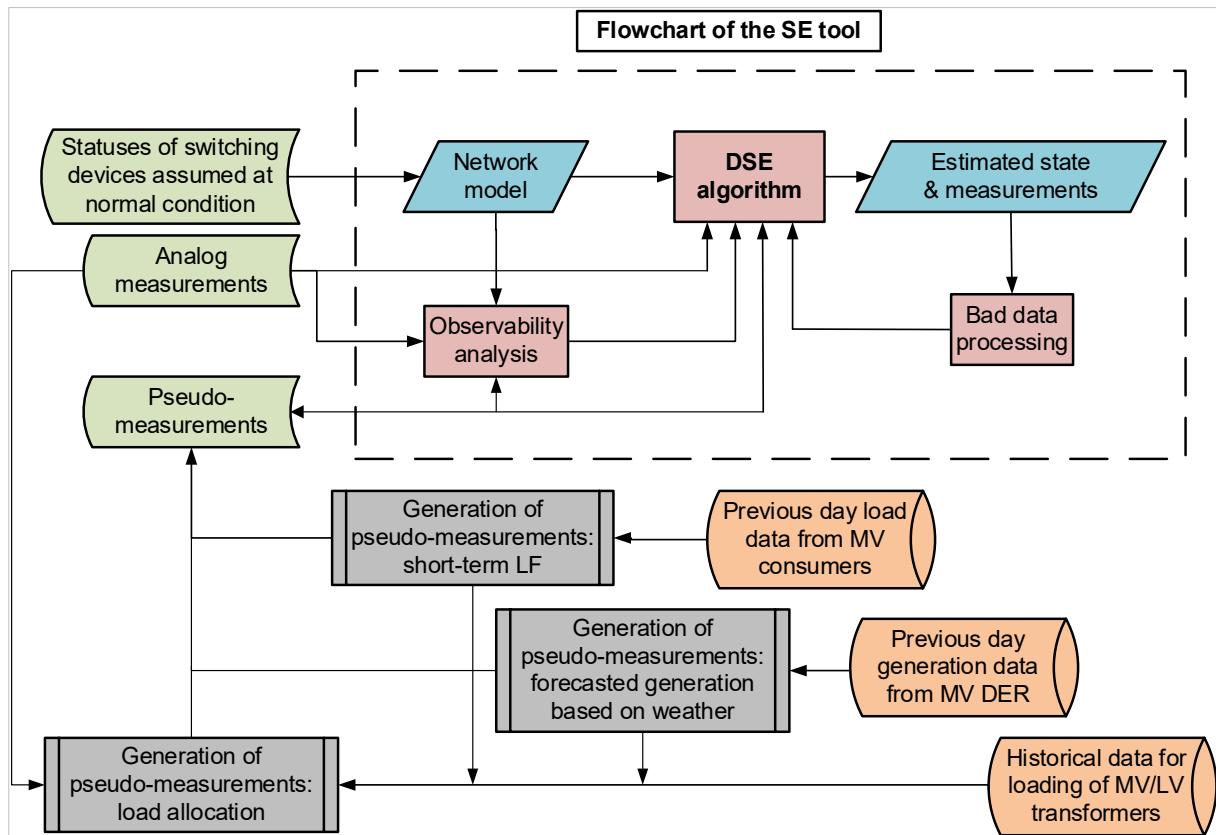


Figure 3: Structure of the SE tool.

### 3.4 WLS based modelling of the DSE problem

#### 3.4.1 Assumptions

The distribution network is assumed to operate in the steady state. The slowly varying conditions of the network in its normal operating state allows for the tolerance of a certain volume of time skewness between measurements included in the same snapshot [6]. Evidently, this assumption is unneeded if the measurement set is exclusively composed of synchronized phasor data.

Furthermore, with a view to avoiding modelling complexities, the network is assumed to be balanced and the single phase equivalent network model is considered for the execution of power flow analysis and the DSE algorithm. This hypothetical is justifiable, as mentioned in subchapter 2.2.

#### 3.4.2 Problem formulation

The formulation of the DSE problem is grounded in the following nonlinear measurement model [7]:

$$\mathbf{z} = \begin{bmatrix} z_1 \\ z_2 \\ \vdots \\ z_m \end{bmatrix} = \begin{bmatrix} h_1(\mathbf{x}) \\ h_2(\mathbf{x}) \\ \vdots \\ h_m(\mathbf{x}) \end{bmatrix} + \begin{bmatrix} e_1 \\ e_2 \\ \vdots \\ e_m \end{bmatrix} = \mathbf{h}(\mathbf{x}) + \mathbf{e} \quad (1)$$

where  $\mathbf{z}$  is the measurement vector which contains  $m$  values – measured, estimated or forecasted – introduced into the DSE algorithm as a dataset,  $\mathbf{h}(\mathbf{x})$  is the vector of nonlinear functions mapping the measurements to the state variables, that is, all bus voltage magnitudes and phase angles except for the one of the slack bus (assumed to be known, equal to zero) which define the state  $\mathbf{x}$ , and  $\mathbf{e}$  is the vector of measurement errors.

The WLS based approach is founded upon the assumption that the measurement errors follow the normal (or Gaussian) distribution with zero mean values and are, also, independent, symbolically,  $\mathbf{E}(\mathbf{e}) = \mathbf{0}$  and  $\mathbf{E}(\mathbf{e}\mathbf{e}^T) = \Sigma_{\mathbf{z}} = \text{diag}(\sigma_1^2, K, \sigma_i^2, K, \sigma_m^2)$ , where  $\sigma_i^2$  is the variance of the  $i$ th measurement error.

In the context of the aforementioned statistical model, the desideratum based on equation (1) is to find a value of  $\mathbf{x}$ , let it be  $\hat{\mathbf{x}}$ , which leads to the overall minimization of errors  $\mathbf{e} = \mathbf{z} - \mathbf{h}(\mathbf{x})$ . It is proven that the value  $\hat{\mathbf{x}}$  is the maximum likelihood estimate of  $\mathbf{x}$ , that is, this exact value which maximizes the probability of the measurement data. As a result, the DSE problem is conceptualized as an optimization task which amounts to the minimization of the sum of squares of weighted measurement residuals

$r_i = \frac{\mathbf{z} - h_i(\mathbf{x})}{\sigma_i}$ ,  $i = 1, K, m$ . Hence, a WLS estimator is built in order to solve the DSE problem by

minimizing the following objective function [7]:

$$\min_{\mathbf{x}} J(\mathbf{x}) = \sum_{i=1}^m r_i^2 = \sum_{i=1}^m \frac{(\mathbf{z}_i - h_i(\mathbf{x}))^2}{\sigma_i^2} = \mathbf{r}^T \Sigma_{\mathbf{z}}^{-1} \mathbf{r} \quad (2)$$

As observed,  $J(\mathbf{x})$  is a nonlinear function of the state  $\mathbf{x}$  and in fact, its minimization belongs to nonconvex optimization. Consequently, a solution to problem (2) can be approximated only via iterative procedures.

### 3.4.3 Solution algorithm

The solution scheme originates from the application of the first order optimality condition to  $J(\mathbf{x})$  [7]:

$$\mathbf{g}(\mathbf{x}) = \nabla_{\mathbf{x}} J(\mathbf{x}) = -\mathbf{H}^T(\mathbf{x}) \Sigma_{\mathbf{z}}^{-1} (\mathbf{z} - \mathbf{h}(\mathbf{x})) = 0 \quad (3)$$

where  $\mathbf{H}(\mathbf{x}) = \frac{\partial \mathbf{h}(\mathbf{x})}{\partial \mathbf{x}}$  is the Jacobian matrix.

In order to linearize the problem, the derivative  $\mathbf{g}(\mathbf{x})$  is expanded into Taylor series at the proximity of a point  $\mathbf{x} = \mathbf{x}_k$  and the higher order terms are ignored, as follows:

$$\mathbf{g}(\mathbf{x}_k) + \mathbf{G}(\mathbf{x}_k)(\mathbf{x} - \mathbf{x}_k) = 0 \quad (4)$$

where  $\mathbf{G}(\mathbf{x}) = \frac{\partial \mathbf{g}(\mathbf{x})}{\partial \mathbf{x}} = \mathbf{H}^T(\mathbf{x}) \Sigma_{\mathbf{z}}^{-1} \mathbf{H}(\mathbf{x})$  is the gain matrix of the model.

By combining the expressions (3) and (4), the following iterative scheme is obtained:

$$\mathbf{G}(\mathbf{x}_k) \Delta \mathbf{x}_k = \mathbf{H}^T(\mathbf{x}_k) \Sigma_{\mathbf{z}}^{-1} (\mathbf{z} - \mathbf{h}(\mathbf{x}_k)) \Rightarrow \mathbf{x}_{k+1} = \mathbf{x}_k - \mathbf{G}^{-1}(\mathbf{x}_k) \mathbf{H}^T(\mathbf{x}_k) \Sigma_{\mathbf{z}}^{-1} (\mathbf{z} - \mathbf{h}(\mathbf{x}_k)) \quad (5)$$

where  $\Delta \mathbf{x}_k = \mathbf{x}_{k+1} - \mathbf{x}_k$ ,  $k$  denotes the ascending number of the iteration and all matrices and vectors are evaluated at  $\mathbf{x} = \mathbf{x}_k$ .

The iterative solution scheme is known as the Newton's method, whereas the set of linear equations at the left side of (5) are referred as the Normal Equations of the problem [5], [6]. As noticed, the invertibility of  $\mathbf{G}(\mathbf{x})$  is the necessary condition for the derivation of the formula at the right side of (5).

### 3.4.4 Insight into the WLS model

The analysis of the solution algorithm was necessary in order to define the crucial parameters of the WLS model and highlight their importance.

The vector of measurement functions  $\mathbf{h}(\mathbf{x})$  contains the mathematical expressions for the electrical quantities comprising the measurement dataset, which are obtained via the application of Kirchhoff's circuit laws to power networks. Apparently, they are the same equations used for power flow analysis with the major difference that measurement errors are also considered. The analytical expressions for all types of conventional measurements, that is, line power flows, bus power injections, bus voltage magnitudes and line current now magnitudes, as well as the models of network components, are described in Annex B.

The Jacobian  $\mathbf{H}(\mathbf{x})$  is composed of all first order partial derivatives of the vector of measurement

functions with respect to the state variables. Its  $ij$ th entry is  $\mathbf{H}_{ij}(\mathbf{x}) = \frac{\partial \mathbf{h}_i(\mathbf{x})}{\partial \mathbf{x}_j}$ , where  $\mathbf{h}_i(\mathbf{x})$  is the

measurement function referring to the  $i$ th measurement and  $\mathbf{x}_j$  is the  $j$ th state variable. Given that

$\mathbf{G}(\mathbf{x})$  is calculated based on  $\mathbf{H}(\mathbf{x})$ , the linear approximation of the measurement model (1) is intrinsically dependent upon the properties of the Jacobian matrix. The occurrence of undefined Jacobian elements for certain linearization points or abrupt changes in values of specific entries due to nonlinearities, are among the most serious issues raised during the solution of the problem [6]. The structure of  $\mathbf{H}(\mathbf{x})$  is provided in Annex B.

As regards the gain matrix  $\mathbf{G}(\mathbf{x})$ , its role is crucial for solving the iterative scheme in (5) and related computational techniques leverage its sparsity in order to achieve good convergence [5]. Additionally, the importance of  $\mathbf{G}(\mathbf{x})$  is significant since, by definition, it encompasses all the information about the available measurements (type, location, and accuracy) and serves as an accuracy indicator for the DSE procedure. More specifically, the covariance matrix of the SE errors is computed based on [16]:

$$\text{cov}_{\mathbf{x}}(\hat{\mathbf{x}}) = \mathbf{G}^{-1}(\hat{\mathbf{x}}) = \left[ \mathbf{H}^T(\hat{\mathbf{x}}) \Sigma_z^{-1} \mathbf{H}(\hat{\mathbf{x}}) \right]^{-1} \quad (6)$$

The  $i$ th diagonal entry of the inverse matrix  $\mathbf{G}^{-1}(\hat{\mathbf{x}})$  is the variance of the computed estimate  $\hat{\mathbf{x}}_i$  of the state variable  $\mathbf{x}_i$ , thus, it quantifies its accuracy level.

Finally, the study of  $\mathbf{G}(\mathbf{x})$  is included into the numerical methods for observability analysis. Intuitively, a distribution grid is said to be observable if the set of available measurements is adequately informative to achieve an estimate  $\hat{\mathbf{x}}$  via the WLS estimator. The observability status can be checked numerically by calculating the rank of  $\mathbf{H}(\mathbf{x})$ . The necessary and sufficient condition for observability is that the number of linearly independent measurements is equal to the number of state variables, thus,  $\mathbf{H}(\mathbf{x})$  has a full rank. This property results in a non-singular gain matrix  $\mathbf{G}(\mathbf{x})$  [5]. Consequently, the observability status can be identified by checking whether  $\mathbf{G}(\mathbf{x})$  is invertible or not.

## 3.5 Generation of pseudo-measurements

### 3.5.1 Short term load forecasting

As detailed in subchapter 3.3, the first stage for the generation of pseudo-measurements refers to the application of a short term LF method to the measured load data of the previous day from the MV consumers, aiming at the estimation of their loads in real time. To this direction, a one day-ahead LF technique is deployed, based on a simple autoregressive model [43], for the estimation of load consumption per individual MV consumer, on an hourly basis. It exploits the load measurements of the same hour from the previous day as well as the same day of previous week. Moreover, real-time measurements of temperature along with day-specific information, are used. Supposing that the day of

estimation is divided into 24 time intervals, the formula of the proposed LF model for the  $i$ th time interval is given below:

$$P_{D,i} = c + a_1 P_{D,i \text{ prevday}} + a_2 P_{D,i \text{ prevweek}} + a_3 T_i + a_4 T_{i-1} + a_5 T_{i-2} + a_6 DL_{\text{today}} + a_7 WD + a_8 WE \quad (7)$$

where  $i$  is the time interval corresponding to the real-time load estimate,  $i-1$ ,  $i-2$  are the two previous time intervals, respectively, *today*, *prevday*, *prevweek* denote the current day, the previous day and the same day of the previous week, respectively,  $P_{D,i}$  is the estimated demand for active load in power units and  $T$  symbolizes the temperature.

As regards day-specific data,  $DL$  denotes the duration of daylight in hours, and  $WD$  ( $WE$ ) is a dummy variable which is equal to 1 (0) if the current day is a weekday (weekend).

The parameters  $a_1, \dots, a_8$  and  $c$  are calculated based on the application of an ordinary least square estimator to a large sample of actual load data, e.g. for a whole season from consecutive years.

The corresponding reactive part of the load, let it be  $Q_{D,i}$ , is estimated based on the power factor of the MV consumer, which is calculated via the historical load data. Moreover, it is noted that the time resolution of the estimates can be increased; for example, considering that an estimated value for hourly load refers to average power consumption, the load estimate for 15 minutes is a quarter of the value.

Summing up, the load consumptions of every MV consumer who is supported by the AMR system are estimated in real time based on the formula (6) and their power factor. Given that every MV consumer is fed by its individual substation, the estimated active and reactive loads are equal to the pair of active and reactive power injections at this exact bus.

### 3.5.2 Load allocation

At second stage, an LA procedure is executed with a view to obtaining load estimates for the rest of load buses, which are not supported by the AMR system. Before allocating the loads, the computation of the generation of all DER units, that is, the PV units hosted in the Mesogeia site, is required. Given that the AMR system supports all PV units, yet, the most recent data available in real time come from the previous day, an estimation technique needs to be introduced.

Considering that solar irradiance as well as the hours of daytime barely change between consecutive days, the real-time power generation of PV units at the  $i$ th time interval can be approximated by the corresponding measured data from the previous day as long as the weather conditions are similar, mainly referring to sunlight. Therefore, the real-time information about the weather is sufficient in order to acquire estimates of PV generation.

As a result, the following, simple formula is used for every PV unit:

$$P_{G,i} = P_{G,i \text{ prevday}}, \text{ in case of similar weather conditions} \quad (8)$$

where  $P_{G,i}$  is the estimated power generation in real time and  $P_{G,i \text{ prevday}}$  is the measured power value of the corresponding time interval from the previous day.

Apparently, if the weather conditions differ, the approximation in (7) is adjusted accordingly. For example, in case of partly cloudy, real-time weather contrarily to a sunny previous day, the estimate  $P_{G,i}$  is set to the half value of  $P_{G,i \text{ prevday}}$ .

Given that every PV unit is connected to the grid via its individual transformer, the estimated power generation is equal to the power injection at the corresponding bus. It is noted that a unity power factor is considered, thus, there are no reactive components.

Finally, in order to perform the LA, the actual measurements of active and reactive power flows from the upstream HV/MV substation are also used. The main idea is to calculate the amount of power to be allocated at the  $i$ th time interval and, subsequently, to allot it based on normalized load profiles for MV/LV transformers [40]. These profiles are created using sample data for loading conditions of MV/LV transformers from the past. The seasonality of loads, as well as the nominal capacities of the transformers are also taken into account.

The amount of load to be allocated, let it be  $P_{dtotal,i}$ , is calculated by subtracting the aggregated MV consumption from the sum of actual, active power flowing to the grid, denoted by  $P_{flow,i}$ , and the total DER generation, as follows:

$$P_{dtotal,i} = P_{flow,i} + \sum_{j=1}^{m_G} P_{G,i}^j - \sum_{k=1}^{m_D} P_{D,i}^k \quad (9)$$

where  $m_G$  and  $m_D$  are the numbers of PV units and MV consumers served by the AMR system, respectively,  $P_{G,i}^j$  is the PV generation at the  $j$ th bus, and  $P_{D,i}^k$  is the MV consumption at the  $k$ th bus.

In essence, the LA technique exploits the radial topology of distribution grids in order to estimate loads of all buses which are located downstream a point, either bus or branch, for which actual power measurements are available. Therefore, individual LA procedures are carried out for every part of the grid that is downstream a measured point. In respect to the Mesogeia pilot site, the LA formula in (8) is implemented for every feeder separately, since the actual power measurements obtained via the SCADA refer to power flows at the top of the feeders.

As a result, the allocated active power for every bus without AMR equipment is calculated based on:

$$P_{d,i} = NLP_{d,i} P_{dtotal,i} \quad (10)$$

where  $NLP_{d,i}$  is the value of the normalized load profile which corresponds to the nominal capacity of the MV/LV transformer of the bus, the season and the type of the day of the estimation.

Assuming a constant power factor, an estimate of the reactive power  $Q_{d,i}$  is also obtained. In this way, a pair of active and reactive power injections is provided for the rest of the load buses.

### 3.6 Integration of PMU data

With a view to merging the synchronized measurements from PMUs into the WLS estimator, the related mathematical model needs to be revised. Modifications of the WLS model for PMU purposes have been widely discussed in the existing literature [44]–[47].

First and foremost, the matter of the reference angle is reconsidered. Without PMUs, there are no measurements of phase angles, neither voltages nor currents. Hence, the use of a reference bus in terms of phase angle is required. This reference is simply assigned to the voltage phase angle of the slack bus which is arbitrarily set equal to zero and is excluded from the problem formulation. The DSE algorithm estimates the relative phase angles of all buses with regard to this angle of zero value. Contrarily, in the presence of PMUs, this practice is unnecessary, since there is availability of measured phase angles with a reference point dictated by the GPS. Hence, all measurements of phase angles are processed by the DSE algorithm and their estimated values are calculated based on the GPS reference.

In the light of the analysis above, no reference angle of zero value is used in case of installed PMUs. All data of phase angles is included in the measurement set and introduced into the DSE algorithm. The measured phase angle of one bus, determined based on the GPS, is used as a reference. All bus phase angles, measured or not, are estimated in reference to the one of the aforementioned bus, which is also estimated. Accordingly, the state vector  $\mathbf{x}$  comprises all bus voltage magnitudes and phase angles.

A second issue to be taken into account is the formulation of phasor measurements. The incorporation of current phasors in the form of polar coordinates, that is, magnitude and phase angle, into the measurement model increases the possibilities for the occurrence of undefined entries in the Jacobian matrix, since the corresponding partial derivatives include denominators. The solution to this problem is the formulation of the related measurements in rectangular coordinates, that is, their expression in real and imaginary parts, which yield derivatives with simpler structure. Therefore, this choice minimizes the risk for undefined Jacobian elements and simplifies the related computations. Nonetheless, it has a negative impact on the accuracy of the measured PMU data, amplifying their measurement errors. This accuracy loss is much smaller than the overall improvement achieved after the installation of PMUs, though. Overall, this trade-off is determined in favor of the rectangular coordinates, which are used within the framework of the SE tool. The analytical formulas for the aforementioned measurements and partial derivatives are provided in Annex B.

For the purposes of the present study, all the issues discussed refer to the effective integration of the PMU into the SE tool. Apparently, the integration of PMUs in technical level is another, major issue which is out of scope for the study. In short, the equipment deployed for installation of a system of PMUs must not only have a great deal of processing capability but also be able to collect data from local sensors. Also, an adequate and flexible communication link for the support of several data acquisition points, must be guaranteed. In this way, real-time availability of PMU data can be ensured and, thus, exploited by the SE tool.

## 4 Simulations studies of the SE tool

### 4.1 The test network of the Mesogeia site

The test bed for the Greek demo is a portion of real-world distribution network operating in the geographical site of Mesogeia, which is located at the south-eastern part of Attica region. For the simulation studies of the SE tool, two radial distribution feeders from the Mesogeia pilot site are used. Both feeders, with the code names 210 and 490, originate from the HV/MV substation of Nea Makri and deliver electric power via overhead lines with nominal operating voltage at 20 kV. Overall, the test network consists of 335 nodes, each one pertaining to one bus, and 334 branches, each one referring to one line connecting two buses. The composition of the set of nodes is analyzed in Table 1.

**Table 1: Description of nodes (type and number) of the test network.**

Feeder	No. of nodes with injections			No. of nodes with zero injection	Total no. of nodes
	Slack bus	DER units	Load buses		
210	1	7	104	160	272
490	Common with 210	0	31	32	63
<b>Aggregate</b>	<b>1</b>	<b>7</b>	<b>135</b>	<b>192</b>	<b>335</b>

The common slack bus of the two feeders is identified with the HV/MV substation of Nea Makri and is used as the reference node on condition that only conventional measurements are available. As noticed, a considerable number of nodes refer to zero injection buses, over 50% of the total number of buses. The individual substations of MV consumers and the MV/LV transformers comprise the set of load buses. The configuration of the two feeders, as well as the structure of the HV/MV substation of Nea Makri are provided in Annex A.

As far as the measurement set is concerned, Table 2 provides a detailed list of all available measurement data given the pre-existing metering infrastructure of the test network. The measurements acquired from the RTUs of the HV/MV substation are considered as the only actual, real-time measured data, whereas the virtual measurements convey error-free information about zero injections. Before its introduction into the DSE algorithm, the dataset is supplemented with pseudo-measurements which are obtained according to the design of the SE tool given in subchapter 3.3. The pseudo-measurements are either AMR based, namely the load forecasts for MV consumers and the estimates of generation of DER units, or LA based, that is, allocated loads for MV/LV transformers.

With a simple summation, the complete dataset comprises 673 measurements. Provided that the grid state  $\mathbf{x}$  consists of 335 bus voltage magnitudes and 334 phase angles, the measurement redundancy which is defined as the ratio of the total number of measurements, let it be  $m$ , to the number of state variables, let it be  $n$  [16], is equal to  $m / n = 673 / 669 = 1,006$ . This value is appreciably low and is expected to affect negatively the error filtering capability of the SE tool. Apparently, the dataset and the corresponding measurement redundancy are revised at the last stage of the simulations, where the installation of PMUs is considered.

**Table 2: Type, number and source of available pre-existing measurements**

Network part	Available measurement set			Location	Generic symbol
	Type	No.	Source		
Feeder 210	Pair of power injections	3	Pseudo-measurements from AMR based LF	MV consumers	$P_D, Q_D$
	Pair of power injections	7	Pseudo-measurements from AMR based estimation	DER – PV units	$P_G, Q_G$
	Pair of power injections	101	LA	MV/LV transformers	$P_d, Q_d$
	Pair of zero injections	160	Virtual	Zero injection buses	$P_{ZI}, Q_{ZI}$
Feeder 490	Pair of power injections	2	Pseudo-measurements from AMR based LF	MV consumers	$P_D, Q_D$
	Pair of power injections	29	LA	MV/LV transformers	$P_d, Q_d$
	Pair of zero injections	32	Virtual	Zero injection buses	$P_{ZI}, Q_{ZI}$
HV/MV substation	Voltage magnitude	1	SCADA	MV busbar of the HV/MV transformer	$V_S$
	Pair of power flows	2	SCADA	Top of distribution feeders 210 and 490	$P_{FL}, Q_{FL}$

## 4.2 Description of the UCs

For the implementation of the Greek demo, five high level Use Cases have been conceptualized and rigorously defined by a joint working group of HEDNO and NTUA in D4.1. Their general objective is to provide a rigid framework for the development of the tools and services within the Greek demo, and to systematize the study of the impact of Platone solutions implemented in the Mesogeia pilot site. The performance of the tools and services is assessed by means of certain KPIs.

The Use Cases UC-GR-01 and UC-GR-02, described in subchapters 3.3.1 and 3.3.2 of D4.1 [2], respectively, refer to the SE tool. These two Use Cases are linked to the requirements which were reported in subchapter 3.2 of the present document, since they establish an operational framework within which the SE tool is required to provide specific services in a reliable and effective manner. To this direction, meaningful operational scenarios are conceived and used as the benchmarks for testing the SE tool. Finally, 6 KPIs are deployed for the quantification of its performance.

The Use Case UC-GR-01 is dedicated to the examination of the capability of the SE tool to achieve observability for the Mesogeia pilot site based on the pre-existing metering infrastructure and, subsequently, to perform data cleansing in order to attain an accurate estimate of the actual grid state. The Use Case includes two different scenarios. In the baseline scenario, a typical operational framework is considered. The HEDNO operates the test network of the Mesogeia site and all switching devices are

at their normal condition, thus, the network model is known with a good degree of certainty. The conventional measurements available for purposes of real-time monitoring, are obtained via the metering infrastructure which is described comprehensively in subchapter 3.2. The SE tool is required to render the grid observable using the methodology detailed in subchapter 3.4 for generation of pseudo-measurements, and to filter the measurement dataset by means of the WLS based DSE algorithm with a view to obtaining the maximum likelihood estimate of the grid state. The quality of the obtained results is evaluated in terms of accuracy, that is, the deviation of the state estimate from the actual grid state, and convergence, which refers to the capability of the iterative solution algorithm to converge to the optimal solution as well as the associated rate. As regards the second scenario, the occurrence of missing or inconsistent measurement data which render the test network unobservable, is considered. With the object of achieving observability, realistic options for additional or alternative data which can substitute for the missing ones, are examined. The impact of the modified measurement set on the performance of the DSE algorithm is assessed.

The Use Case UC-GR-02 follows as an extension to the aforementioned one, aiming at the proper integration of PMU data into the SE tool. The related scenario assumes that a prespecified number of PMUs are installed in the test network at strategical locations. As a result, synchronized phasor data are fused with the pre-existing conventional measurements, boosting the overall information content. Smooth integration of PMU data needs to be performed by the SE tool, so that all related problems, described in subchapter 3.2.3., can be circumvented. The modelling techniques proposed in subchapter 3.6, are followed. The performance of the SE tool is assessed in order to quantify the improvement that the use of high quality information provided by PMUs entail, compared to the pre-existing metering infrastructure.

## 4.3 Description of simulations

### 4.3.1 Simulation framework for UC-GR-01

Provided that the short term LF delivers hourly load estimates, the operation of the SE tool is simulated at hourly intervals for the Use Case UC-GR-01. The simulations are based on actual data obtained from SCADA and AMR systems of the HEDNO. The period of simulations covers a whole week of July 2019. This selection is justifiable; in general, summer months are characterized by heavy loading conditions, which have been associated with deterioration of SE errors [48]. Hence, the SE tool is tested with regard to the operating conditions close to the worst case.

As regards the evaluation of the performance of the SE tool, it is apparent that, since the actual grid state  $\mathbf{x}$  is never known, another reference state has to be assumed in order to quantify the accuracy of the DSE algorithm. The reference state vector is obtained through the execution of the DSE algorithm based on the SCADA measurements as well as the delayed AMR data of the same day of the estimation. Apparently, the LA scheme for the MV/LV transformers is based on these actual data. This implementation is equivalent to a hypothetical situation where, in addition to SCADA measurements, the measured data from AMR system are also available in real time and not with a one-day delay. Hence, this reference state is assumed to be the true state vector. In Figure 4, the simulation framework for the  $i$ th hourly time interval of a day of estimation, is visualized.

The MATLAB based open-source toolbox for electric power system simulation and optimization, MATPOWER [49] has been used for testing of the SE tool. Related scripts have been developed to read the load flow data stored in ASCII files with the PTI PSS/E “raw” format [50], whereas separate files were created in order to store in exploitable format the available measurement data. Existing SE oriented functions have been modified and new ones have been created in order to implement the design of the SE tool.

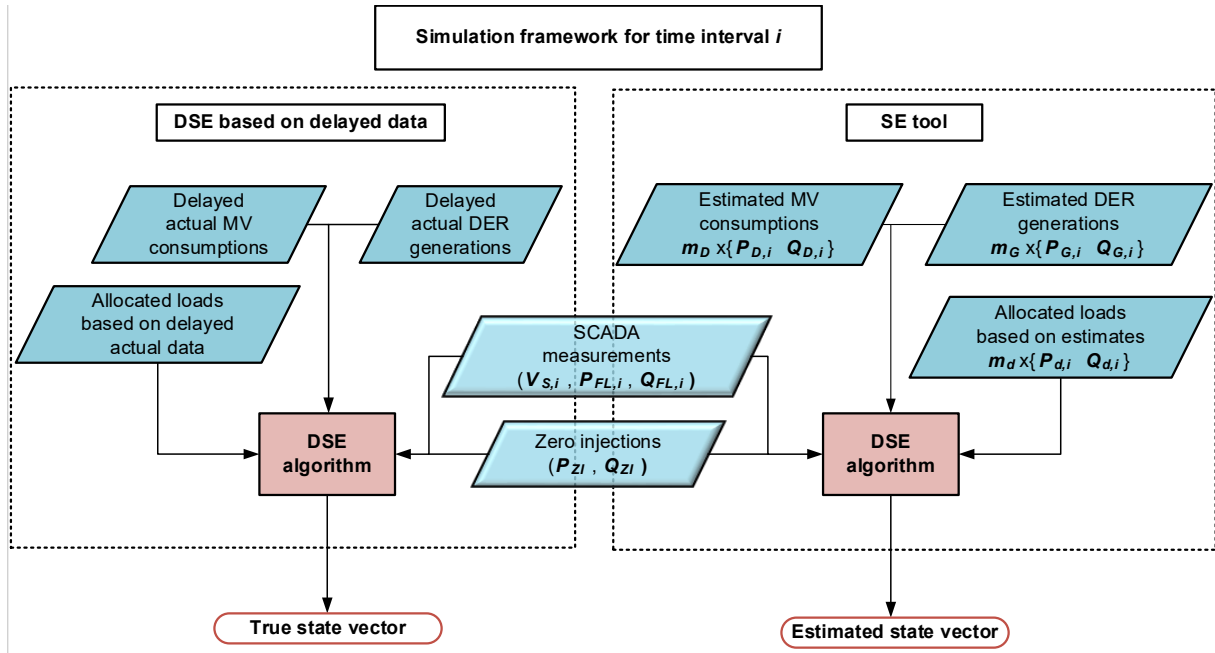


Figure 4: Simulation framework for UC-GR-01

The KPIs used for evaluation of accuracy and convergence, are summarized in the sequel [51], [52]. Analytical descriptions of them can be found in D4.1. The accuracy metrics are essentially different norms for calculating the difference between the true and the estimated state. The convergence metrics are computed based on specific values occurring during the execution of DSE algorithm.

- Accuracy KPIs

- The relative percentage error  $RPE_j$  is the relative difference between true  $V_j^{true}$  and estimated voltage magnitude  $V_j^{est}$  of the  $j$ th node:

$$RPE_j = \left| \frac{V_j^{true} - V_j^{est}}{V_j^{true}} \right| 100\% \quad (11)$$

- The root mean square error  $RMSE$  is the root of the mean of the squared differences between true and estimated nodal voltage magnitudes:

$$RMSE = \sqrt{\frac{1}{n} \sum_{j=1}^n (V_j^{true} - V_j^{est})^2} \quad (12)$$

- The accuracy metric for estimation of voltage phasors  $Macc_V$  is the Euclidean norm of the deviations between true  $V_j^{true}$  and estimated nodal complex voltages  $V_j^{est}$ :

$$Macc_V = \|V^{error}\|_2 = \sqrt{\sum_{j=1}^n |V_j^{true} - V_j^{est}|^2} \quad (13)$$

- Bearing in mind the analysis in subchapter 3.4.4, the maximum diagonal entry of covariance matrix of the DSE problem evaluated at the estimated state  $\hat{\mathbf{x}}$ , captures the variance of the worst estimated state variable:

$$\Psi_M = \max_{j=1,K,n} [\text{cov}_{\mathbf{x}}(\hat{\mathbf{x}})]_{jj} = [\mathbf{G}^{-1}(\hat{\mathbf{x}})]_{jj} \quad (14)$$

It is worth noting that, contrarily to the aforementioned accuracy KPIs, the KPI  $\Psi_M$  is computed as a standalone value, that is, there is no need to assume a true, reference

state for its calculation. The value  $\Psi_M$  is referred hereinafter as worst case coordinate error variance.

- Convergence KPIs
  - The indicator  $Mconv_{obj}$  quantifies the relative change in the value of the objective function  $J$  at the terminal iteration of the solution algorithm, which is denoted via the ascending number  $k_{term}$  :

$$Mconv_{obj} = \left| 1 - \frac{J^{k_{term}}}{J^{k_{term}-1}} \right| \quad (15)$$

- The indicator  $Mconv_V$  is the maximum relative change in absolute value, calculated for the nodal voltage magnitudes  $V_j, j = 1, K, n$  at the last iteration:

$$Mconv_V = \max_{j \in n} \left| 1 - \frac{V_j^{k_{term}}}{V_j^{k_{term}-1}} \right| \quad (16)$$

- The indicator  $Mconv_\delta$  is the maximum difference in absolute value, calculated for the nodal voltage phase angles  $\delta_j, j = 1, K, n$  at the last iteration:

$$Mconv_\delta = \max_{j \in n} \left| \delta_j^{k_{term}} - \delta_j^{k_{term}-1} \right| \quad (17)$$

In respect to measurements, a constant power factor, let it be  $PF$ , equal to 0,95 is assumed for the MV/LV transformers. Hence, the corresponding reactive power consumption for the  $i$ th time interval is:

$$Q_{d,i} = P_{d,i} \tan(\arccos(0.95)) \quad (18)$$

The power factors for MV consumers and DER units have already been reported in subchapter 3.5.

Tuning of measurement weights is the final issue that needs to be taken into consideration. As showed in subchapter 3.4.2, the measurement weights are included in  $\Sigma_z^{-1} = \text{diag}(1/\sigma_1^2, K, 1/\sigma_i^2, K, 1/\sigma_m^2)$ , where  $1/\sigma_i^2$  is the weight of the  $i$ th measurement, inversely proportional to its variance. Hence, the calculation of the associated variances is necessary.

For all measurements, the approach of expressing the standard deviation of a measurement as a function of its value [51] is adopted. This approach is founded upon the assumption that all measurements errors follow the Gaussian distribution [39], stated in subchapter 3.4.2. Hence, the formula for the standard deviation  $\sigma$  of any measurement is given as follows:

$$\sigma = \frac{\mu \times \text{error}\%}{3 \times 100} \quad (19)$$

where  $\mu$  is the actually measured value, in case of SCADA or AMR data, or the value of pseudo-measurement, in case of data from short term LF, estimation of PV generation or LA, and  $\text{error}\%$  denotes the maximum percentage error around  $\mu$ .

The approximation of  $\text{error}\%$  is a matter of major importance, since it is a decisive parameter for the quantification of standard deviation based on (19). With regard to data from SCADA, the voltage magnitude from the MV busbar of the HV/MV substation is the most accurate measurement type given that the power flow measurements are derivative data based on measured voltage and current flows. Moreover, the accuracy of the AMR data is considered to at the same level with that of power flows from SCADA.

As far as the pseudo-measurements are concerned, the approximation of maximum error is different between the DSE based on delayed data and the SE tool. In particular, the simulated DSE on actual, delayed data uses only LA for MV/LV transformers, thus, it includes only a single type of pseudo-measurements. Their error is set 10 times bigger than the one for AMR data. Contrarily, the SE tool makes use of 3 different types of pseudo-measurements, obtained from short term LF, estimated PV generation and, finally, LA. Taking into account the results in [19], the maximum error for load forecasts is set to 10%. The estimated injections from PV units are associated with an error of 20%, given that they are based on measurements from the previous day. Finally, the load estimates from LA are considered as the most inaccurate pseudo-measurement with a maximum error of 40%.

The values for *error%* per measurement type are summarized in Table 3. As observed, the maximum error for pseudo-measurements obtained from LA is bigger for the simulation of the SE tool compared to the one for the DSE based on delayed data. The LA scheme for the former depends on the estimates from LF and of PV generation whereas, for the latter, exploits actual data. Besides, no maximum error is considered for virtual measurements. Their standard deviation is assigned an extremely low value, equal to  $10^{-6}$ .

**Table 3: Maximum errors considered for tuning of measurement weights.**

Measurement type	Maximum error <i>error%</i>	
	DSE based on delayed data	SE tool
Voltage magnitude (SCADA)	0.2	0.2
Power flows (SCADA)	2	2
Power injections (AMR)	2	–
Pseudo-measurements from AMR based LF	–	10
Pseudo-measurements from AMR based estimation of PV generation	–	20
Pseudo-measurements from LA	20	40
Virtual measurements	0	0

### 4.3.2 Simulation framework for UC-GR-02

Similarly to UC-GR-01, the concept of the simulations for UC-GR-02 is based on the assumption that the SE tool operates at hourly intervals during a period of increased loading conditions. The only difference is the addition of synchronized phasor data to the pre-existing measurement set, which is assumed to be delivered by a prespecified number of PMUs placed at specific points of the Mesogeia pilot site. Given that no actual PMU data are available for the test network, the only way to evaluate the operation of the SE tool in case of installed PMUs is the deployment of the power flow algorithm for the construction of realistic measurement sets. This is a well-established practice which is routinely performed by SE vendors worldwide during the refinement and tuning of their algorithms [52].

More specifically, no actual SCADA and AMR data are used for simulations. The actual values of all available data, i.e., pre-existing, conventional and PMU measurements, for the *i*th time interval are obtained via a power flow solution presuming high loading conditions for all load buses (MV consumers and MV/LV transformers) and maximum feasible PV generation during daylight. In order to generate a realistic dataset, each value is perturbed by adding a normally distributed random error, whose standard deviation is computed based on (19).

The corresponding formula for the  $k$ th measurement is the following:

$$\mu_{k,i}^{meas} = \mu_{k,i}^{true} + rand \times \sigma_k \tag{20}$$

where  $\mu_{k,i}^{meas}$  is the assumed value of the  $k$ th measurement for the  $i$ th time interval,  $\mu_{k,i}^{true}$  is the corresponding actual value (obtained from a power flow solution),  $rand$  is a pseudo-random number following the Gaussian distribution  $\mathcal{N}(0,1)$  and  $\sigma_k$  is the associated standard deviation.

For the calculation of standard deviations, the same maximum errors as the ones provided in Table 3 for the SE tool, are considered for all pre-existing measurements. Regarding voltage and current magnitudes and phase angles delivered by PMUs, a fixed, maximum error of 0.1% is assumed, since they are regarded as more accurate data than SCADA measurements [51], [53].

The simulation framework is executed for a whole day. In order to produce snapshots of measurements at time intervals of 15 minutes, the power flow measurements from SCADA are leveraged in order to capture the intraday variation of loading conditions. An average load profile is generated and, then, applied to all load buses in order to extract their hourly actual values via the power flow algorithm. In Figure 5, the simulation framework for the  $i$ th time interval of the day of estimation is displayed. As observed, the assumed, true state of the grid is also obtained via the power flow algorithm. The same KPIs given in (11)–(17), are computed in order to assess the SE tool.

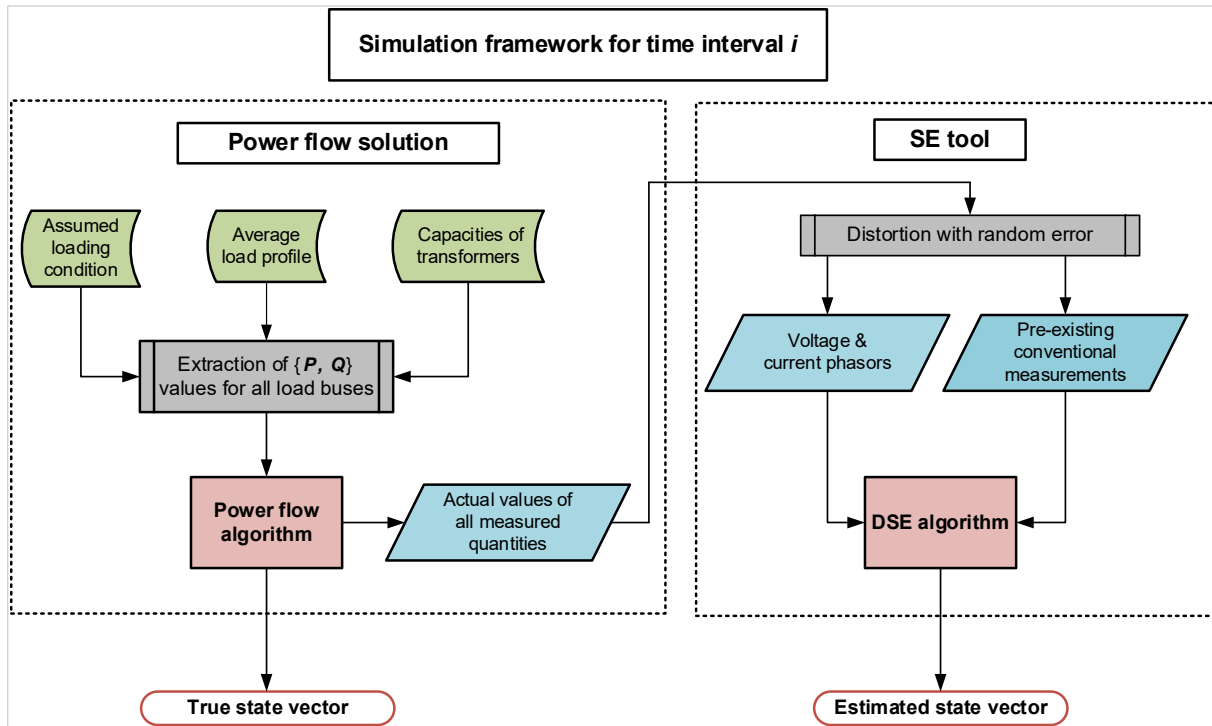


Figure 5: Simulation framework for UC-GR-02

## 4.4 Simulation studies

### 4.4.1 Results for UC-GR-01

#### 4.4.1.1 Scenario 1

In Scenario 1, the full set of pre-existing measurements listed in Table 2, is considered available. For this set, the gain matrix of the problem has full rank, so, it is invertible. According to subchapter 3.4.4, this property entails that the test network is observable. Besides, the formation of the dataset is such that there are at least two measurements per node, which constitutes a general empirical rule for achievement of observability.

Table 4 lists the maximum daily values of the worst case coordinate error variance  $\Psi_M$  which were obtained from the operation of the DSE based on delayed data and the SE tool at hourly intervals.

**Table 4: Daily values of worst case coordinate error variance of SE tool compared to DSE based on delayed data**

Day of estimation	Worst case coordinate error variance $\Psi_M$ ( $10^{-7}$ )	
	DSE based on delayed data	SE tool
Monday	0.482	2.357
Tuesday	0.484	2.467
Wednesday	0.496	2.426
Thursday	0.464	2.119
Friday	0.493	2.334
Saturday	0.479	2.801
Sunday	0.492	2.506

As expected, the DSE based on delayed actual AMR data yields estimated states of lower variance compared to the SE tool, thus, it is confirmed that its output can be used as a reference, true state in order to evaluate the accuracy of the SE tool.

Figure 6 refer to the estimation of nodal voltage magnitudes. The overall, weekly fluctuation of hourly *RPEs* per node, is displayed using internal (contiguous) node numbering, i.e., from 1 to 335.

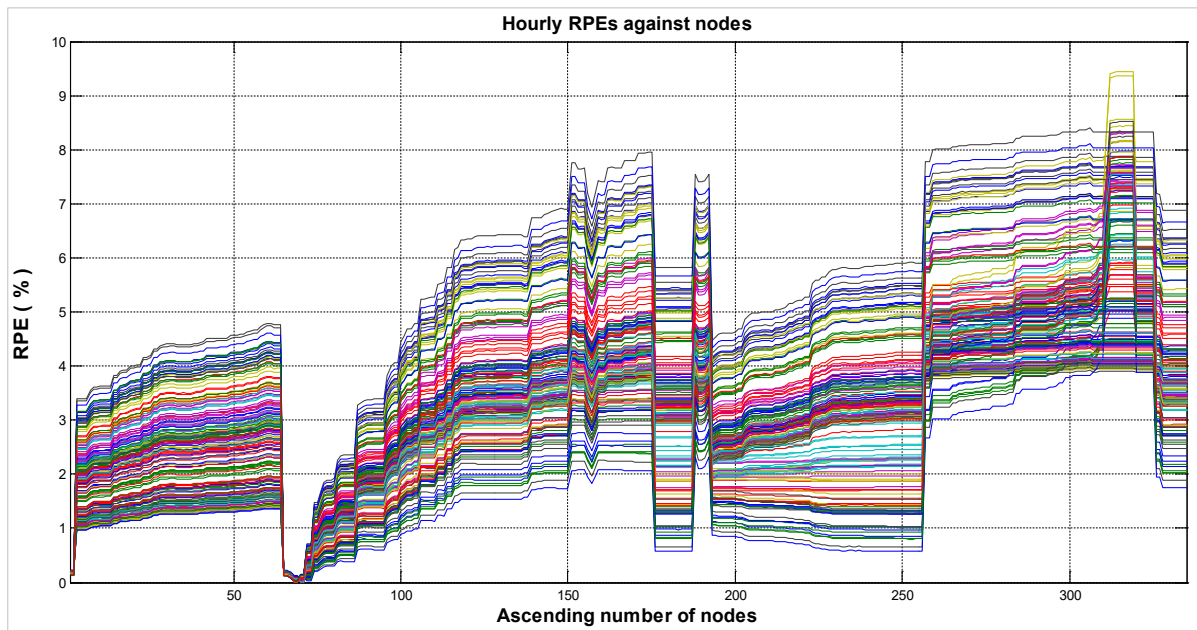


**Figure 6: Weekly distribution of hourly *RPEs* per node**

The related diagram depicts 168 values of *RPE* per node, that is, 24 values per day since the SE tool operates on hourly time intervals, for 7 consecutive days. Each curve refers to the distribution of *RPEs* per node for a specific hourly time interval of a specific day. As noticed, most values exceed 1%, which

is set as the quality threshold for this KPI in D4.1 [2]. The values of errors are minimized close to the slack bus, that is, at the proximity of node 1 and of node 65. Node 1 identifies with the slack bus and its vicinity includes the nodes at the top of feeder 490. In addition, node 65 identifies with the upper point of feeder 210 and its vicinity includes the nodes at top of the feeder. Hence, the estimated voltage magnitudes of the aforesaid nodes are associated with low errors due to their closeness to the slack bus, which is the only node with measured voltage magnitude. The highest errors occur at the bottom of feeder 210, which is considerably longer than feeder 490, and get values close to 9%.

Furthermore, a wide nodal range of feeder 290, which lies between nodes 200 and 250, is characterized by relatively low errors; a plausible explanation for this finding is the increased number of zero injection buses at this area, which are linked to error-free, virtual measurements. In general, the hourly curves of the distribution of errors per node have similar shapes, which means that there is a regularity regarding the relative levels of nodal errors per hour. Indisputably, the deployment of the same LA formula (10) for both the SE tool and the DSE based on delayed data, is the reason for this fact, since the majority of pseudo-measurements pertain to MV/LV transformers whose power injections are obtained via LA. The relatively low accuracy of this data leads to high levels of errors localized to certain nodal areas which embrace increased number of MV/LV transformers, for example, between nodes 120 and 180, as well as nodes 260 and 320. The same argument holds true for the nodes between 10 and 60, which belong to feeder 490, yet, the corresponding errors are kept at lower levels due to the short length of the feeder.

In Figures 7 and 8, the fluctuation of hourly values of  $RMSE$  and  $Macc_V$  on daily basis, is provided.

Given that both  $RMSE$  and  $Macc_V$  are average values, they capture a clear tendency for deterioration of errors during specific periods per day. For example, values of  $RMSE$  rise gradually from approximately 10 a.m. since PV generation starts to get significant, non-zero values which, apparently, are estimated with higher errors. Also, large values are observed from the evening until midnight of each day. This trend is even more noticeable for the values of  $Macc_V$ , that is, the estimated complex voltages. Since power demand as well as load variations intensify during evenings due to increased residential loads, maximized loading conditions occur, thus, leading to higher errors for the estimates obtained from the SE tool. Overall, the quality threshold of 0.2, determined for  $Macc_V$  in [2], is not met.

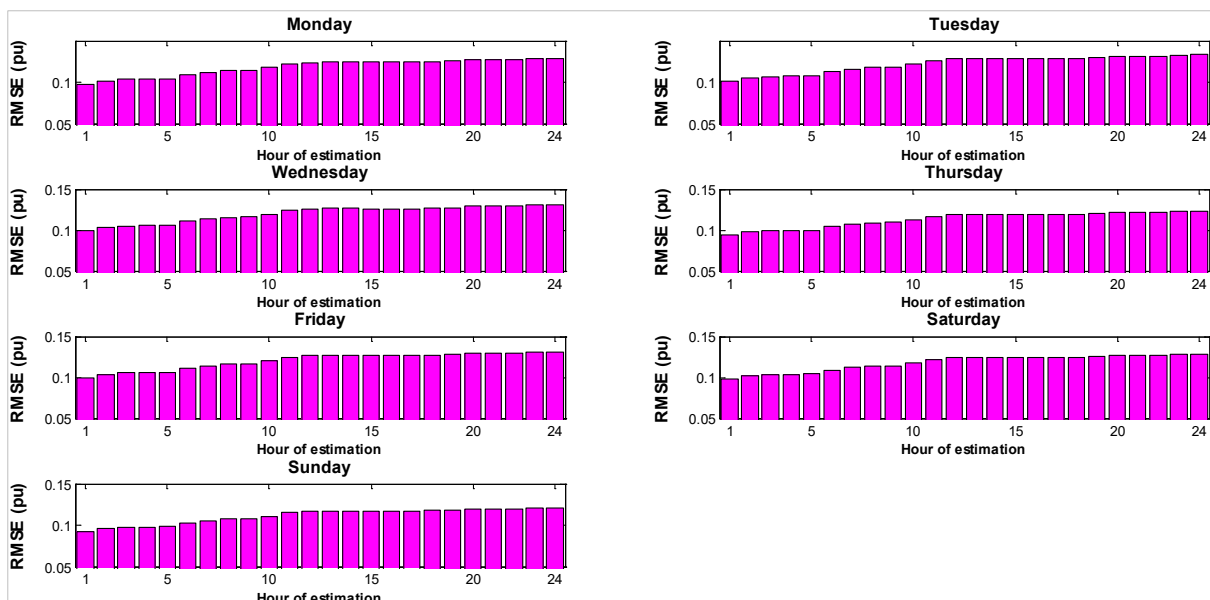


Figure 7: Hourly values of  $RMSE$  for the whole week of estimation

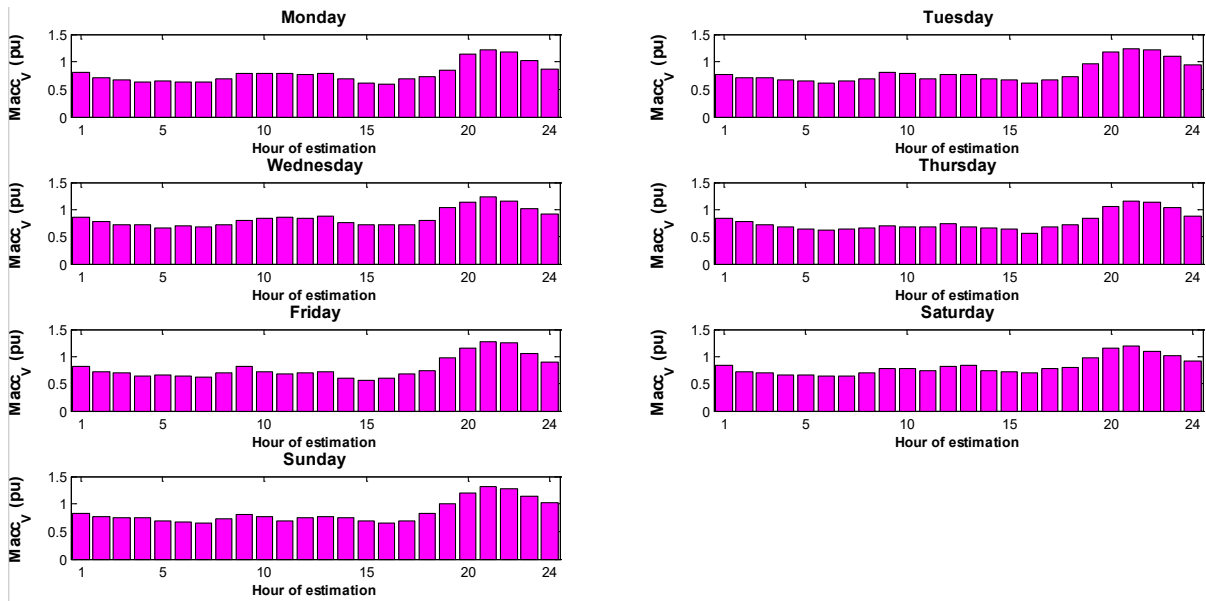


Figure 8: Hourly values of  $Macc_v$  for the whole week of estimation

In order to draw an overall conclusion about the difference in state estimates between the SE tool and the reference DSE based on delayed data, the corresponding mean, weekly profiles of estimated voltage magnitudes are illustrated in Figure 9. For reasons of comparison, the mean voltage magnitude obtained from the DSE based on delayed data, is also depicted. It is observed that the weekly profile from the SE tool lies below the mean voltage magnitude for the majority of the nodes. As expected, the largest differences between the two profiles arise in the areas of high  $RPEs$ , which were mentioned above. For example, in the area between nodes 260 and 320 the accuracy of the SE tool gets significantly low, indicating false violation of the voltage limit of 0,95 pu. Consequently, the reliability of the related results is poor.

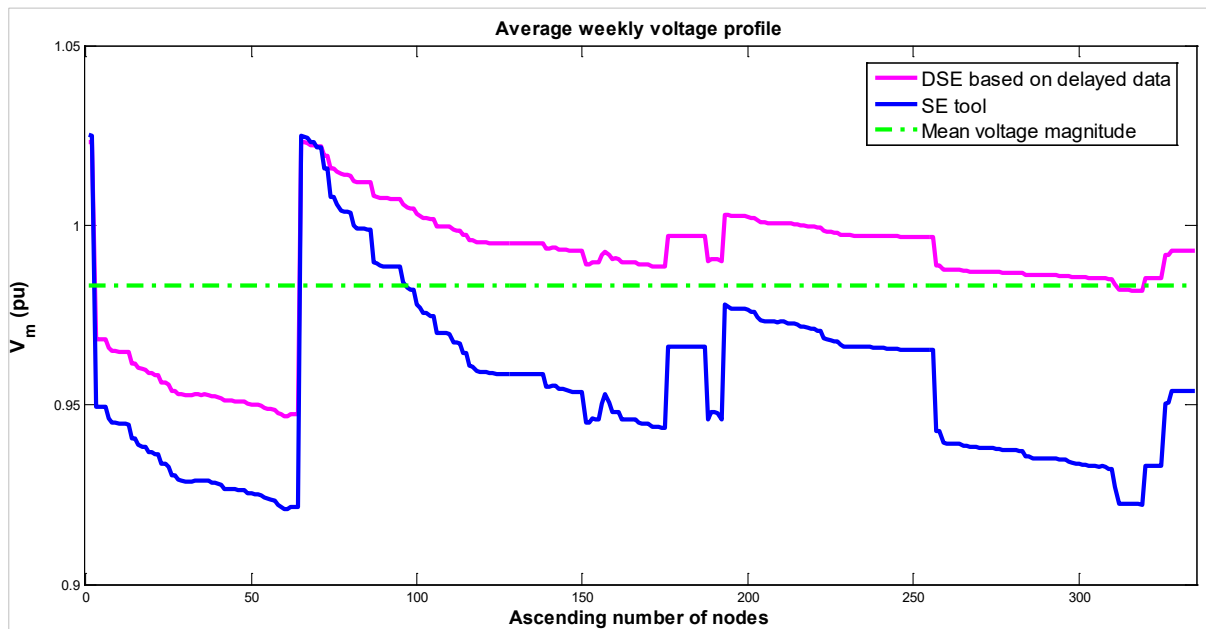


Figure 9: Average weekly profiles of voltage magnitudes obtained from SE tool and DSE based on delayed data

In view of convergence rate, the diagrams of the hourly fluctuation of the three related KPIs  $Mconv_{obj}$ ,  $Mconv_v$  and  $Mconv_s$  for all the days of simulations, are provided in Figures 10, 11 and 12, respectively.

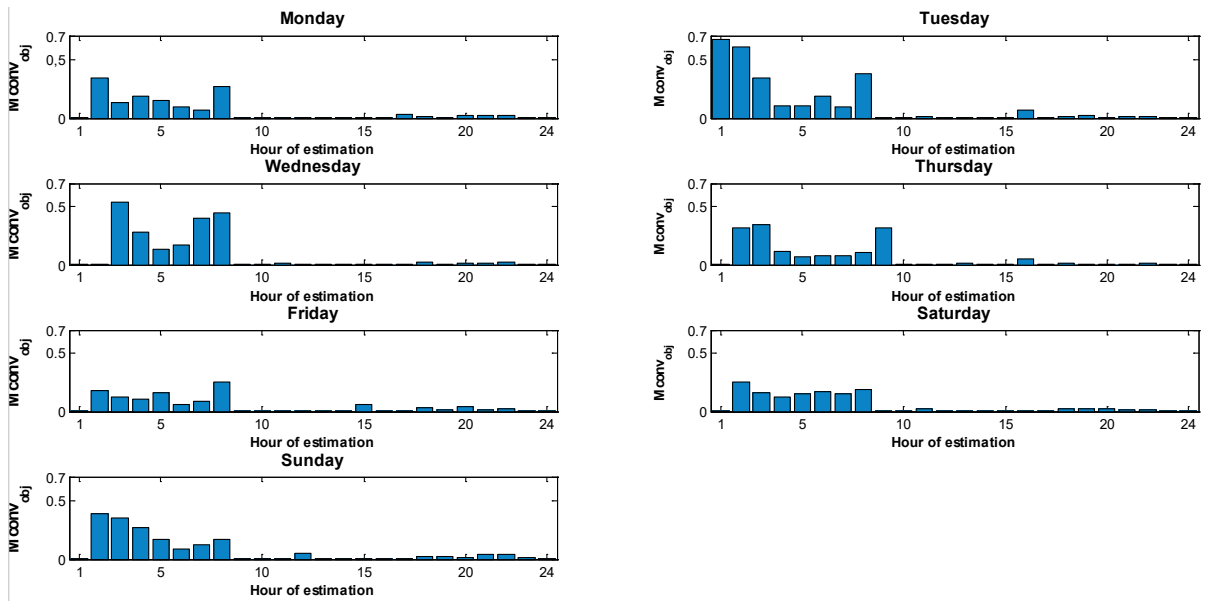


Figure 10: Hourly values of  $Mconv_{obj}$  for the whole week of estimation

As regards  $Mconv_{obj}$ , it is noteworthy that low values imply that the DSE algorithm approaches the optimal (minimum) value of  $J(\mathbf{x})$  with small steps. Conversely, high values of  $Mconv_{obj}$  are observed during small hours, which implies that the solution is approached rapidly, with a single, rather big step.

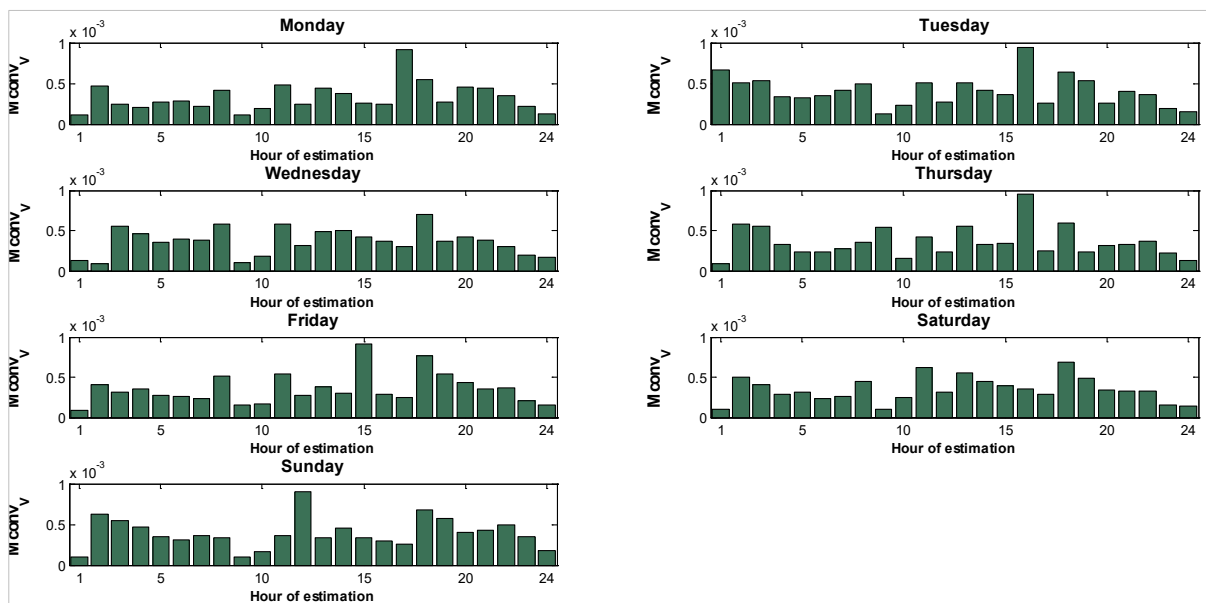
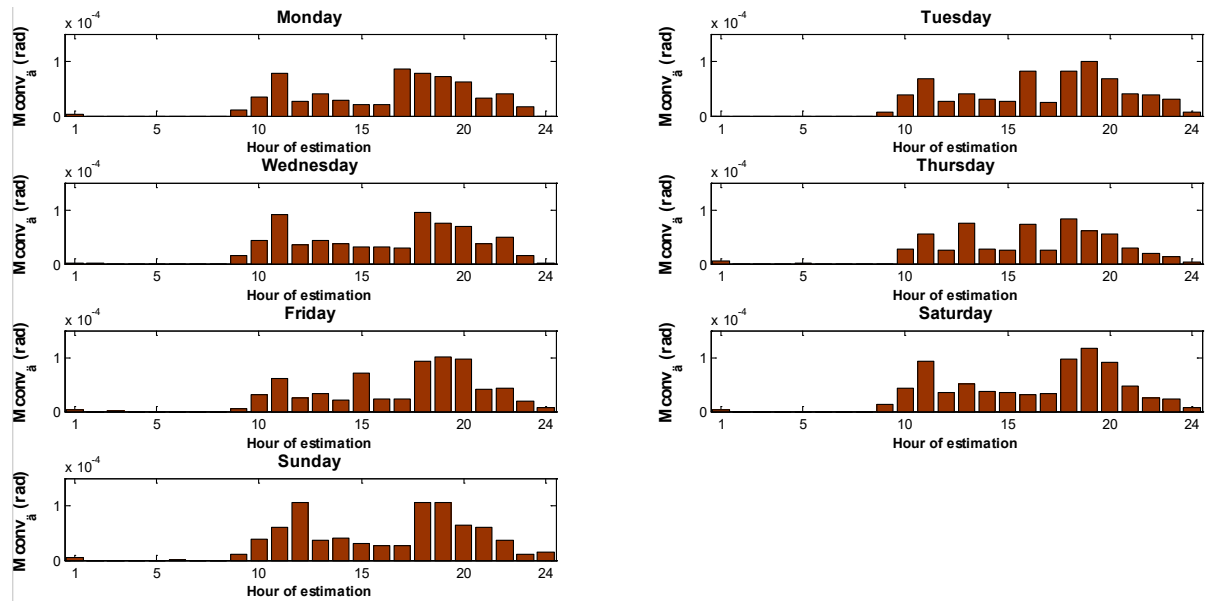


Figure 11: Hourly values  $Mconv_V$  of for the whole week of estimation



**Figure 12: Hourly values of  $M_{conv_a}$  for the whole week of estimation**

In [52], a prespecified threshold of  $2 \times 10^{-3}$  is set for the values of  $M_{conv_V}$  in order to determine acceptable SE solutions. The related results provided in Figure 11, indicate that the SE tool meets this level of quality. Finally, concerning the KPI  $M_{conv_\delta}$ , it is clear that high values occur for hourly intervals during daytime, that is, when the loading conditions of the network are increased. In general, though, the related values are kept low, a fact which means that the SE tool exhibits good convergence rate in terms of voltage phase angles.

In conclusion, the adverse effect of the low measurement redundancy on the error filtering capacity of the SE tool is confirmed. The limited amount of pre-existing data (actual and pseudo-measurements) provides marginal measurement redundancy, which is not sufficient in order to achieve high quality suppression of measurement errors. Besides, although they can provide several benefits to DSE, pseudo-measurements cannot compete with actual data in terms of measurement redundancy [11]. The comparison of the SE tool with the reference DSE based on delayed actual data, showed that the accuracy of the former is satisfactory only for specific areas of the test network.

The critical role of tuning measurement weights is also ascertained. The extensive use of pseudo-measurements, which are linked to low weights compared to actual SCADA or AMR data, exacerbates the problem of poor conditioned gain matrices, thus, augmenting the sensitivity of the state estimates to errors. However, the accomplishment of consistent algorithmic convergence shows that the relative levels of measurement weights are adjusted properly. In other words, the high values of maximum errors for pseudo-measurements lead to decreased accuracy of the SE tool, yet, the ratios of maximum errors between different measurement types, which determine the escalation from the most to the least accurate data, are tuned effectively in terms of convergence rate.

Overall, the performance of the SE tool given the pre-existing metering infrastructure, is low as regards accuracy and satisfactory as regards convergence rate. With a view to improving accuracy, the measurement redundancy should be boosted via the addition of actual, real-time measurements to the available dataset. To this end, the reinforcement of the metering infrastructure is necessary.

#### 4.4.1.2 Scenario 2

In addition to accuracy problems, the low level of measurement redundancy also jeopardizes the observability of the test network. Besides, redundancy quantifies how robust the observability state of the network is to measurement loss. The aforementioned issue is investigated in Scenario 2 by assuming that the network is not observable at a certain time interval due to missing or inconsistent measurement data. In particular, the study is focused on the contingency of temporary unavailability of the single measurement of voltage magnitude from the HV/MV substation. This scenario is of high

importance due to the criticality of the forenamed measurement, since its loss renders the Mesogeia pilot site non-observable. In general, the existence of at least one measured voltage magnitude in the available dataset is essential for the maintenance of observability [6].

A meticulous analysis of historical recordings from RTUs revealed that missing values frequent occurred. For a limited number of hourly intervals, there were no data of voltage magnitude delivered by RTUs. The issue got worse for data with 15-min resolution; instead of 4 measured values per hour, in many cases only 3 or 2 measurements were obtained. In addition, inconsistency issues were also identified. For example, it was observed that, for quite a few hourly intervals, the time stamp of the measurement was appreciably far from the exact time to which it referred. Latencies up to 20 minutes with reference to the expected time were discovered. Figure 13 depicts two representative examples for the aforementioned problems considering hourly time intervals. Altogether, addressing the issue of missing or inconsistent data regarding critical measurements is crucial for solving the DSE problem.

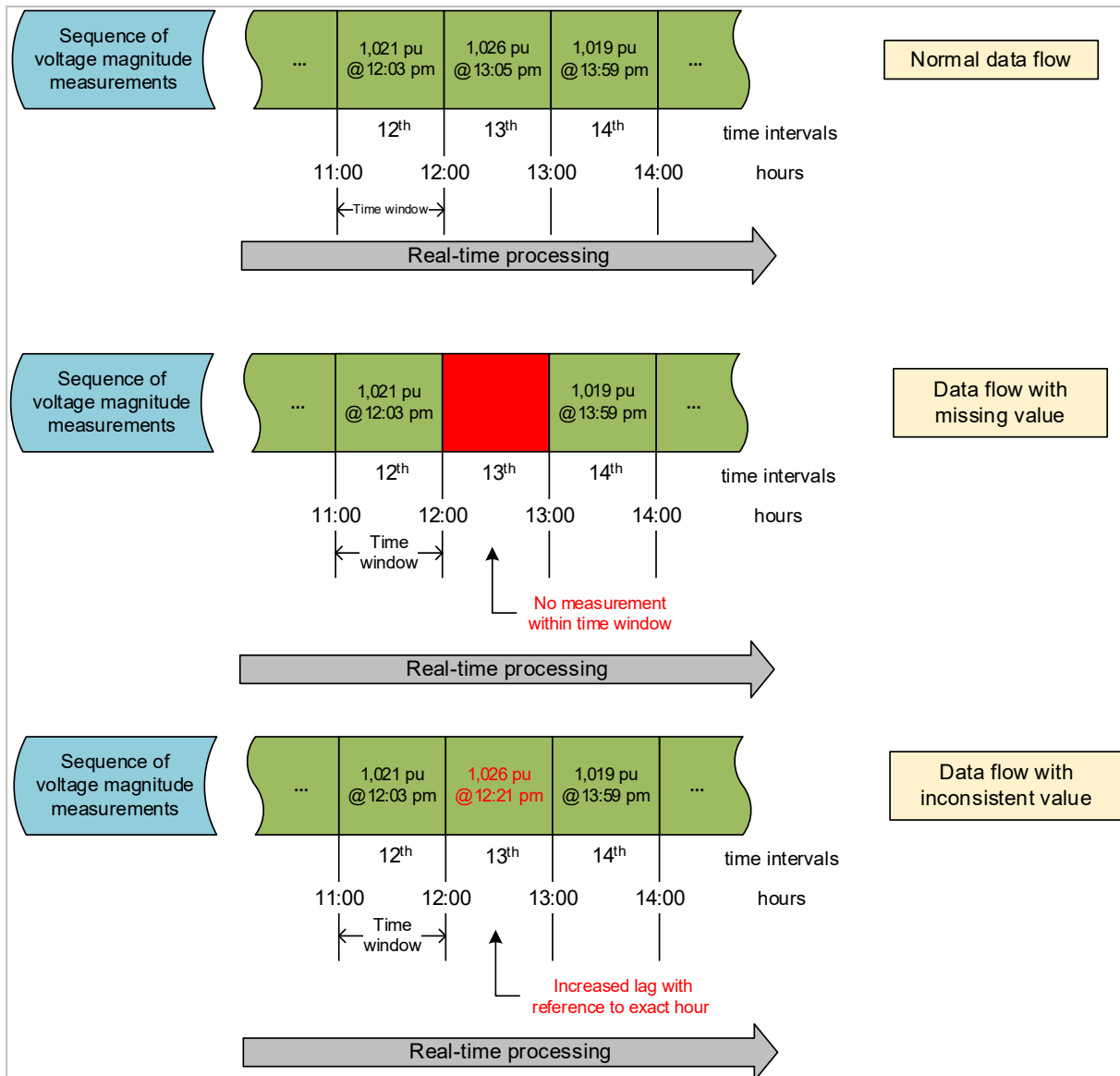


**Figure 13: Illustrative examples of data flows with missing and inconsistent values**

The easiest solution in case of missing voltage magnitude, is to use the measured value at the HV side of the HV/MV transformer combined with the corresponding tap position of the HV winding. In this way, the voltage magnitude at the MV side is easily computed by dividing the HV value by the voltage ratio at this tap placement. This simple technique provides a derivative piece of data that can substitute for the actual measurement which is not available. Apparently, a negative impact on the accuracy of the SE tool is highly possible, since the related measurement weight needs to be lowered. In addition to the

reduction in accuracy, the forenamed technique does not boost the measurement redundancy, thus, the risk for loss of observability persists. Taking into consideration the trade-off between its convenience and the related drawbacks, it is considered as a backup plan in case of urgent need for data. It is worth noting that co-operation with the TSO may be required, considering that the HV/MV substations make up the boundaries between transmission and distribution grids.

Undoubtedly, the most reliable solution is the addition of new measurements of voltage magnitude to the pre-existing dataset. In this way, the redundancy will be augmented, while the accuracy of the state estimated will improve as the number of new voltage magnitudes increase. This data can become available by upgrading the AMR equipment installed at MV consumers or PV units. The total number of these nodes is 12, thus, some of them can be selected for the upgrade based on their accessibility. The availability of these additional data render the measurement of voltage magnitude at HV/MV substation non-critical and the observability state of the test network is reinforced. Evidently, this solution is costly bearing in mind that this data, similar to SCADA measurements, is required to be available in real time.

In Table 5, the effect of the aforementioned solutions to the accuracy of the SE tool is investigated via the presentation of the worst case coordinate error variances per individual case study. The covariance matrix  $\text{cov}_x(\mathbf{x})$  was recalculated based on the pre-existing set of measurements excluding the actual measurement of voltage magnitude at the slack bus, which is replaced by:

- a derivative value for voltage magnitude based on measured voltage at the HV side and the tap position (Case study 1),
- 3 voltage magnitudes from nodes of PV units (Case study 2),
- 6 voltage magnitudes from nodes of MV consumers and PV units (Case study 3), and
- 9 voltage magnitudes from nodes of MV consumers and PV units (Case study 4).

Since no actual voltage data was available, the covariance matrix  $\text{cov}_x(\mathbf{x})$  was evaluated at hourly, estimated states  $\hat{\mathbf{x}}$  obtained from the SE tool for the whole day of Sunday in Scenario 1. Hence, Table 6 presents the maximum value of worst case coordinate error variance per case study. All the aforementioned measurements were associated with an error of 2%.

**Table 5: Worst case coordinate error variance of SE tool for Case studies 1–4**

Case study	Worst case coordinate error variance $\Psi_M$ ( $10^{-7}$ )
1	4.926
2	3.128
3	1.906
4	1.127

As observed, the accuracy of the SE tool deteriorates considerably in Case study 1, since the original value using the actual measurement of voltage magnitude provided in Table 4, is  $2.506 \times 10^{-7}$ . Hence, the related solution ensures the observability of the grid, yet, it is not reliable in terms of precision. Contrarily, the addition of new voltage magnitudes to the pre-existing set of measurements, is a more advantageous choice; the values of  $\Psi_M$  are lower in Cases studies 2–4 compared to Case study 1. Additionally, in Cases 3 and 4, the attained values are better than the original value in Table 4, whereas this does not hold true for Case study 2. Evidently, the 3 new voltage magnitudes from PV units cannot outperform the single voltage magnitude from the slack bus due to their higher maximum error – 2% instead of 0,2% – and their locations (nodes) which are at the downstream part of feeder 210.

#### 4.4.2 Results for UC-GR-02

Primarily, the placement of PMUs is required to be decided. The low cost PMU originally presented in [54], is deemed the reference device for the determination of the configuration of installed PMUs. All nodes which pertain to MV consumers and PV units are excluded from the placement, since they are already equipped with AMR devices. Taking into account the schemes of placed PMUs in [37] and [47], the eligible nodes pertain to load buses which have at least two adjacent branches, that is, they are not terminal end points of the MV feeders. No zero injection bus is considered for installation.

As regards the number of PMUs, in [55] it is stated that one fourth to one third of the grid nodes need to be equipped with PMUs in order to attain observability – assuming, of course, no pre-existing measurements. This rule provides a value to start from; it is under 100 PMUs on average for the Mesogeia pilot site. Given that the observability is ensured prior to PMU installation, the number to be considered for purposes of UC-GR-02 is much smaller. Considering the trade-off between the desired gain in measurement redundancy and accuracy, and the technical complications related to the development of an extended PMU system, a total number of 20 PMUs is assumed to be placed.

In Table 6, the assumed configuration of PMUs is presented. As observed, the distribution of PMUs between the two feeders is proportional to the ratio of their nodes ( $63/271 \approx 1/4$ ). Each PMU can process up to 8 channels [54] with one phase of a voltage or current red per individual channel. Thus, a pair of voltage and current phasors is recorded by the PMUs installed at the feeders. On the contrary, the PMU at the HV/MV substation is assumed to record the two phasors of the current flows through the top of the feeders 210 kai 490, respectively. Besides, the voltage magnitude of the slack bus is a pre-existing SCADA measurement.

**Table 6: Configuration of installed PMUs**

Network part	No. of PMUs	Measured node and corresponding branches
Feeder 210	5	125 {125–130}, 141 {141–154}, 223 {223–227}, 279 {279–283}, 302 {302–306}
Feeder 490	14	605 {605–609}, 734 {734–739}, 761 {761–765}, 1037 {1037–1041}, 1103 {1103–1107}, 1289 {1289–1293}, 1304 {1304–1990}, 2028 {2028–2032}, 2889 {2889–2893}, 2928 {2928–2932}, 3015 {3015–3019}, 3155 {3155–3159}, 3209 {3209–3213}, 3506 {3506–3510}
HV/MV substation	1	1 {1–2}, {1–583}

The procedure adopted to evaluate the accuracy of the SE tool is discussed in subchapter 4.3.2. Concisely, for each time step of 15 minutes, the power flow algorithm is executed in order to determine the true state of the test network as well as the true values of the measured quantities. All related measurements (conventional and PMU), which comprise the dataset to be introduced into the SE tool, are obtained by perturbing the true values with errors following the Gaussian distribution, according to formula (20). Hence, realistic measurement sets are created for a whole day.

In Table 7, the worst values of the accuracy KPIs  $RMSE$ ,  $Macc_V$  and  $\Psi_M$  that occurred at the operation of the SE tool in 15-min time intervals, are provided. As noticed, all values are considerably lower than the ones achieved in Scenario 1 of UC-GR-01. For example, the value of  $\Psi_M$  is 10 times smaller than the minimum value that the SE tool achieved in Table 4 (column 2). Also, the reduction in  $Macc_V$  is significant; the worst value is 0.0261, while the corresponding value in Scenario 1 of UC-GR-01, as showed in Figure 8, is above unity. Such a finding is anticipated, since PMUs provide measurements of voltage phase angles.

**Table 7: Worst values of accuracy KPIs for estimation in 15-min time intervals**

SE tool with integrated PMU data	Maximum value of $RMSE$	Maximum value of $Mac_{c_V}$	Worst case coordinate error variance $\Psi_M (10^{-7})$
Estimation for a day, in 15-min time intervals	0.0251	0.0261	0.2068

In Figures 14 and 15, the fluctuation of the values of  $RMSE$  and  $Mac_{c_V}$  per quarter of hour, is displayed. As observed, the values are very low with reference to the thresholds determined in D4.1 [2], indicating appreciable improvement in terms of accuracy of estimated voltages. The values increase during daytime due to non-zero PV generation, as explained in subchapter 4.4.1. It is reminded that no PMUs are assumed to be installed at PV sites, thus, higher estimation errors occur for their voltages.

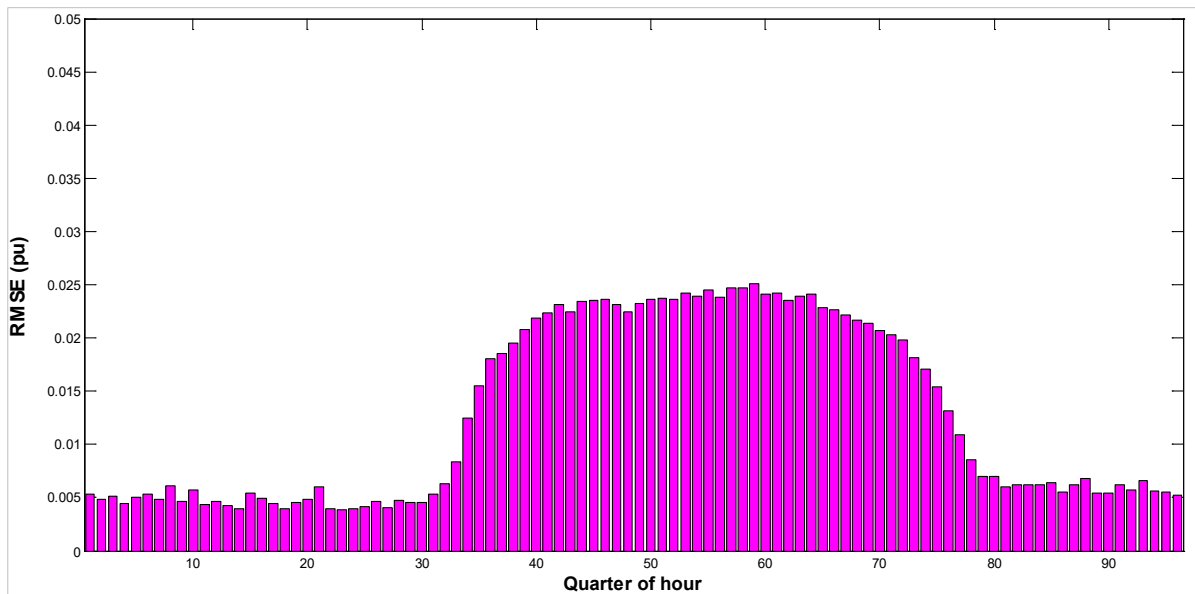


**Figure 14: Values of  $RMSE$  for the day of estimation**

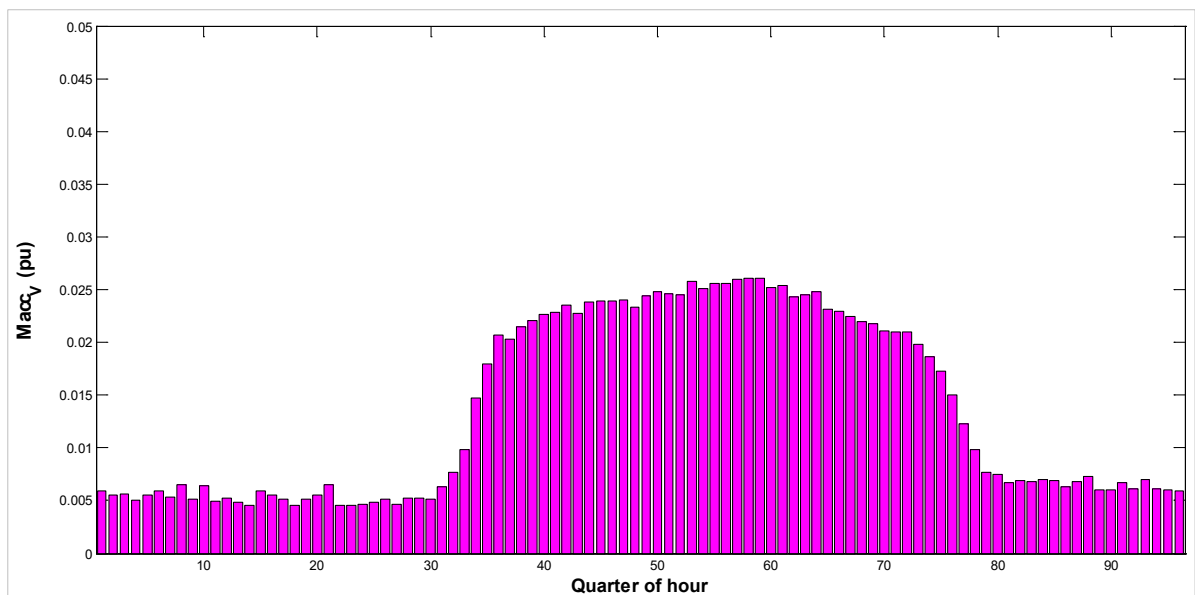


**Figure 15: Values of  $Mac_{c_V}$  for the day of estimation**

The major effect of integration of PMU data into the SE tool is better understood via Figure 16, which illustrates the fluctuation of *RPEs* per node is, using internal (contiguous) node numbering similarly to Figure 6 of UC-GR-01. All errors are below 1% and, overall, significantly improve compared to the ones displayed in Figure 6. Hence, the selection of loads buses for installation of PMUs is proven to be effective in order to reduce errors substantially. It is noteworthy that the relatively higher values, which are approximately 10 times less than the ones in Figure 6, correspond to nodes of PV units.

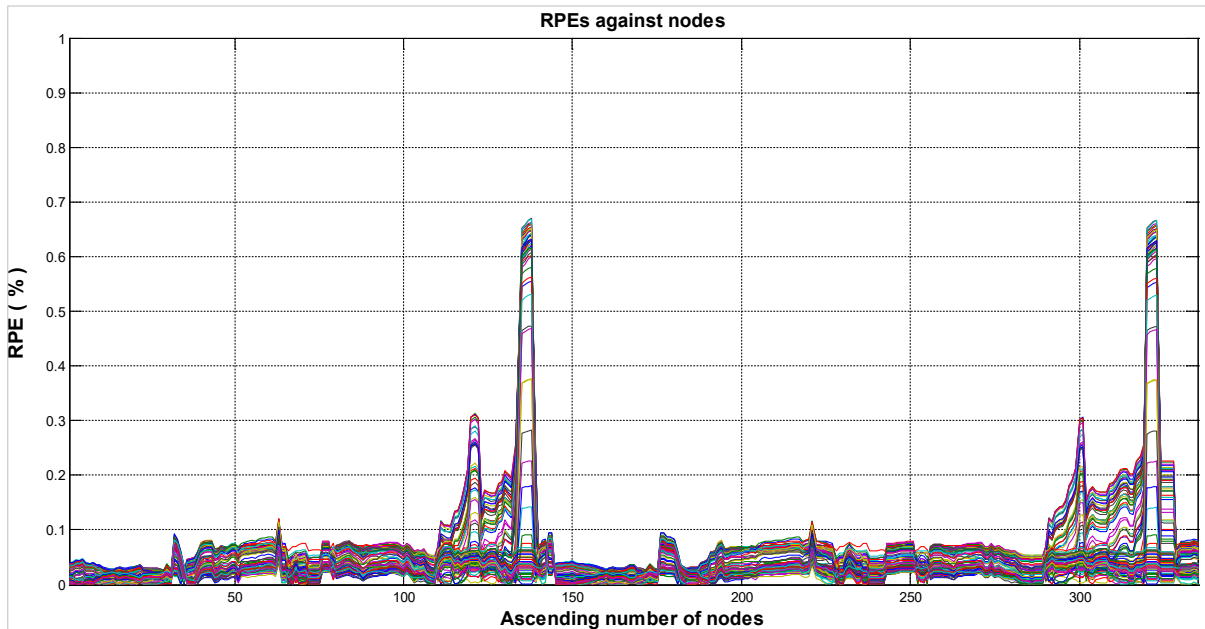


Figure 16 : Distribution of *RPEs* per node for estimation in 15-min time intervals

In respect to convergence rate, the addition of PMU data minimizes the values of the related KPIs  $Mconv_{obj}$ ,  $Mconv_V$  and  $Mconv_\delta$ , as viewed in Figures 17, 18 and 19, respectively. All the values are much smaller than ones for UC-GR-01. Apparently, the prespecified quality threshold of  $2 \times 10^{-3}$  for  $Mconv_V$  and  $Mconv_\delta$  is satisfied.

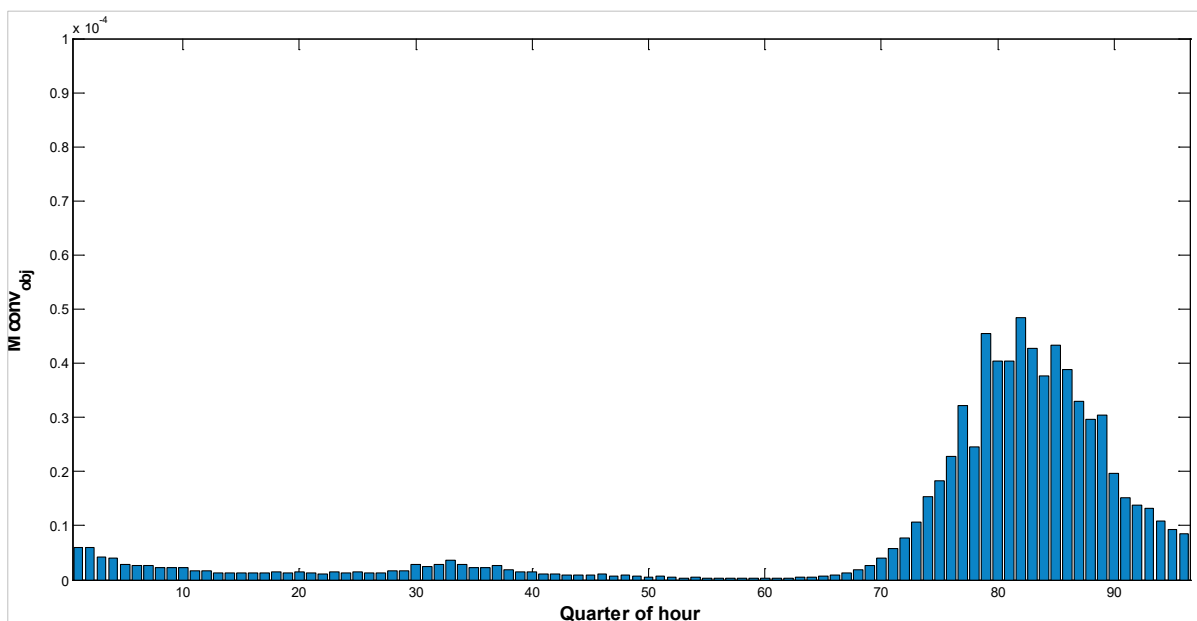


Figure 17: Values of  $Mconv_{obj}$  for the day of estimation

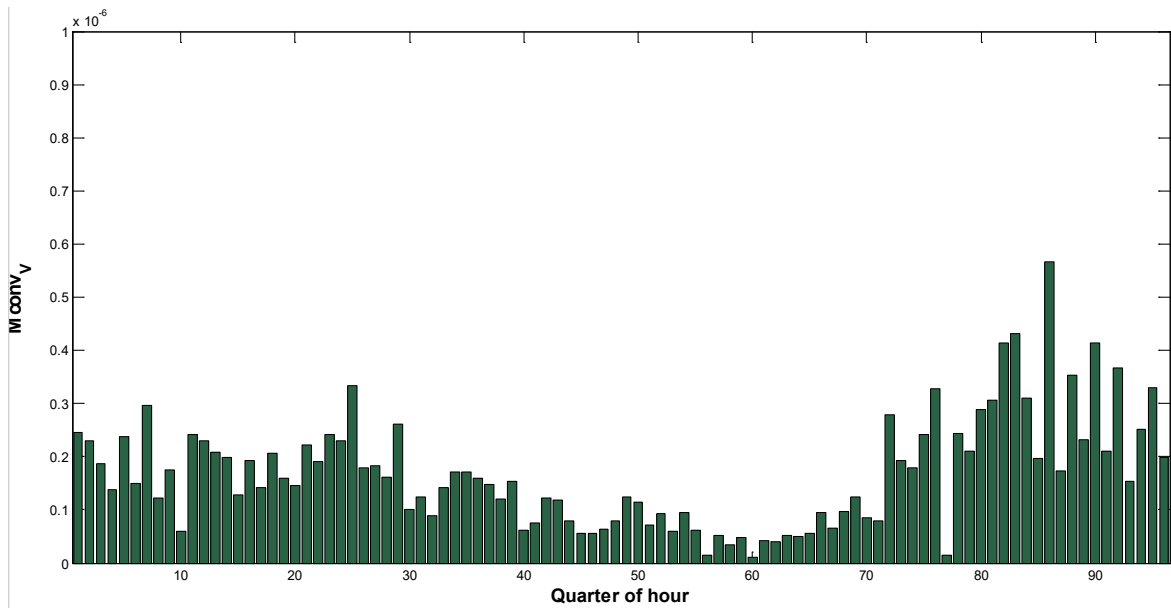


Figure 18: Values of  $M_{conv_v}$  for the day of estimation

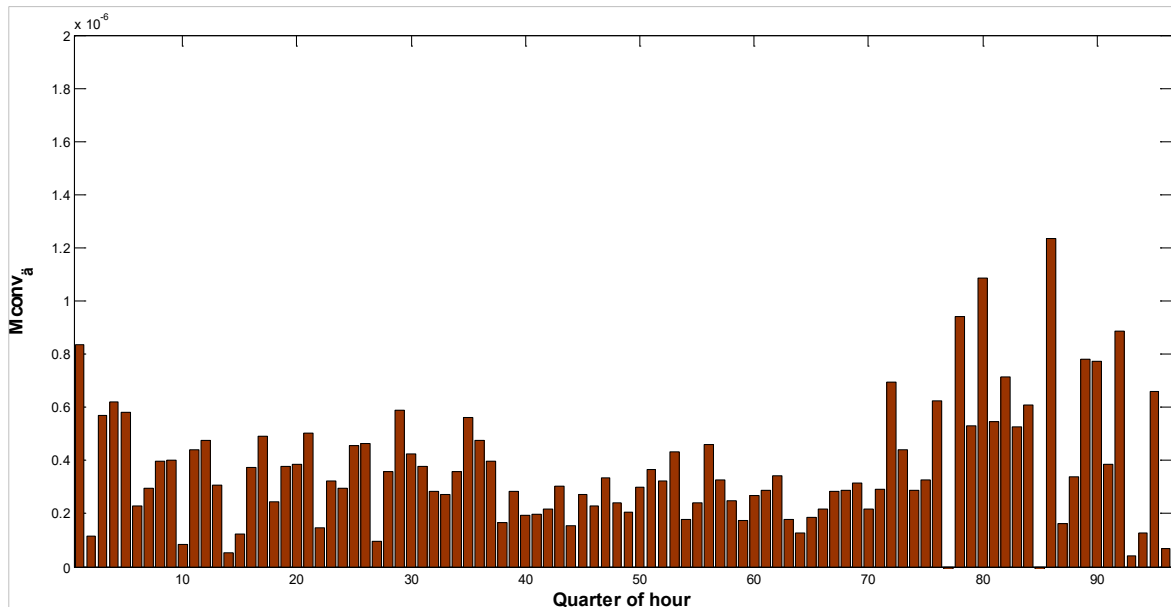


Figure 19: Values of  $M_{conv_a}$  for the day of estimation

As expected, the addition of PMU data into the pre-existing set of measurements helps the SE tool to achieve high quality performance with increased convergence speed and to deliver precise state estimates for the Mesogeia pilot site. In particular, the increased measurement redundancy reinforces the error filtering capacity of the SE tool, thus, highly accurate state estimates are provided. Moreover, the integration of precise PMU data, which are linked to large weights, into the pre-existing dataset, is smooth in terms of convergence. The solution algorithm converges with excellent rates, a finding which means that measurement weights are tuned effectively. Overall, taking into account that the assumed number of installed PMUs is reasonable, the outcomes are remarkable and demonstrate that the deployment of PMUs, even in small numbers, is an effective solution for the development of quality DSE.

---

## 5 Conclusion

The current report presents the design and development of the SE tool, which comprises one of the main components of the Greek demo for real-time monitoring and control. The study of the international literature regarding DSE promoted the use of the WLS-based model because it constitutes the most appropriate method for the formulation of the problem, co-operates effectively with LE/LF methods for the provision of pseudo-measurements and processes mixed measurement sets of conventional and PMU data. These characteristics are of vital importance for the pilot site of the Greek demo, Mesogeia. Its existing metering infrastructure furnishes a limited number of actual measurements, thus, rendering the use of a large number of pseudo-measurements necessary for purposes of observability. The potential upgrade of the infrastructure via installation of PMUs will boost the set of available measurements, yet, proper modifications of the WLS based SE tool are required for their fertile integration. These two major issues were investigated through Use Cases UC-GR-01 and UC-GR-02.

The main conclusion that can be drawn from UC-GR-01 is that the developed SE tool can ensure the observability of the test network of Mesogeia pilot site and converge without problems to the optimal network state given the pre-existing set of measurements, a fact which confirms that measurement weights were tuned properly. Yet, the obtained results demonstrate the strong effect of the minimal actual, real-time measurements and the subsequent extensive use of pseudo-measurements on the accuracy of the SE tool; related KPIs showed that its accuracy is low compared to a reference DSE algorithm based on delayed (i.e. not available in real time), actual data. Furthermore, the impact of missing or inconsistent data on the reliable operation of the SE tool, was examined by focusing on the single measurement of voltage magnitude, which is critical for observability achievement. The related analysis led to the conclusion that the addition of new measurement of voltage magnitudes to the pre-existing dataset is a prerequisite for the reinforcement of grid observability and improved accuracy of the SE tool. The findings of UC-GR-01 can be used as a useful feedback for HEDNO in order to identify the issues raised during the implementation of a real-world DSE procedure.

What became evident after the completion of UC-GR-02 is that the integration of PMU data into the SE tool is advantageous in terms of accuracy and convergence speed. Given the lack of actual measurements from PMUs, the simulations were based on a well-established practice which deploys the power flow algorithm for the construction of realistic measurement sets. Importantly, the related results for the KPIs provide evidence for drastic reduction of errors in state estimates and enhanced convergence rate. Hence, it is safe to claim that the proposed methodology for fusing PMU data with conventional measurements is effective and that the tuning of measurement weights was also performed correctly. Furthermore, other crucial aspects that were addressed, such as the selection of locations for placement of PMUs and the phasors to be measured per individual PMU, provide a basis for the determination of the configuration of PMUs by HEDNO, when they become available for installation within Platone framework.

Overall, the developed SE tool is capable of ensuring the observability of the Mesogeia pilot site, exhibits high convergence speed and, with the advent of PMUs, is expected to deliver highly accurate state estimates. Hence, it can be used by the DSOTP of HEDNO for real-time monitoring of the Mesogeia pilot site and for the support of advanced algorithms aiming at the effective use of DER and flexible loads, as envisaged within the Platone framework. Importantly, the optimized performance of the SE tool should be one of the criteria considered for the installation of PMUs. HEDNO in collaboration with NTUA will streamline its operation before and during Mesogeia demonstration. The experience and related results from the operation of the SE tool in real-time conditions, with installed PMUs will be documented in D4.5, "Mesogeia demonstration report".

---

## 6 List of Tables

Table 1: Description of nodes (type and number) of the test network. .... 27

Table 2: Type, number and source of available pre-existing measurements ..... 28

Table 3: Maximum errors considered for tuning of measurement weights. .... 32

Table 4: Daily values of worst case coordinate error variance of SE tool compared to DSE based on delayed data ..... 34

Table 5: Worst case coordinate error variance of SE tool for Case studies 1–4 ..... 40

Table 6: Configuration of installed PMUs ..... 41

Table 7: Worst values of accuracy KPIs for estimation in 15-min time intervals..... 42

Table 8 Nominal apparent power at load and generation nodes of feeder R490 ..... 52

Table 9 Zero injection nodes of feeder R490 ..... 53

Table 10 Nominal apparent power at load and generation nodes of feeder R210 ..... 53

Table 11 Zero injection nodes of feeder R210 ..... 54

Table 12 Types and electric parameters of overhead and underground cables ..... 57

Table 13 Line data for feeder R490..... 58

Table 14 Line data for feeder R210..... 60

## 7 List of Figures

Figure 1: Time frames of components in energy management systems [24].	15
Figure 2: Typical structure of a state estimator.	16
Figure 3: Structure of the SE tool.	21
Figure 4: Simulation framework for UC-GR-01	30
Figure 5: Simulation framework for UC-GR-02	33
Figure 6: Weekly distribution of hourly $RPEs$ per node.	34
Figure 7: Hourly values of $RMSE$ for the whole week of estimation.	35
Figure 8: Hourly values of $M_{accr}$ for the whole week of estimation	36
Figure 9: Average weekly profiles of voltage magnitudes obtained from SE tool and DSE based on delayed data	36
Figure 10: Hourly values of $M_{conv_{obj}}$ for the whole week of estimation.	37
Figure 11: Hourly values $M_{convr}$ of for the whole week of estimation.	37
Figure 12: Hourly values of $M_{conv_{\delta}}$ for the whole week of estimation	38
Figure 13: Illustrative examples of data flows with missing and inconsistent values	39
Figure 14: Values of $RMSE$ for the day of estimation.	42
Figure 15: Values of $M_{accr}$ for the day of estimation	42
Figure 16 : Distribution of $RPEs$ per node for estimation in 15-min time intervals.	43
Figure 17: Values of $M_{conv_{obj}}$ for the day of estimation.	43
Figure 18: Values of $M_{convr}$ for the day of estimation	44
Figure 19: Values of $M_{conv_{\delta}}$ for the day of estimation	44
Figure 20: Configuration of Nea Makri substation	52
Figure 21: $\pi$ -model of a power distribution line.	71

## 8 List of References

- [1] European Commission, “2050 long-term strategy”. [Online]. Available: [https://ec.europa.eu/clima/policies/strategies/2050\\_en](https://ec.europa.eu/clima/policies/strategies/2050_en)
- [2] Platone, “Deliverable 4.1: Report on the definitions of KPIs and UCs,” Work Package 4, 2020.
- [3] Platone, “Deliverable 1.2: Project KPIs definition and measurement methods,” Work Package 1, 2020.
- [4] “Platone Use Case development on smart-grid-use-cases Github Repository,” [Online]. Available: <https://github.com/smart-grid-use-cases/github-pages/tree/master/content/en/docs/Platone>.
- [5] A. Monticelli, *State estimation in Electric Power Systems: A Generalized Approach*. Boston, MA: Kluwer Academic Publishers, 1999
- [6] A. Abur and A. Gomez Exposito, *Power System State Estimation: Theory and Implementation*. New York, NY: Marcel Dekker, 2004.
- [7] F. C. Schweppe, J. Wildes, and D. B. Rom, “Power system static state estimation – Part I, II, III,” *IEEE Trans. Power App. Syst.*, vol. PAS-89, no. 1, pp. 120–135, Jan. 1970.
- [8] A. Primadianto and C.-N. Lu, “A review on distribution system state estimation,” *IEEE Trans. Power Syst.*, vol. 32, no. 5, pp. 3875–3883, Sep. 2017.
- [9] K. Dehghanpour, Z. Wang, J. Wang, Y. Yuan and F. Bu, “A survey on state estimation techniques and challenges in smart distribution systems,” *IEEE Trans. Smart Grid*, vol. 10, no. 2, pp. 2312–2322, Mar. 2019.
- [10] H. Farhangi, “The path of the smart grid,” *IEEE Power Energy Mag.*, vol. 8, no. 1, pp. 18–28, Jan./Feb. 2010.
- [11] M. Razanousky and K. Morrissey, “Fundamental research challenges for DSE to enable high-performing grids,” NYSERDA: Albany, NY, USA, Rep. No. 18–37, May 2018.
- [12] N. Hatzigiorgiou, J. Amantegui, B. Andersen, M. Armstrong, P. Boss, B. Dalle, G. de Montravel, A. Negri, C. A. Nucci, and P. Southwell, CIGRE WG “Network of the Future” Electricity Supply Systems of the Future,” *Electra*, vol. 256, pp. 42–49, Jun. 2011.
- [13] G. Mauri, F. Pilo, J. Taylor, G. Bruno, E. Kampf, F. Silvestro, C. Pecas Lopez, B. Bak-Jensen, J. R. Pillai, and H. Sprongl, “Control and automation systems for electricity distribution networks (edn) of the future,” CIGRE/CIGRE joint working group: Paris, France, Rep. No. C6/B5.25/CIGRE, Dec. 2017.
- [14] F. Ahmad, A. Rasool, E. Ozsoy, S. Rajasekar, A. Sabanovic, and M. Elitas, “Distribution system state estimation-A step towards smart grid,” *Renewable Sustain. Energy Rev.*, vol. 81, pp. 2659–2671, Jan. 2018.
- [15] N. Uribe-Pérez, L. Hernández, D. de la Vega, and I. Angulo, “State of the art and trends review of smart metering in electricity grids,” *Appl. Sci.*, vol. 6, no. 3, pp. 68–92, Feb. 2016.
- [16] L. Mili, A. Abur, S. Nuthalapati, C. Evrenosoglu, et al., “State estimation concepts and terminology,” Power systems operations committee, State estimation algorithms working group IEEE PES Society.: Piscataway, NJ, Rep. No. PES TR-20, May 2016.
- [17] A. Gómez-Expósito, C. Gómez-Quiles and I. Džafić, “State estimation in two time scales for smart distribution systems,” *IEEE Trans. Smart Grid*, vol. 6, no. 1, pp. 421–430, Jan. 2015.
- [18] K. Samarakoon, J. Wu, J. Ekanayake and N. Jenkins, “Use of delayed smart meter measurement for distribution state estimation,” *IEEE PES General Meeting*, Detroit, MI, USA, 2011, pp. 1–6.
- [19] T. Xygkis, G. Karlis, I. Siderakis, and G. Korres, “Use of near real-time and delayed smart meter data for distribution system load and state estimation,” *9<sup>th</sup> Mediterranean Conf. Power Gener. Transm. Distrib. Energy Convers. (MedPower)*, Athens, Greece, 2014, pp. 1–6.

- 
- [20] Y.-F. Huang, S. Werner, J. Huang, N. Kashyap, and V. Gupta, "State estimation in electric power grids: Meeting new challenges presented by the requirements of the future grid", *IEEE Signal Process. Mag.*, vol. 29, no. 5, pp. 33–43, Sep. 2012.
- [21] J. Ekanayake, K. Liyanage, J. Wu, A. Yokoyama, and N. Jenkins, *Smart Grid: Technology and Applications*. New York, NY: John Wiley and Sons, 2012.
- [22] A. Gomez-Exposito, A. Abur, A. V. Jaen, and C. Gomez-Quiles, "A multilevel state estimation paradigm for smart grids," *Proc. IEEE*, vol. 99, no. 6, pp. 952–976, Jun. 2011.
- [23] A. Del Rosso, T. Borst, R. Jamielson, et al., "Advanced utility data management and analytics for improved operation situational awareness for EPU operations," CIGRE joint working group: Paris, France, Rep. No. D2/C2.41, Jun. 2018.
- [24] M. S. Thomas and J. D. McDonald, *Power System SCADA and Smart Grids*. Boca Raton, FL: CRC Press, 2015.
- [25] D. L. Lubkeman, J. Zhang, A. K. Ghosh, and R. H. Jones, "Field results for a distribution circuit state estimator implementation," *IEEE Trans. Power Del.*, vol. 15, no. 1, pp. 399–406, Jan. 2000.
- [26] V. Thornley, N. Jenkins, and S. White, "State estimation applied to active distribution networks with minimal measurements," *15th Power Syst. Comp. Conf. (PSCC)*, Liege, Belgium, 2005, pp. 1–7.
- [27] M. Pau, P. A. Pegoraro, and S. Sulis, "Performance of three-phase WLS distribution system state estimation approaches," *IEEE Int. Workshop Appl. Meas. Power Syst.*, Aachen, Germany, 2015, pp. 138–143.
- [28] Y. Deng, Y. He, and B. Zhang, "A branch estimation-based state estimation method for radial distribution systems," *IEEE Trans. Power Del.*, vol. 17, no. 4, pp. 1057–1062, Oct. 2002.
- [29] H. Wang and N. N. Schulz, "A revised branch current based distribution system state estimation algorithm and meter placement impact," *IEEE Trans. Power Syst.*, vol. 19, no. 1, pp. 207–213, Feb. 2004.
- [30] J. Wu, Y. He, and N. Jenkins, "A robust state estimator for medium voltage distribution networks," *IEEE Trans. Power Syst.*, vol. 28, no. 2, pp. 1008–1016, May 2012.
- [31] A. Al-Wakeel, J. Wu, and N. Jenkins, "State estimation of medium voltage distribution networks using smart meter measurements," *Appl. Energy*, vol. 184, pp. 207–218, Dec. 2016.
- [32] I. Roytelman and S. M. Shahidepour, "State estimation for electric power distribution systems in quasi real time conditions," *IEEE Trans. Power Del.*, vol. 8, no. 4, pp. 2009–2015, Oct. 1993.
- [33] A. K. Ghosh, D. L. Lubkeman, M. J. Downey, and R. H. Jones, "Distribution circuit state estimation using probabilistic approach," *IEEE Trans. Power Syst.*, vol. 12, no. 1, pp. 45–51, Feb. 1997.
- [34] Y. Hu, A. Kuh, T. Yang, and A. Kavcic, "A belief propagation based power distribution system state estimator," *IEEE Comput. Intell. Mag.*, vol. 6, no. 3, pp. 36–46, Aug. 2011.
- [35] P. A. Pegoraro et al., "Bayesian approach for distribution system state estimation with non-Gaussian uncertainty models," *IEEE Trans. Instrum. Meas.*, vol. 66, no. 11, pp. 2957–2966, Nov. 2017,
- [36] J. Zhang, G. Welch, and G. Bishop, "Lodim: A novel power system state estimation method with dynamic measurement selection," *IEEE Power & Energy Soc. General Meeting*, Detroit, MI, 2011, pp. 1–7.
- [37] S. Sarri, M. Paolone, R. Cherkaoui, A. Borghetti, F. Napolitano, and C. A. Nucci, "State estimation of active distribution networks: comparison between WLS and iterated Kalman-filter algorithm integrating PMUs," *3rd IEEE PES Innovative Smart Grid Technol. Eur.*, Berlin, Germany, 2012, pp. 1–8.
- [38] M. Brown Do Coutto Filho and J. C. S. de Souza, "Forecasting-aided state estimation-Part I: Panorama," *IEEE Trans. Power Syst.*, vol. 24, no. 4, pp. 1667–1677, Nov. 2009.

- 
- [39] R. Singh, B. C. Pal, and R. A. Jabr, "Choice of estimator for distribution system state estimation," *IET Gener., Transm. Distrib.*, vol. 3, no. 7, pp. 666–678, Jul. 2009.
- [40] A. Ghosh, D. Lubkeman, M. Downey and R. Jones, "Load modeling for distribution circuit state estimation," *IEEE Trans. Power Del.*, vol. 12, no. 2, pp. 999–1005, Apr. 1997.
- [41] H. Wang, and N. N. Schulz, "A load modeling algorithm for distribution system state estimation," *2001 IEEE PES Transm. Distrib. Conf. Expo.*, Atlanta, GE, USA, 2001, pp. 102–106.
- [42] C. Carmona-Delgado, E. Romero-Ramos, and J. Riquelme-Santos, "Fast and reliable distribution load and state estimator," *Electr. Power Syst. Res.*, vol. 101, pp. 110–124, Aug. 2013.
- [43] M. Z. Degefa, R. J. Millar, M. Koivisto, M. Humayun and M. Lehtonen, "Load flow analysis framework for active distribution networks based on smart meter reading system," *Eng.*, vol. 5, pp. 1–8, Oct. 2013.
- [44] R. F. Nuqui and A. G. Phadke, "Hybrid Linear State Estimation Utilizing Synchronized Phasor Measurements," *2007 IEEE Lausanne Power Tech*, Lausanne, 2007, pp. 1665–1669.
- [45] S. Chakrabarti, E. Kyriakides, G. Valverde and V. Terzija, "State estimation including synchronized measurements," *2009 IEEE Bucharest PowerTech*, Bucharest, 2009, pp. 1–5.
- [46] G. N. Korres and N. M. Manousakis, "A state estimator including conventional and synchronized phasor measurements," *Comput. Electr. Eng.*, vol. 38, no. 2, pp. 294–305, Mar. 2012.
- [47] J. Liu, J. Tang, F. Ponci, A. Monti, C. Muscas, and P. A. Pegoraro, "Trade-offs in PMU deployment for state estimation in active distribution grids," *IEEE Trans. Smart Grid*, vol. 3, no. 2, pp. 915–924, Jun. 2012.
- [48] M. G. Damavandi, V. Krishnamurthy, and J. R. Martí "Robust meter placement for state estimation in active distribution systems," *IEEE Trans. Smart Grid*, vol. 6, no. 4, pp.1972–1982, Feb. 2015.
- [49] R. D. Zimmerman, C. E. Murillo-Sanchez, and R. J. Thomas, "MATPOWER: Steady-state operations, planning and analysis tools for power systems research and education," *IEEE Trans. Power Syst.*, vol. 26, no. 1, pp. 12–19, Feb. 2011.
- [50] PTI Load Flow Data Format. [Online]. Available: <https://www.ee.washington.edu/research/pstca/formats/pti.txt>
- [51] M. Yucra, F. Schmidt, and M. C. de Almeida, "A comparative analysis inclusion of PMUs in the power system state estimator," *2015 IEEE 6th Latin American Symp. Circuits & Syst. (LASCAS)*, Montevideo, 2015, pp. 1–4,
- [52] "Metrics for determining the impact of phasor measurements on power system state estimation", Eastern Interconnection Phasor Project, KEMA: Arnhem, Netherlands, Mar. 2006.
- [53] B. A. Alcaide-Moreno, C. R. Fuerte-Esquivel, M. Glavic, and T. Van Cutsem, "Hybrid processing of SCADA and synchronized phasor measurements for tracking network state," *2015 IEEE PES General Meeting*, Denver, CO, 2015, pp. 1–5.
- [54] A. Angioni, G. Lipari, M. Pau, F. Ponci, and A. Monti, "A Low Cost PMU to Monitor Distribution Grids," *2017 IEEE Int. Workshop Applied Meas. Power Syst. (AMPS)*, Liverpool, 2017, pp. 1–6.
- [55] T. L. Baldwin, L. Milli, M. B. Boisen, and R. Adapa, "Power system observability with minimal phasor measurement placement," *IEEE Trans. Power Syst.*, vol. 8, no. 2, pp. 701–715, May 1993.

## 9 List of Abbreviations

Abbreviation	Term
AMI	Advanced metering infrastructure
AMR	Automated meter reading
DER	Distributed energy resources
DMS	Distribution management system
DSE	Distribution state estimation
DSO	Distribution system operator
DSOTP	Distribution system operator technical platform
GPS	Global positioning system
HEDNO	Hellenic distribution network operator
HV	High voltage
IED	Intelligent electronic device
IEEE	Institute of Electrical and Electronics Engineers
KPI	Key performance indicator
LA	Load allocation
LE	Load estimation
LF	Load forecasting
LV	Low voltage
MV	Medium voltage
PMU	Phasor measurement unit
PV	Photovoltaics
RTU	Remote terminal unit
SCADA	Supervisory control and data acquisition
SE	State estimation
SM	Smart meter
TSO	Transmission system operator
WLS	Weighted least squares

## Annex A Data of the Mesogeia pilot site

For the simulation studies of the SE tool, the two 20 kV distribution feeders 210 and 490, originating from the HV/MV substation of Nea Makri, are used. The single line diagram for the feeders originating from the HV/MV transformer 1 of the substation of Nea Makri is provided in Figure 20. The top of the feeders 210 and 490 are circled with dashed, yellow line.

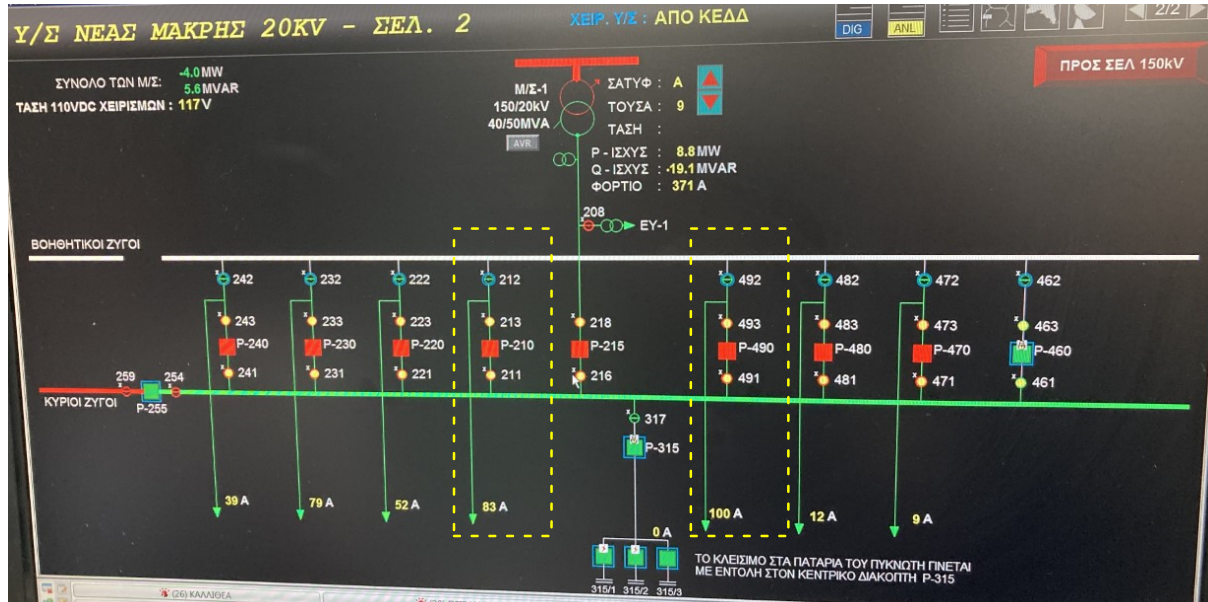


Figure 20: Configuration of Nea Makri substation

In Tables 8–11, the apparent power at nodes pertaining to load buses (type PQ), PV units (type PV) and zero injection (type ZI) buses for the two feeders, are listed. Apparently, a zero value means that the corresponding node refers to a zero injection bus.

Table 8 Nominal apparent power at load and generation nodes of feeder R490

Bus	Type	kVA	Bus	Type	kVA
8	PQ	150	223	PQ	250
42	PQ	250	229	PQ	630
48	PQ	160	235	PQ	400
56	PQ	160	241	PQ	400
60	PQ	250	256	PQ	250
75	PQ	250	262	PQ	250
92	PQ	400	279	PQ	400
98	PQ	250	283	PQ	400
104	PQ	630	298	PQ	400
110	PQ	400	302	PQ	630
125	PQ	630	306	PQ	400
141	PQ	630	321	PQ	400
173	PQ	630	325	PQ	400
177	PQ	630	343	PQ	630
194	PQ	400	357	PQ	160
209	PQ	400			

Table 9 Zero injection nodes of feeder R490

Bus	Type	kVA	Bus	Type	kVA
2	ZI	0	179	ZI	0
5	ZI	0	192	ZI	0
7	ZI	0	193	ZI	0
9	ZI	0	227	ZI	0
46	ZI	0	233	ZI	0
52	ZI	0	239	ZI	0
54	ZI	0	245	ZI	0
73	ZI	0	260	ZI	0
79	ZI	0	266	ZI	0
90	ZI	0	277	ZI	0
96	ZI	0	287	ZI	0
102	ZI	0	310	ZI	0
Bus	Type	kVA	Bus	Type	kVA
108	ZI	0	329	ZI	0
114	ZI	0	331	ZI	0
130	ZI	0	346	ZI	0
154	ZI	0	369	ZI	0

Bus 1 is considered as the slack bus for feeder R490, identified with the substation of Nea Makri.

Table 10 Nominal apparent power at load and generation nodes of feeder R210

Bus	Type	kVA	Bus	Type	kVA
605	PQ	50	2954	PQ	400
629	PV	250	2958	PQ	100
635	PQ	100	2961	PQ	250
641	PQ	250	2967	PQ	100
711	PQ	160	2982	PQ	250
715	PQ	400	2988	PQ	150
719	PQ	160	3005	PQ	250
734	PQ	250	3011	PQ	250
743	PQ	250	3015	PQ	200
747	PQ	250	3030	PQ	100
753	PQ	250	3036	PQ	160
757	PQ	250	3040	PQ	100
761	PQ	250	3047	PQ	250
778	PQ	250	3062	PQ	160
798	PQ	160	3069	PQ	250
1025	PQ	400	3097	PQ	400
1033	PQ	400	3103	PQ	50
1037	PQ	160	3111	PQ	100
1041	PQ	160	3115	PQ	50
1049	PQ	400	3131	PQ	250

1055	PQ	160	3151	PQ	160
1071	PQ	250	3155	PQ	400
1099	PQ	400	3193	PQ	100
1103	PQ	160	3199	PQ	160
1109	PQ	400	3205	PQ	100
1116	PQ	250	3209	PQ	100
<b>Bus</b>	<b>Type</b>	<b>kVA</b>	<b>Bus</b>	<b>Type</b>	<b>kVA</b>
1124	PQ	250	3213	PQ	100
1131	PQ	250	3219	PQ	250
1137	PQ	160	3225	PQ	160
1143	PQ	250	3243	PQ	400
1162	PQ	250	3249	PQ	50
1191	PQ	1000	3266	PQ	160
1285	PQ	400	3272	PV	315
1289	PQ	400	3278	PV	315
1304	PQ	630	3282	PQ	160
1327	PQ	400	3288	PQ	250
1969	PQ	400	3296	PQ	50
1975	PQ	400	3306	PQ	100
1981	PQ	160	3312	PQ	100
1985	PQ	250	3319	PQ	50
2024	PQ	400	3336	PQ	50
2028	PQ	400	3353	PQ	400
2053	PQ	400	3359	PQ	100
2057	PQ	400	3388	PQ	400
2774	PQ	100	3395	PQ	400
2782	PQ	160	3417	PQ	100
2788	PQ	50	3421	PQ	50
2810	PQ	50	3432	PV	500
2889	PQ	250	3440	PV	630
2893	PQ	160	3446	PV	630
2899	PQ	160	3451	PV	630
2903	PQ	100	3468	PQ	50
2907	PQ	50	3506	PQ	400
2924	PQ	160	3580	PQ	630
2928	PQ	250	3596	PQ	800
2948	PQ	250			

Table 11 Zero injection nodes of feeder R210

Bus	Type	kVA	Bus	Type	kVA
583	ZI	0	2878	ZI	0
594	ZI	0	2897	ZI	0
609	ZI	0	2911	ZI	0

612	ZI	0	2922	ZI	0
627	ZI	0	2932	ZI	0
633	ZI	0	2943	ZI	0
639	ZI	0	2946	ZI	0
645	ZI	0	2952	ZI	0
651	ZI	0	2965	ZI	0
662	ZI	0	2971	ZI	0
673	ZI	0	2986	ZI	0
684	ZI	0	2992	ZI	0
696	ZI	0	3003	ZI	0
707	ZI	0	3009	ZI	0
709	ZI	0	3019	ZI	0
723	ZI	0	3034	ZI	0
739	ZI	0	3044	ZI	0
741	ZI	0	3050	ZI	0
751	ZI	0	3064	ZI	0
765	ZI	0	3066	ZI	0
776	ZI	0	3067	ZI	0
782	ZI	0	3074	ZI	0
784	ZI	0	3085	ZI	0
795	ZI	0	3101	ZI	0
1023	ZI	0	3107	ZI	0
1029	ZI	0	3109	ZI	0
1031	ZI	0	3119	ZI	0
1045	ZI	0	3135	ZI	0
1047	ZI	0	3146	ZI	0
1053	ZI	0	3149	ZI	0
1060	ZI	0	3159	ZI	0
1075	ZI	0	3168	ZI	0
<b>Bus</b>	<b>Type</b>	<b>kVA</b>	<b>Bus</b>	<b>Type</b>	<b>kVA</b>
1077	ZI	0	3174	ZI	0
1088	ZI	0	3180	ZI	0
1107	ZI	0	3191	ZI	0
1113	ZI	0	3197	ZI	0
1120	ZI	0	3203	ZI	0
1122	ZI	0	3217	ZI	0
1128	ZI	0	3223	ZI	0
1135	ZI	0	3229	ZI	0
1141	ZI	0	3241	ZI	0
1147	ZI	0	3247	ZI	0
1158	ZI	0	3253	ZI	0
1166	ZI	0	3264	ZI	0
1168	ZI	0	3270	ZI	0
1180	ZI	0	3276	ZI	0

1195	ZI	0	3286	ZI	0
1197	ZI	0	3293	ZI	0
1208	ZI	0	3300	ZI	0
1211	ZI	0	3304	ZI	0
1283	ZI	0	3310	ZI	0
1293	ZI	0	3317	ZI	0
1302	ZI	0	3323	ZI	0
1309	ZI	0	3334	ZI	0
1315	ZI	0	3340	ZI	0
1338	ZI	0	3351	ZI	0
1364	ZI	0	3357	ZI	0
1375	ZI	0	3363	ZI	0
1378	ZI	0	3365	ZI	0
1966	ZI	0	3386	ZI	0
1973	ZI	0	3393	ZI	0
1979	ZI	0	3399	ZI	0
1990	ZI	0	3403	ZI	0
2001	ZI	0	3415	ZI	0
2013	ZI	0	3427	ZI	0
2032	ZI	0	3437	ZI	0
<b>Bus</b>	<b>Type</b>	<b>kVA</b>	<b>Bus</b>	<b>Type</b>	<b>kVA</b>
2061	ZI	0	3443	ZI	0
2070	ZI	0	3449	ZI	0
2072	ZI	0	3455	ZI	0
2765	ZI	0	3466	ZI	0
2768	ZI	0	3472	ZI	0
2770	ZI	0	3478	ZI	0
2772	ZI	0	3484	ZI	0
2786	ZI	0	3510	ZI	0
2792	ZI	0	3554	ZI	0
2795	ZI	0	3565	ZI	0
2804	ZI	0	3567	ZI	0
2807	ZI	0	3569	ZI	0
2813	ZI	0	3579	ZI	0
2824	ZI	0	3584	ZI	0

Bus 580 is originally the top of the feeder R210. Since R210 and R490 originate from the HV/MV substation of Nea Makri, the bus 580 is merged with bus 1.

Table 12 shows the various types of single circuit overhead and underground cables and their associated electrical parameters.

**Table 12 Types and electric parameters of overhead and underground cables**

	<b>R (Ohm/km)</b>	<b>X (Ohm/km)</b>	<b>C (nF/km)</b>	<b>B (mho/km)</b>
<b>1/0 6/1 ACSR Raven</b>	0.576	0.397	9.896	3.10892E-06
<b>16mm<sup>2</sup> Cu</b>	1.274	0.417	8.802	2.76523E-06
<b>35mm<sup>2</sup> Cu</b>	0.596	0.393	9.383	2.94776E-06
<b>95mm<sup>2</sup> Cu</b>	0.220	0.358	10.268	3.22579E-06
<b>70mm<sup>2</sup> AAAC</b>	0.562	0.370	9.927	3.11866E-06
<b>185mm<sup>2</sup> AAAC</b>	0.204	0.337	10.992	3.45324E-06
<b>3 6/1 ACSR Shallow</b>	1.268	0.422	9.248	2.90534E-06
<b>300 26/7 ACSR Ostrich</b>	0.215	0.334	10.89	3.42119E-06
<b>240 AL XLPE (TS)</b>	0.162	0.115	530	0.000166504
<b>240 AL NAEKBA (TS)</b>	0.150	0.108	530	0.000166504

The electric parameters for the overhead lines and underground cables of feeders 490 and 210 are given in Tables 13 and 14, respectively.

**Table 13 Line data for feeder R490**

From	To	Type	Length (m)	R (Ohm)	X (Ohm)	B (mho)	R (pu)	X (pu)	B (pu)
1	2	300 26/7 ACSR Ostrich	20.0	0.0043	0.0067	0.0000000684	0.00005	0.00008	0.0000054739
2	5	240 AL XLPE (TS)	9630.0	1.5601	1.1075	0.0016034375	0.01950	0.01384	0.1282749980
5	7	300 26/7 ACSR Ostrich	140.0	0.0301	0.0468	0.0000004790	0.00038	0.00058	0.0000383174
5	42	300 26/7 ACSR Ostrich	240.0	0.0516	0.0802	0.0000008211	0.00065	0.00100	0.0000656869
7	8	1/0 6/1 ACSR Raven	60.0	0.0346	0.0238	0.0000001865	0.00043	0.00030	0.0000149228
7	9	300 26/7 ACSR Ostrich	40.0	0.0086	0.0134	0.0000001368	0.00011	0.00017	0.0000109478
42	46	300 26/7 ACSR Ostrich	100.0	0.0215	0.0334	0.0000003421	0.00027	0.00042	0.0000273696
46	48	3 6/1 ACSR Shallow	330.0	0.4184	0.1393	0.0000009588	0.00523	0.00174	0.0000767011
46	52	300 26/7 ACSR Ostrich	30.0	0.0065	0.0100	0.0000001026	0.00008	0.00013	0.0000082109
52	54	70mm <sup>2</sup> AAAC	100.0	0.0562	0.0370	0.0000003119	0.00070	0.00046	0.0000249493
54	56	70mm <sup>2</sup> AAAC	230.0	0.1293	0.0851	0.0000007173	0.00162	0.00106	0.0000573833
54	60	35mm <sup>2</sup> Cu	730.0	0.4351	0.2869	0.0000021519	0.00544	0.00359	0.0001721490
52	73	300 26/7 ACSR Ostrich	320.0	0.0688	0.1069	0.0000010948	0.00086	0.00134	0.0000875826
73	75	1/0 6/1 ACSR Raven	10.0	0.0058	0.0040	0.0000000311	0.00007	0.00005	0.0000024871
73	79	300 26/7 ACSR Ostrich	140.0	0.0301	0.0468	0.0000004790	0.00038	0.00058	0.0000383174
79	90	95mm <sup>2</sup> Cu	30.0	0.0066	0.0107	0.0000000968	0.00008	0.00013	0.0000077419
90	92	35mm <sup>2</sup> Cu	220.0	0.1311	0.0865	0.0000006485	0.00164	0.00108	0.0000518805
90	96	95mm <sup>2</sup> Cu	120.0	0.0264	0.0430	0.0000003871	0.00033	0.00054	0.0000309676
From	To	Type	Length (m)	R (Ohm)	X (Ohm)	B (mho)	R (pu)	X (pu)	B (pu)
96	98	3 6/1 ACSR Shallow	230.0	0.2916	0.0971	0.0000006682	0.00365	0.00121	0.0000534583
96	102	95mm <sup>2</sup> Cu	50.0	0.0110	0.0179	0.0000001613	0.00014	0.00022	0.0000129031
102	104	35mm <sup>2</sup> Cu	30.0	0.0179	0.0118	0.0000000884	0.00022	0.00015	0.0000070746
102	108	95mm <sup>2</sup> Cu	220.0	0.0484	0.0788	0.0000007097	0.00061	0.00098	0.0000567739
108	110	1/0 6/1 ACSR Raven	10.0	0.0058	0.0040	0.0000000311	0.00007	0.00005	0.0000024871
108	114	95mm <sup>2</sup> Cu	80.0	0.0176	0.0286	0.0000002581	0.00022	0.00036	0.0000206450

114	125	240 AL XLPE (TS)	340.0	0.0551	0.0391	0.0000566115	0.00069	0.00049	0.0045289200
125	130	240 AL XLPE (TS)	500.0	0.0810	0.0575	0.0000832522	0.00101	0.00072	0.0066601764
125	141	240 AL XLPE (TS)	210.0	0.0340	0.0242	0.0000349659	0.00043	0.00030	0.0027972741
141	154	35mm <sup>2</sup> Cu	30.0	0.0179	0.0118	0.0000000884	0.00022	0.00015	0.0000070746
141	223	95mm <sup>2</sup> Cu	30.0	0.0066	0.0107	0.0000000968	0.00008	0.00013	0.0000077419
154	192	35mm <sup>2</sup> Cu	30.0	0.0179	0.0118	0.0000000884	0.00022	0.00015	0.0000070746
154	173	240 AL XLPE (TS)	220.0	0.0356	0.0253	0.0000366310	0.00045	0.00032	0.0029304776
173	177	240 AL XLPE (TS)	230.0	0.0373	0.0265	0.0000382960	0.00047	0.00033	0.0030636812
177	179	240 AL XLPE (TS)	130.0	0.0211	0.0150	0.0000216456	0.00026	0.00019	0.0017316459
192	193	35mm <sup>2</sup> Cu	50.0	0.0298	0.0197	0.0000001474	0.00037	0.00025	0.0000117910
192	194	35mm <sup>2</sup> Cu	40.0	0.0238	0.0157	0.0000001179	0.00030	0.00020	0.0000094328
193	209	240 AL XLPE (TS)	70.0	0.0113	0.0081	0.0000116553	0.00014	0.00010	0.0009324247
223	227	95mm <sup>2</sup> Cu	70.0	0.0154	0.0251	0.0000002258	0.00019	0.00031	0.0000180644
227	229	35mm <sup>2</sup> Cu	40.0	0.0238	0.0157	0.0000001179	0.00030	0.00020	0.0000094328
227	233	95mm <sup>2</sup> Cu	60.0	0.0132	0.0215	0.0000001935	0.00017	0.00027	0.0000154838
<b>From</b>	<b>To</b>	<b>Type</b>	<b>Length (m)</b>	<b>R (Ohm)</b>	<b>X (Ohm)</b>	<b>B (mho)</b>	<b>R (pu)</b>	<b>X (pu)</b>	<b>B (pu)</b>
233	235	1/0 6/1 ACSR Raven	350.0	0.2016	0.1390	0.0000010881	0.00252	0.00174	0.0000870498
233	239	95mm <sup>2</sup> Cu	240.0	0.0528	0.0859	0.0000007742	0.00066	0.00107	0.0000619351
239	241	95mm <sup>2</sup> Cu	120.0	0.0264	0.0430	0.0000003871	0.00033	0.00054	0.0000309676
239	277	95mm <sup>2</sup> Cu	260.0	0.0572	0.0931	0.0000008387	0.00072	0.00116	0.0000670964
241	245	95mm <sup>2</sup> Cu	30.0	0.0066	0.0107	0.0000000968	0.00008	0.00013	0.0000077419
245	256	95mm <sup>2</sup> Cu	310.0	0.0682	0.1110	0.0000010000	0.00085	0.00139	0.0000799995
256	260	70mm <sup>2</sup> AAAC	310.0	0.1742	0.1147	0.0000009668	0.00218	0.00143	0.0000773427
260	262	35mm <sup>2</sup> Cu	60.0	0.0358	0.0236	0.0000001769	0.00045	0.00029	0.0000141492
260	266	70mm <sup>2</sup> AAAC	60.0	0.0337	0.0222	0.0000001871	0.00042	0.00028	0.0000149696
277	279	95mm <sup>2</sup> Cu	120.0	0.0264	0.0430	0.0000003871	0.00033	0.00054	0.0000309676
277	287	95mm <sup>2</sup> Cu	90.0	0.0198	0.0322	0.0000002903	0.00025	0.00040	0.0000232257
279	283	35mm <sup>2</sup> Cu	156.0	0.0930	0.0613	0.0000004598	0.00116	0.00077	0.0000367880
287	298	95mm <sup>2</sup> Cu	40.0	0.0088	0.0143	0.0000001290	0.00011	0.00018	0.0000103225

298	302	95mm <sup>2</sup> Cu	190.0	0.0418	0.0680	0.0000006129	0.00052	0.00085	0.0000490320
302	306	95mm <sup>2</sup> Cu	140.0	0.0308	0.0501	0.0000004516	0.00039	0.00063	0.0000361288
306	310	95mm <sup>2</sup> Cu	150.0	0.0330	0.0537	0.0000004839	0.00041	0.00067	0.0000387094
310	321	95mm <sup>2</sup> Cu	70.0	0.0154	0.0251	0.0000002258	0.00019	0.00031	0.0000180644
321	325	95mm <sup>2</sup> Cu	750.0	0.1650	0.2685	0.0000024193	0.00206	0.00336	0.0001935472
325	329	95mm <sup>2</sup> Cu	450.0	0.0990	0.1611	0.0000014516	0.00124	0.00201	0.0001161283
329	331	70mm <sup>2</sup> AAAC	280.0	0.1574	0.1036	0.0000008732	0.00197	0.00130	0.0000698580
329	346	95mm <sup>2</sup> Cu	30.0	0.0066	0.0107	0.0000000968	0.00008	0.00013	0.0000077419
<b>From</b>	<b>To</b>	<b>Type</b>	<b>Length (m)</b>	<b>R (Ohm)</b>	<b>X (Ohm)</b>	<b>B (mho)</b>	<b>R (pu)</b>	<b>X (pu)</b>	<b>B (pu)</b>
329	357	95mm <sup>2</sup> Cu	670.0	0.1474	0.2399	0.0000021613	0.00184	0.00300	0.0001729022
331	343	240 AL XLPE (TS)	30.0	0.0049	0.0035	0.0000049951	0.00006	0.00004	0.0003996106
357	369	95mm <sup>2</sup> Cu	220.0	0.0484	0.0788	0.0000007097	0.00061	0.00098	0.0000567739

Table 14 Line data for feeder R210

From	To	Type	Length (m)	R (Ohm)	X (Ohm)	B (mho)	R (pu)	X (pu)	B (pu)
580	583	300 26/7 ACSR Ostrich	20.0	0.0043	0.0067	0.0000000684	0.00005	0.00008	0.0000054739
583	594	240 AL NAEKBA (TS)	10.0	0.0015	0.0011	0.0000016650	0.00002	0.00001	0.0001332035
594	605	300 26/7 ACSR Ostrich	40.0	0.0086	0.0134	0.0000001368	0.00011	0.00017	0.0000109478
605	609	300 26/7 ACSR Ostrich	110.0	0.0237	0.0367	0.0000003763	0.00030	0.00046	0.0000301065
609	612	185mm <sup>2</sup> AAAC	90.0	0.0184	0.0303	0.0000003108	0.00023	0.00038	0.0000248633
609	627	185mm <sup>2</sup> AAAC	110.0	0.0224	0.0371	0.0000003799	0.00028	0.00046	0.0000303885
627	629	1/0 6/1 ACSR Raven	20.0	0.0115	0.0079	0.0000000622	0.00014	0.00010	0.0000049743
627	633	185mm <sup>2</sup> AAAC	530.0	0.1081	0.1786	0.0000018302	0.00135	0.00223	0.0001464173
633	635	1/0 6/1 ACSR Raven	20.0	0.0115	0.0079	0.0000000622	0.00014	0.00010	0.0000049743
633	639	185mm <sup>2</sup> AAAC	700.0	0.1428	0.2359	0.0000024173	0.00179	0.00295	0.0001933814
639	641	1/0 6/1 ACSR Raven	30.0	0.0173	0.0119	0.0000000933	0.00022	0.00015	0.0000074614
639	645	300 26/7 ACSR Ostrich	180.0	0.0387	0.0601	0.0000006158	0.00048	0.00075	0.0000492652
645	651	300 26/7 ACSR Ostrich	160.0	0.0344	0.0534	0.0000005474	0.00043	0.00067	0.0000437913

651	662	240 AL XLPE (TS)	60.0	0.0097	0.0069	0.0000099903	0.00012	0.00009	0.0007992212
662	673	300 26/7 ACSR Ostrich	40.0	0.0086	0.0134	0.0000001368	0.00011	0.00017	0.0000109478
<b>From</b>	<b>To</b>	<b>Type</b>	<b>Length (m)</b>	<b>R (Ohm)</b>	<b>X (Ohm)</b>	<b>B (mho)</b>	<b>R (pu)</b>	<b>X (pu)</b>	<b>B (pu)</b>
662	684	300 26/7 ACSR Ostrich	30.0	0.0065	0.0100	0.0000001026	0.00008	0.00013	0.0000082109
684	696	95mm <sup>2</sup> Cu	290.0	0.0638	0.1038	0.0000009355	0.00080	0.00130	0.0000748383
696	707	95mm <sup>2</sup> Cu	70.0	0.0154	0.0251	0.0000002258	0.00019	0.00031	0.0000180644
707	709	70mm <sup>2</sup> AAAC	160.0	0.0899	0.0592	0.0000004990	0.00112	0.00074	0.0000399188
707	723	95mm <sup>2</sup> Cu	790.0	0.1738	0.2828	0.0000025484	0.00217	0.00354	0.0002038698
709	711	70mm <sup>2</sup> AAAC	10.0	0.0056	0.0037	0.0000000312	0.00007	0.00005	0.0000024949
709	715	70mm <sup>2</sup> AAAC	190.0	0.1068	0.0703	0.0000005925	0.00133	0.00088	0.0000474036
715	719	70mm <sup>2</sup> AAAC	270.0	0.1517	0.0999	0.0000008420	0.00190	0.00125	0.0000673630
723	734	95mm <sup>2</sup> Cu	40.0	0.0088	0.0143	0.0000001290	0.00011	0.00018	0.0000103225
734	739	95mm <sup>2</sup> Cu	30.0	0.0066	0.0107	0.0000000968	0.00008	0.00013	0.0000077419
739	741	1/0 6/1 ACSR Raven	730.0	0.4205	0.2898	0.0000022695	0.00526	0.00362	0.0001815609
739	761	95mm <sup>2</sup> Cu	410.0	0.0902	0.1468	0.0000013226	0.00113	0.00183	0.0001058058
741	743	1/0 6/1 ACSR Raven	40.0	0.0230	0.0159	0.0000001244	0.00029	0.00020	0.0000099485
741	747	70mm <sup>2</sup> AAAC	260.0	0.1461	0.0962	0.0000008109	0.00183	0.00120	0.0000648681
747	751	1/0 6/1 ACSR Raven	80.0	0.0461	0.0318	0.0000002487	0.00058	0.00040	0.0000198971
751	753	1/0 6/1 ACSR Raven	60.0	0.0346	0.0238	0.0000001865	0.00043	0.00030	0.0000149228
751	757	1/0 6/1 ACSR Raven	170.0	0.0979	0.0675	0.0000005285	0.00122	0.00084	0.0000422813
761	765	95mm <sup>2</sup> Cu	150.0	0.0330	0.0537	0.0000004839	0.00041	0.00067	0.0000387094
765	776	95mm <sup>2</sup> Cu	50.0	0.0110	0.0179	0.0000001613	0.00014	0.00022	0.0000129031
776	778	1/0 6/1 ACSR Raven	30.0	0.0173	0.0119	0.0000000933	0.00022	0.00015	0.0000074614
776	782	95mm <sup>2</sup> Cu	350.0	0.0770	0.1253	0.0000011290	0.00096	0.00157	0.0000903220
<b>From</b>	<b>To</b>	<b>Type</b>	<b>Length (m)</b>	<b>R (Ohm)</b>	<b>X (Ohm)</b>	<b>B (mho)</b>	<b>R (pu)</b>	<b>X (pu)</b>	<b>B (pu)</b>
782	784	95mm <sup>2</sup> Cu	100.0	0.0220	0.0358	0.0000003226	0.00028	0.00045	0.0000258063
782	2878	300 26/7 ACSR Ostrich	90.0	0.0194	0.0301	0.0000003079	0.00024	0.00038	0.0000246326
784	795	95mm <sup>2</sup> Cu	140.0	0.0308	0.0501	0.0000004516	0.00039	0.00063	0.0000361288
795	798	3 6/1 ACSR Shallow	220.0	0.2790	0.0928	0.0000006392	0.00349	0.00116	0.0000511341

795	1023	95mm <sup>2</sup> Cu	110.0	0.0242	0.0394	0.0000003548	0.00030	0.00049	0.0000283869
1023	1025	1/0 6/1 ACSR Raven	30.0	0.0173	0.0119	0.0000000933	0.00022	0.00015	0.0000074614
1023	1029	95mm <sup>2</sup> Cu	480.0	0.1056	0.1718	0.0000015484	0.00132	0.00215	0.0001238702
1029	1031	1/0 6/1 ACSR Raven	47.0	0.0271	0.0187	0.0000001461	0.00034	0.00023	0.0000116895
1029	1045	95mm <sup>2</sup> Cu	300.0	0.0660	0.1074	0.0000009677	0.00083	0.00134	0.0000774189
1031	1033	3 6/1 ACSR Shallow	100.0	0.1268	0.0422	0.0000002905	0.00159	0.00053	0.0000232428
1033	1037	3 6/1 ACSR Shallow	580.0	0.7354	0.2448	0.0000016851	0.00919	0.00306	0.0001348080
1037	1041	70mm <sup>2</sup> AAC	540.0	0.3035	0.1998	0.0000016841	0.00379	0.00250	0.0001347261
1045	1047	1/0 6/1 ACSR Raven	200.0	0.1152	0.0794	0.0000006218	0.00144	0.00099	0.0000497427
1045	1053	95mm <sup>2</sup> Cu	350.0	0.0770	0.1253	0.0000011290	0.00096	0.00157	0.0000903220
1047	1049	3 6/1 ACSR Shallow	290.0	0.3677	0.1224	0.0000008426	0.00460	0.00153	0.0000674040
1053	1055	300 26/7 ACSR Ostrich	180.0	0.0387	0.0601	0.0000006158	0.00048	0.00075	0.0000492652
1053	1060	95mm <sup>2</sup> Cu	380.0	0.0836	0.1360	0.0000012258	0.00105	0.00170	0.0000980639
1060	1071	95mm <sup>2</sup> Cu	30.0	0.0066	0.0107	0.0000000968	0.00008	0.00013	0.0000077419
1071	1075	95mm <sup>2</sup> Cu	160.0	0.0352	0.0573	0.0000005161	0.00044	0.00072	0.0000412901
1075	1077	300 26/7 ACSR Ostrich	80.0	0.0172	0.0267	0.0000002737	0.00022	0.00033	0.0000218956
1075	1158	300 26/7 ACSR Ostrich	90.0	0.0194	0.0301	0.0000003079	0.00024	0.00038	0.0000246326
<b>From</b>	<b>To</b>	<b>Type</b>	<b>Length (m)</b>	<b>R (Ohm)</b>	<b>X (Ohm)</b>	<b>B (mho)</b>	<b>R (pu)</b>	<b>X (pu)</b>	<b>B (pu)</b>
1077	1088	300 26/7 ACSR Ostrich	30.0	0.0065	0.0100	0.0000001026	0.00008	0.00013	0.0000082109
1088	1099	1/0 6/1 ACSR Raven	50.0	0.0288	0.0199	0.0000001554	0.00036	0.00025	0.0000124357
1088	1103	300 26/7 ACSR Ostrich	560.0	0.1204	0.1870	0.0000019159	0.00151	0.00234	0.0001532695
1103	1107	300 26/7 ACSR Ostrich	200.0	0.0430	0.0668	0.0000006842	0.00054	0.00084	0.0000547391
1107	1109	300 26/7 ACSR Ostrich	140.0	0.0301	0.0468	0.0000004790	0.00038	0.00058	0.0000383174
1107	1113	300 26/7 ACSR Ostrich	70.0	0.0151	0.0234	0.0000002395	0.00019	0.00029	0.0000191587
1113	1116	3 6/1 ACSR Shallow	260.0	0.3297	0.1097	0.0000007554	0.00412	0.00137	0.0000604312
1113	1120	300 26/7 ACSR Ostrich	80.0	0.0172	0.0267	0.0000002737	0.00022	0.00033	0.0000218956
1120	1122	1/0 6/1 ACSR Raven	130.0	0.0749	0.0516	0.0000004042	0.00094	0.00065	0.0000323328
1120	1128	300 26/7 ACSR Ostrich	580.0	0.1247	0.1937	0.0000019843	0.00156	0.00242	0.0001587434
1122	1124	70mm <sup>2</sup> AAC	528.0	0.2967	0.1954	0.0000016467	0.00371	0.00244	0.0001317322

1128	1131	300 26/7 ACSR Ostrich	90.0	0.0194	0.0301	0.0000003079	0.00024	0.00038	0.0000246326
1128	1135	300 26/7 ACSR Ostrich	150.0	0.0323	0.0501	0.0000005132	0.00040	0.00063	0.0000410543
1135	1137	70mm <sup>2</sup> AAAC	190.0	0.1068	0.0703	0.0000005925	0.00133	0.00088	0.0000474036
1135	1141	300 26/7 ACSR Ostrich	480.0	0.1032	0.1603	0.0000016422	0.00129	0.00200	0.0001313739
1141	1143	1/0 6/1 ACSR Raven	30.0	0.0173	0.0119	0.0000000933	0.00022	0.00015	0.0000074614
1141	1147	300 26/7 ACSR Ostrich	170.0	0.0366	0.0568	0.0000005816	0.00046	0.00071	0.0000465282
1158	1162	35mm <sup>2</sup> Cu	30.0	0.0179	0.0118	0.0000000884	0.00022	0.00015	0.0000070746
1158	1166	300 26/7 ACSR Ostrich	470.0	0.1011	0.1570	0.0000016080	0.00126	0.00196	0.0001286369
1166	1168	185mm <sup>2</sup> AAAC	70.0	0.0143	0.0236	0.0000002417	0.00018	0.00029	0.0000193381
1166	1195	300 26/7 ACSR Ostrich	90.0	0.0194	0.0301	0.0000003079	0.00024	0.00038	0.0000246326
<b>From</b>	<b>To</b>	<b>Type</b>	<b>Length (m)</b>	<b>R (Ohm)</b>	<b>X (Ohm)</b>	<b>B (mho)</b>	<b>R (pu)</b>	<b>X (pu)</b>	<b>B (pu)</b>
1168	1180	185mm <sup>2</sup> AAAC	1190.0	0.2428	0.4010	0.0000041094	0.00303	0.00501	0.0003287483
1180	1191	240 AL NAEKBA (TS)	250.0	0.0375	0.0270	0.0000416261	0.00047	0.00034	0.0033300882
1195	1197	1/0 6/1 ACSR Raven	70.0	0.0403	0.0278	0.0000002176	0.00050	0.00035	0.0000174100
1195	1364	300 26/7 ACSR Ostrich	230.0	0.0495	0.0768	0.0000007869	0.00062	0.00096	0.0000629500
1197	1208	1/0 6/1 ACSR Raven	110.0	0.0634	0.0437	0.0000003420	0.00079	0.00055	0.0000273585
1208	1211	1/0 6/1 ACSR Raven	90.0	0.0518	0.0357	0.0000002798	0.00065	0.00045	0.0000223842
1208	1283	70mm <sup>2</sup> AAAC	280.0	0.1574	0.1036	0.0000008732	0.00197	0.00130	0.0000698580
1211	3554	240 AL XLPE (TS)	20.0	0.0032	0.0023	0.0000033301	0.00004	0.00003	0.0002664071
1283	1285	70mm <sup>2</sup> AAAC	220.0	0.1236	0.0814	0.0000006861	0.00155	0.00102	0.0000548884
1283	1289	70mm <sup>2</sup> AAAC	110.0	0.0618	0.0407	0.0000003431	0.00077	0.00051	0.0000274442
1289	1293	1/0 6/1 ACSR Raven	150.0	0.0864	0.0596	0.0000004663	0.00108	0.00074	0.0000373070
1302	1304	1/0 6/1 ACSR Raven	140.0	0.0806	0.0556	0.0000004352	0.00101	0.00069	0.0000348199
1304	1309	1/0 6/1 ACSR Raven	240.0	0.1382	0.0953	0.0000007461	0.00173	0.00119	0.0000596913
1304	1990	1/0 6/1 ACSR Raven	70.0	0.0403	0.0278	0.0000002176	0.00050	0.00035	0.0000174100
1309	1315	1/0 6/1 ACSR Raven	30.0	0.0173	0.0119	0.0000000933	0.00022	0.00015	0.0000074614
1309	1378	1/0 6/1 ACSR Raven	330.0	0.1901	0.1310	0.0000010259	0.00238	0.00164	0.0000820755
1309	1973	1/0 6/1 ACSR Raven	250.0	0.1440	0.0993	0.0000007772	0.00180	0.00124	0.0000621784
1315	1327	1/0 6/1 ACSR Raven	40.0	0.0230	0.0159	0.0000001244	0.00029	0.00020	0.0000099485

1338	3506	240 AL XLPE (TS)	70.0	0.0113	0.0081	0.0000116553	0.00014	0.00010	0.0009324247
1364	1375	300 26/7 ACSR Ostrich	390.0	0.0839	0.1303	0.0000013343	0.00105	0.00163	0.0001067413
1375	1966	300 26/7 ACSR Ostrich	410.0	0.0882	0.1369	0.0000014027	0.00110	0.00171	0.0001122152
<b>From</b>	<b>To</b>	<b>Type</b>	<b>Length (m)</b>	<b>R (Ohm)</b>	<b>X (Ohm)</b>	<b>B (mho)</b>	<b>R (pu)</b>	<b>X (pu)</b>	<b>B (pu)</b>
1966	1969	1/0 6/1 ACSR Raven	60.0	0.0346	0.0238	0.0000001865	0.00043	0.00030	0.0000149228
1966	2807	300 26/7 ACSR Ostrich	40.0	0.0086	0.0134	0.0000001368	0.00011	0.00017	0.0000109478
1973	1975	70mm <sup>2</sup> AAAC	190.0	0.1068	0.0703	0.0000005925	0.00133	0.00088	0.0000474036
1973	1979	1/0 6/1 ACSR Raven	30.0	0.0173	0.0119	0.0000000933	0.00022	0.00015	0.0000074614
1979	1981	1/0 6/1 ACSR Raven	40.0	0.0230	0.0159	0.0000001244	0.00029	0.00020	0.0000099485
1979	1985	1/0 6/1 ACSR Raven	70.0	0.0403	0.0278	0.0000002176	0.00050	0.00035	0.0000174100
1990	2001	1/0 6/1 ACSR Raven	20.0	0.0115	0.0079	0.0000000622	0.00014	0.00010	0.0000049743
2001	2028	1/0 6/1 ACSR Raven	560.0	0.3226	0.2223	0.0000017410	0.00403	0.00278	0.0001392796
2001	2013	240 AL XLPE (TS)	80.0	0.0130	0.0092	0.0000133204	0.00016	0.00012	0.0010656282
2013	2024	1/0 6/1 ACSR Raven	110.0	0.0634	0.0437	0.0000003420	0.00079	0.00055	0.0000273585
2028	2032	1/0 6/1 ACSR Raven	20.0	0.0115	0.0079	0.0000000622	0.00014	0.00010	0.0000049743
2032	2057	1/0 6/1 ACSR Raven	300.0	0.1728	0.1191	0.0000009327	0.00216	0.00149	0.0000746141
2032	2053	240 AL XLPE (TS)	120.0	0.0194	0.0138	0.0000199805	0.00024	0.00017	0.0015984423
2057	2061	1/0 6/1 ACSR Raven	220.0	0.1267	0.0873	0.0000006840	0.00158	0.00109	0.0000547170
2072	2070	1/0 6/1 ACSR Raven	40.0	0.0230	0.0159	0.0000001244	0.00029	0.00020	0.0000099485
2072	3064	70mm <sup>2</sup> AAAC	110.0	0.0618	0.0407	0.0000003431	0.00077	0.00051	0.0000274442
2765	2072	70mm <sup>2</sup> AAAC	50.0	0.0281	0.0185	0.0000001559	0.00035	0.00023	0.0000124746
2765	2768	185mm <sup>2</sup> AAAC	440.0	0.0898	0.1483	0.0000015194	0.00112	0.00185	0.0001215540
2768	2770	300 26/7 ACSR Ostrich	310.0	0.0667	0.1035	0.0000010606	0.00083	0.00129	0.0000848456
2770	2772	70mm <sup>2</sup> AAAC	50.0	0.0281	0.0185	0.0000001559	0.00035	0.00023	0.0000124746
2770	2786	300 26/7 ACSR Ostrich	400.0	0.0860	0.1336	0.0000013685	0.00108	0.00167	0.0001094782
<b>From</b>	<b>To</b>	<b>Type</b>	<b>Length (m)</b>	<b>R (Ohm)</b>	<b>X (Ohm)</b>	<b>B (mho)</b>	<b>R (pu)</b>	<b>X (pu)</b>	<b>B (pu)</b>
2772	2774	70mm <sup>2</sup> AAAC	200.0	0.1124	0.0740	0.0000006237	0.00141	0.00093	0.0000498985
2772	2782	1/0 6/1 ACSR Raven	410.0	0.2362	0.1628	0.0000012747	0.00295	0.00203	0.0001019726
2786	2788	70mm <sup>2</sup> AAAC	170.0	0.0955	0.0629	0.0000005302	0.00119	0.00079	0.0000424138

2786	2792	300 26/7 ACSR Ostrich	270.0	0.0581	0.0902	0.0000009237	0.00073	0.00113	0.0000738978
2792	2795	185mm <sup>2</sup> AAAC	290.0	0.0592	0.0977	0.0000010014	0.00074	0.00122	0.0000801151
2807	2810	1/0 6/1 ACSR Raven	2260.0	1.3018	0.8972	0.0000070262	0.01627	0.01122	0.0005620928
2807	2813	300 26/7 ACSR Ostrich	90.0	0.0194	0.0301	0.0000003079	0.00024	0.00038	0.0000246326
2813	2824	300 26/7 ACSR Ostrich	510.0	0.1097	0.1703	0.0000017448	0.00137	0.00213	0.0001395847
2824	2804	185mm <sup>2</sup> AAAC	30.0	0.0061	0.0101	0.0000001036	0.00008	0.00013	0.0000082878
2824	3191	300 26/7 ACSR Ostrich	1030.0	0.2215	0.3440	0.0000035238	0.00277	0.00430	0.0002819064
2878	2889	300 26/7 ACSR Ostrich	310.0	0.0667	0.1035	0.0000010606	0.00083	0.00129	0.0000848456
2889	2893	300 26/7 ACSR Ostrich	300.0	0.0645	0.1002	0.0000010264	0.00081	0.00125	0.0000821087
2893	2897	300 26/7 ACSR Ostrich	110.0	0.0237	0.0367	0.0000003763	0.00030	0.00046	0.0000301065
2897	2899	1/0 6/1 ACSR Raven	290.0	0.1670	0.1151	0.0000009016	0.00209	0.00144	0.0000721269
2897	2911	1/0 6/1 ACSR Raven	80.0	0.0461	0.0318	0.0000002487	0.00058	0.00040	0.0000198971
2899	2903	1/0 6/1 ACSR Raven	340.0	0.1958	0.1350	0.0000010570	0.00245	0.00169	0.0000845626
2903	2907	1/0 6/1 ACSR Raven	450.0	0.2592	0.1787	0.0000013990	0.00324	0.00223	0.0001119211
2911	2922	1/0 6/1 ACSR Raven	130.0	0.0749	0.0516	0.0000004042	0.00094	0.00065	0.0000323328
2922	2924	70mm <sup>2</sup> AAAC	60.0	0.0337	0.0222	0.0000001871	0.00042	0.00028	0.0000149696
2922	2928	1/0 6/1 ACSR Raven	490.0	0.2822	0.1945	0.0000015234	0.00353	0.00243	0.0001218697
2928	2932	1/0 6/1 ACSR Raven	280.0	0.1613	0.1112	0.0000008705	0.00202	0.00139	0.0000696398
<b>From</b>	<b>To</b>	<b>Type</b>	<b>Length (m)</b>	<b>R (Ohm)</b>	<b>X (Ohm)</b>	<b>B (mho)</b>	<b>R (pu)</b>	<b>X (pu)</b>	<b>B (pu)</b>
2932	2943	1/0 6/1 ACSR Raven	70.0	0.0403	0.0278	0.0000002176	0.00050	0.00035	0.0000174100
2943	2946	1/0 6/1 ACSR Raven	220.0	0.1267	0.0873	0.0000006840	0.00158	0.00109	0.0000547170
2943	2961	1/0 6/1 ACSR Raven	70.0	0.0403	0.0278	0.0000002176	0.00050	0.00035	0.0000174100
2946	2948	1/0 6/1 ACSR Raven	50.0	0.0288	0.0199	0.0000001554	0.00036	0.00025	0.0000124357
2946	2952	1/0 6/1 ACSR Raven	180.0	0.1037	0.0715	0.0000005596	0.00130	0.00089	0.0000447684
2952	2954	1/0 6/1 ACSR Raven	170.0	0.0979	0.0675	0.0000005285	0.00122	0.00084	0.0000422813
2952	2958	1/0 6/1 ACSR Raven	390.0	0.2246	0.1548	0.0000012125	0.00281	0.00194	0.0000969983
2961	2965	70mm <sup>2</sup> AAAC	210.0	0.1180	0.0777	0.0000006549	0.00148	0.00097	0.0000523935
2965	2967	1/0 6/1 ACSR Raven	170.0	0.0979	0.0675	0.0000005285	0.00122	0.00084	0.0000422813
2965	2971	70mm <sup>2</sup> AAAC	40.0	0.0225	0.0148	0.0000001247	0.00028	0.00019	0.0000099797

2971	2982	70mm <sup>2</sup> AAC	70.0	0.0393	0.0259	0.0000002183	0.00049	0.00032	0.0000174645
2982	2986	70mm <sup>2</sup> AAC	320.0	0.1798	0.1184	0.0000009980	0.00225	0.00148	0.0000798377
2986	2988	70mm <sup>2</sup> AAC	70.0	0.0393	0.0259	0.0000002183	0.00049	0.00032	0.0000174645
2986	2992	70mm <sup>2</sup> AAC	180.0	0.1012	0.0666	0.0000005614	0.00126	0.00083	0.0000449087
2992	3003	70mm <sup>2</sup> AAC	110.0	0.0618	0.0407	0.0000003431	0.00077	0.00051	0.0000274442
3003	3005	70mm <sup>2</sup> AAC	50.0	0.0281	0.0185	0.0000001559	0.00035	0.00023	0.0000124746
3003	3009	70mm <sup>2</sup> AAC	260.0	0.1461	0.0962	0.0000008109	0.00183	0.00120	0.0000648681
3009	3011	70mm <sup>2</sup> AAC	110.0	0.0618	0.0407	0.0000003431	0.00077	0.00051	0.0000274442
3009	3015	1/0 6/1 ACSR Raven	1160.0	0.6682	0.4605	0.0000036063	0.00835	0.00576	0.0002885078
3015	3019	70mm <sup>2</sup> AAC	320.0	0.1798	0.1184	0.0000009980	0.00225	0.00148	0.0000798377
3019	3030	70mm <sup>2</sup> AAC	70.0	0.0393	0.0259	0.0000002183	0.00049	0.00032	0.0000174645
<b>From</b>	<b>To</b>	<b>Type</b>	<b>Length (m)</b>	<b>R (Ohm)</b>	<b>X (Ohm)</b>	<b>B (mho)</b>	<b>R (pu)</b>	<b>X (pu)</b>	<b>B (pu)</b>
3030	3034	70mm <sup>2</sup> AAC	260.0	0.1461	0.0962	0.0000008109	0.00183	0.00120	0.0000648681
3034	3036	1/0 6/1 ACSR Raven	40.0	0.0230	0.0159	0.0000001244	0.00029	0.00020	0.0000099485
3034	3040	70mm <sup>2</sup> AAC	510.0	0.2866	0.1887	0.0000015905	0.00358	0.00236	0.0001272413
3040	3044	70mm <sup>2</sup> AAC	280.0	0.1574	0.1036	0.0000008732	0.00197	0.00130	0.0000698580
3044	3047	1/0 6/1 ACSR Raven	180.0	0.1037	0.0715	0.0000005596	0.00130	0.00089	0.0000447684
3044	3050	70mm <sup>2</sup> AAC	30.0	0.0169	0.0111	0.0000000936	0.00021	0.00014	0.0000074848
3050	3066	70mm <sup>2</sup> AAC	40.0	0.0225	0.0148	0.0000001247	0.00028	0.00019	0.0000099797
3064	3062	1/0 6/1 ACSR Raven	200.0	0.1152	0.0794	0.0000006218	0.00144	0.00099	0.0000497427
3066	3067	185mm <sup>2</sup> AAC	440.0	0.0898	0.1483	0.0000015194	0.00112	0.00185	0.0001215540
3066	3074	185mm <sup>2</sup> AAC	100.0	0.0204	0.0337	0.0000003453	0.00026	0.00042	0.0000276259
3067	2765	185mm <sup>2</sup> AAC	760.0	0.1550	0.2561	0.0000026245	0.00194	0.00320	0.0002099569
3067	3069	70mm <sup>2</sup> AAC	50.0	0.0281	0.0185	0.0000001559	0.00035	0.00023	0.0000124746
3074	3085	185mm <sup>2</sup> AAC	410.0	0.0836	0.1382	0.0000014158	0.00105	0.00173	0.0001132662
3085	3097	70mm <sup>2</sup> AAC	230.0	0.1293	0.0851	0.0000007173	0.00162	0.00106	0.0000573833
3085	3101	185mm <sup>2</sup> AAC	140.0	0.0286	0.0472	0.0000004835	0.00036	0.00059	0.0000386763
3101	3103	70mm <sup>2</sup> AAC	100.0	0.0562	0.0370	0.0000003119	0.00070	0.00046	0.0000249493
3101	3107	185mm <sup>2</sup> AAC	520.0	0.1061	0.1752	0.0000017957	0.00133	0.00219	0.0001436547

3107	3109	70mm <sup>2</sup> AAAC	100.0	0.0562	0.0370	0.0000003119	0.00070	0.00046	0.0000249493
3107	3119	185mm <sup>2</sup> AAAC	900.0	0.1836	0.3033	0.0000031079	0.00230	0.00379	0.0002486332
3109	3111	70mm <sup>2</sup> AAAC	50.0	0.0281	0.0185	0.0000001559	0.00035	0.00023	0.0000124746
3109	3115	1/0 6/1 ACSR Raven	1190.0	0.6854	0.4724	0.0000036996	0.00857	0.00591	0.0002959692
<b>From</b>	<b>To</b>	<b>Type</b>	<b>Length (m)</b>	<b>R (Ohm)</b>	<b>X (Ohm)</b>	<b>B (mho)</b>	<b>R (pu)</b>	<b>X (pu)</b>	<b>B (pu)</b>
3119	3131	70mm <sup>2</sup> AAAC	40.0	0.0225	0.0148	0.0000001247	0.00028	0.00019	0.0000099797
3119	3135	185mm <sup>2</sup> AAAC	600.0	0.1224	0.2022	0.0000020719	0.00153	0.00253	0.0001657555
3135	3146	185mm <sup>2</sup> AAAC	60.0	0.0122	0.0202	0.0000002072	0.00015	0.00025	0.0000165755
3146	3149	300 26/7 ACSR Ostrich	80.0	0.0172	0.0267	0.0000002737	0.00022	0.00033	0.0000218956
3146	3168	300 26/7 ACSR Ostrich	560.0	0.1204	0.1870	0.0000019159	0.00151	0.00234	0.0001532695
3149	3151	1/0 6/1 ACSR Raven	50.0	0.0288	0.0199	0.0000001554	0.00036	0.00025	0.0000124357
3149	3155	1/0 6/1 ACSR Raven	110.0	0.0634	0.0437	0.0000003420	0.00079	0.00055	0.0000273585
3155	3159	1/0 6/1 ACSR Raven	140.0	0.0806	0.0556	0.0000004352	0.00101	0.00069	0.0000348199
3168	3174	300 26/7 ACSR Ostrich	490.0	0.1054	0.1637	0.0000016764	0.00132	0.00205	0.0001341108
3174	3180	300 26/7 ACSR Ostrich	310.0	0.0667	0.1035	0.0000010606	0.00083	0.00129	0.0000848456
3191	3193	1/0 6/1 ACSR Raven	90.0	0.0518	0.0357	0.0000002798	0.00065	0.00045	0.0000223842
3191	3197	300 26/7 ACSR Ostrich	1000.0	0.2150	0.3340	0.0000034212	0.00269	0.00418	0.0002736956
3197	3199	1/0 6/1 ACSR Raven	280.0	0.1613	0.1112	0.0000008705	0.00202	0.00139	0.0000696398
3197	3217	300 26/7 ACSR Ostrich	220.0	0.0473	0.0735	0.0000007527	0.00059	0.00092	0.0000602130
3199	3203	1/0 6/1 ACSR Raven	20.0	0.0115	0.0079	0.0000000622	0.00014	0.00010	0.0000049743
3203	3205	1/0 6/1 ACSR Raven	1340.0	0.7718	0.5320	0.0000041660	0.00965	0.00665	0.0003332762
3203	3209	1/0 6/1 ACSR Raven	720.0	0.4147	0.2858	0.0000022384	0.00518	0.00357	0.0001790738
3209	3213	1/0 6/1 ACSR Raven	290.0	0.1670	0.1151	0.0000009016	0.00209	0.00144	0.0000721269
3217	3219	1/0 6/1 ACSR Raven	40.0	0.0230	0.0159	0.0000001244	0.00029	0.00020	0.0000099485
3217	3223	300 26/7 ACSR Ostrich	110.0	0.0237	0.0367	0.0000003763	0.00030	0.00046	0.0000301065
3223	3225	1/0 6/1 ACSR Raven	820.0	0.4723	0.3255	0.0000025493	0.00590	0.00407	0.0002039452
<b>From</b>	<b>To</b>	<b>Type</b>	<b>Length (m)</b>	<b>R (Ohm)</b>	<b>X (Ohm)</b>	<b>B (mho)</b>	<b>R (pu)</b>	<b>X (pu)</b>	<b>B (pu)</b>
3223	3229	300 26/7 ACSR Ostrich	30.0	0.0065	0.0100	0.0000001026	0.00008	0.00013	0.0000082109
3229	3241	1/0 6/1 ACSR Raven	100.0	0.0576	0.0397	0.0000003109	0.00072	0.00050	0.0000248714

3229	3286	300 26/7 ACSR Ostrich	430.0	0.0925	0.1436	0.0000014711	0.00116	0.00180	0.0001176891
3241	3243	1/0 6/1 ACSR Raven	120.0	0.0691	0.0476	0.0000003731	0.00086	0.00060	0.0000298456
3241	3247	1/0 6/1 ACSR Raven	210.0	0.1210	0.0834	0.0000006529	0.00151	0.00104	0.0000522299
3247	3249	1/0 6/1 ACSR Raven	650.0	0.3744	0.2581	0.0000020208	0.00468	0.00323	0.0001616638
3247	3253	1/0 6/1 ACSR Raven	90.0	0.0518	0.0357	0.0000002798	0.00065	0.00045	0.0000223842
3253	3264	1/0 6/1 ACSR Raven	160.0	0.0922	0.0635	0.0000004974	0.00115	0.00079	0.0000397942
3264	3266	1/0 6/1 ACSR Raven	100.0	0.0576	0.0397	0.0000003109	0.00072	0.00050	0.0000248714
3264	3270	1/0 6/1 ACSR Raven	670.0	0.3859	0.2660	0.0000020830	0.00482	0.00332	0.0001666381
3270	3272	1/0 6/1 ACSR Raven	50.0	0.0288	0.0199	0.0000001554	0.00036	0.00025	0.0000124357
3270	3276	1/0 6/1 ACSR Raven	50.0	0.0288	0.0199	0.0000001554	0.00036	0.00025	0.0000124357
3276	3278	1/0 6/1 ACSR Raven	100.0	0.0576	0.0397	0.0000003109	0.00072	0.00050	0.0000248714
3276	3282	1/0 6/1 ACSR Raven	140.0	0.0806	0.0556	0.0000004352	0.00101	0.00069	0.0000348199
3286	3288	1/0 6/1 ACSR Raven	30.0	0.0173	0.0119	0.0000000933	0.00022	0.00015	0.0000074614
3286	3293	300 26/7 ACSR Ostrich	620.0	0.1333	0.2071	0.0000021211	0.00167	0.00259	0.0001696912
3293	3296	1/0 6/1 ACSR Raven	80.0	0.0461	0.0318	0.0000002487	0.00058	0.00040	0.0000198971
3293	3300	300 26/7 ACSR Ostrich	210.0	0.0452	0.0701	0.0000007185	0.00056	0.00088	0.0000574761
3300	3304	1/0 6/1 ACSR Raven	550.0	0.3168	0.2184	0.0000017099	0.00396	0.00273	0.0001367925
3300	3334	300 26/7 ACSR Ostrich	130.0	0.0280	0.0434	0.0000004448	0.00035	0.00054	0.0000355804
3304	3306	1/0 6/1 ACSR Raven	360.0	0.2074	0.1429	0.0000011192	0.00259	0.00179	0.0000895369
<b>From</b>	<b>To</b>	<b>Type</b>	<b>Length (m)</b>	<b>R (Ohm)</b>	<b>X (Ohm)</b>	<b>B (mho)</b>	<b>R (pu)</b>	<b>X (pu)</b>	<b>B (pu)</b>
3304	3310	1/0 6/1 ACSR Raven	300.0	0.1728	0.1191	0.0000009327	0.00216	0.00149	0.0000746141
3310	3312	1/0 6/1 ACSR Raven	410.0	0.2362	0.1628	0.0000012747	0.00295	0.00203	0.0001019726
3310	3317	1/0 6/1 ACSR Raven	270.0	0.1555	0.1072	0.0000008394	0.00194	0.00134	0.0000671527
3317	3319	1/0 6/1 ACSR Raven	120.0	0.0691	0.0476	0.0000003731	0.00086	0.00060	0.0000298456
3317	3323	1/0 6/1 ACSR Raven	60.0	0.0346	0.0238	0.0000001865	0.00043	0.00030	0.0000149228
3334	3336	1/0 6/1 ACSR Raven	40.0	0.0230	0.0159	0.0000001244	0.00029	0.00020	0.0000099485
3334	3340	300 26/7 ACSR Ostrich	60.0	0.0129	0.0200	0.0000002053	0.00016	0.00025	0.0000164217
3340	3351	300 26/7 ACSR Ostrich	200.0	0.0430	0.0668	0.0000006842	0.00054	0.00084	0.0000547391
3351	3353	3 6/1 ACSR Shallow	170.0	0.2156	0.0717	0.0000004939	0.00269	0.00090	0.0000395127

3351	3357	300 26/7 ACSR Ostrich	330.0	0.0710	0.1102	0.0000011290	0.00089	0.00138	0.0000903195
3357	3359	1/0 6/1 ACSR Raven	260.0	0.1498	0.1032	0.0000008083	0.00187	0.00129	0.0000646655
3357	3363	300 26/7 ACSR Ostrich	70.0	0.0151	0.0234	0.0000002395	0.00019	0.00029	0.0000191587
3363	3365	240 AL XLPE (TS)	60.0	0.0097	0.0069	0.0000099903	0.00012	0.00009	0.0007992212
3363	3399	300 26/7 ACSR Ostrich	200.0	0.0430	0.0668	0.0000006842	0.00054	0.00084	0.0000547391
3365	3386	1/0 6/1 ACSR Raven	270.0	0.1555	0.1072	0.0000008394	0.00194	0.00134	0.0000671527
3386	3388	1/0 6/1 ACSR Raven	20.0	0.0115	0.0079	0.0000000622	0.00014	0.00010	0.0000049743
3386	3393	240 AL NAEKBA (TS)	50.0	0.0075	0.0054	0.0000083252	0.00009	0.00007	0.0006660176
3393	3395	1/0 6/1 ACSR Raven	290.0	0.1670	0.1151	0.0000009016	0.00209	0.00144	0.0000721269
3399	3403	1/0 6/1 ACSR Raven	80.0	0.0461	0.0318	0.0000002487	0.00058	0.00040	0.0000198971
3399	3455	300 26/7 ACSR Ostrich	290.0	0.0624	0.0969	0.0000009921	0.00078	0.00121	0.0000793717
3403	3415	1/0 6/1 ACSR Raven	200.0	0.1152	0.0794	0.0000006218	0.00144	0.00099	0.0000497427
<b>From</b>	<b>To</b>	<b>Type</b>	<b>Length (m)</b>	<b>R (Ohm)</b>	<b>X (Ohm)</b>	<b>B (mho)</b>	<b>R (pu)</b>	<b>X (pu)</b>	<b>B (pu)</b>
3415	3417	1/0 6/1 ACSR Raven	110.0	0.0634	0.0437	0.0000003420	0.00079	0.00055	0.0000273585
3415	3421	1/0 6/1 ACSR Raven	1580.0	0.9101	0.6273	0.0000049121	0.01138	0.00784	0.0003929675
3421	3427	1/0 6/1 ACSR Raven	1440.0	0.8294	0.5717	0.0000044768	0.01037	0.00715	0.0003581476
3427	3432	1/0 6/1 ACSR Raven	40.0	0.0230	0.0159	0.0000001244	0.00029	0.00020	0.0000099485
3427	3437	1/0 6/1 ACSR Raven	40.0	0.0230	0.0159	0.0000001244	0.00029	0.00020	0.0000099485
3437	3440	1/0 6/1 ACSR Raven	40.0	0.0230	0.0159	0.0000001244	0.00029	0.00020	0.0000099485
3437	3443	1/0 6/1 ACSR Raven	40.0	0.0230	0.0159	0.0000001244	0.00029	0.00020	0.0000099485
3443	3446	1/0 6/1 ACSR Raven	40.0	0.0230	0.0159	0.0000001244	0.00029	0.00020	0.0000099485
3443	3449	1/0 6/1 ACSR Raven	40.0	0.0230	0.0159	0.0000001244	0.00029	0.00020	0.0000099485
3449	3451	1/0 6/1 ACSR Raven	40.0	0.0230	0.0159	0.0000001244	0.00029	0.00020	0.0000099485
3455	3466	300 26/7 ACSR Ostrich	101.0	0.0217	0.0337	0.0000003455	0.00027	0.00042	0.0000276433
3466	3468	1/0 6/1 ACSR Raven	100.0	0.0576	0.0397	0.0000003109	0.00072	0.00050	0.0000248714
3466	3472	300 26/7 ACSR Ostrich	1930.0	0.4150	0.6446	0.0000066029	0.00519	0.00806	0.0005282324
3472	3478	300 26/7 ACSR Ostrich	40.0	0.0086	0.0134	0.0000001368	0.00011	0.00017	0.0000109478
3478	3484	300 26/7 ACSR Ostrich	30.0	0.0065	0.0100	0.0000001026	0.00008	0.00013	0.0000082109
3506	3510	1/0 6/1 ACSR Raven	130.0	0.0749	0.0516	0.0000004042	0.00094	0.00065	0.0000323328

<b>3510</b>	<b>1375</b>	1/0 6/1 ACSR Raven	60.0	0.0346	0.0238	0.0000001865	0.00043	0.00030	0.0000149228
<b>1378</b>	<b>1966</b>	1/0 6/1 ACSR Raven	40.0	0.0230	0.0159	0.0000001244	0.00029	0.00020	0.0000099485
<b>3554</b>	<b>3565</b>	300 26/7 ACSR Ostrich	20.0	0.0043	0.0067	0.0000000684	0.00005	0.00008	0.0000054739
<b>3565</b>	<b>3567</b>	240 AL NAEKBA (TS)	110.0	0.0165	0.0119	0.0000183155	0.00021	0.00015	0.0014652388
<b>3567</b>	<b>3569</b>	300 26/7 ACSR Ostrich	11.0	0.0024	0.0037	0.0000000376	0.00003	0.00005	0.0000030107
<b>From</b>	<b>To</b>	<b>Type</b>	<b>Length (m)</b>	<b>R (Ohm)</b>	<b>X (Ohm)</b>	<b>B (mho)</b>	<b>R (pu)</b>	<b>X (pu)</b>	<b>B (pu)</b>
<b>3569</b>	<b>3580</b>	300 26/7 ACSR Ostrich	11.0	0.0024	0.0037	0.0000000376	0.00003	0.00005	0.0000030107
<b>3579</b>	<b>3596</b>	240 AL XLPE (TS)	280.0	0.0454	0.0322	0.0000466212	0.00057	0.00040	0.0037296988
<b>3580</b>	<b>3584</b>	300 26/7 ACSR Ostrich	28.0	0.0060	0.0094	0.0000000958	0.00008	0.00012	0.0000076635
<b>3584</b>	<b>3596</b>	240 AL XLPE (TS)	260.0	0.0421	0.0299	0.0000432911	0.00053	0.00037	0.0034632917

## Annex B Measurement model

### B.1 Functions and partial derivatives of conventional measurements

The measurement vector includes the branch active and reactive power flows, the bus active and reactive power injections, and the bus voltage magnitudes. For a system containing  $n$  buses, the state vector comprises  $(2n - 1)$  elements:  $n$  bus voltage magnitudes and  $(n - 1)$  phase angles, where the phase angle of the reference bus is set equal to 0. The state vector  $\mathbf{x}$ , assuming that bus 1 is chosen as the reference, has the following form:

$$\mathbf{x}^T = \left[ \delta^T \mathbf{V}^T \right] = \left[ \delta_2 \text{K} \delta_n \ V_1 \ V_2 \text{K} \ V_n \right]$$

In order to construct the measurement model of the SE problem, the general two-port  $\pi$ -model for a distribution line connecting buses  $i$  and  $j$ , is assumed. The model is shown in Figure 21. For branch  $i - j$ , its series admittance is defined as  $y_{ij} = g_{ij} + jb_{ij}$  and the admittance of the shunt branch connected at bus  $i$  is defined as  $y_{sj} = g_{sj} + jb_{sj}$ . A shunt capacitor or reactor at bus  $i$  is defined by  $y_i = g_i + j b_i$ . Load and generation at bus  $i$  are modelled as equivalent complex power injections,  $\tilde{S}_{Di}$  and  $\tilde{S}_{Gi}$ , respectively, and therefore have no effect on the network model. Exceptions are constant impedance type loads which are included as shunt admittances for the corresponding buses. The bus voltage phasors at buses  $i$  and  $j$  are  $V_i^{\%} = V_i \angle \delta_i$  and  $V_j^{\%} = V_j \angle \delta_j$ .

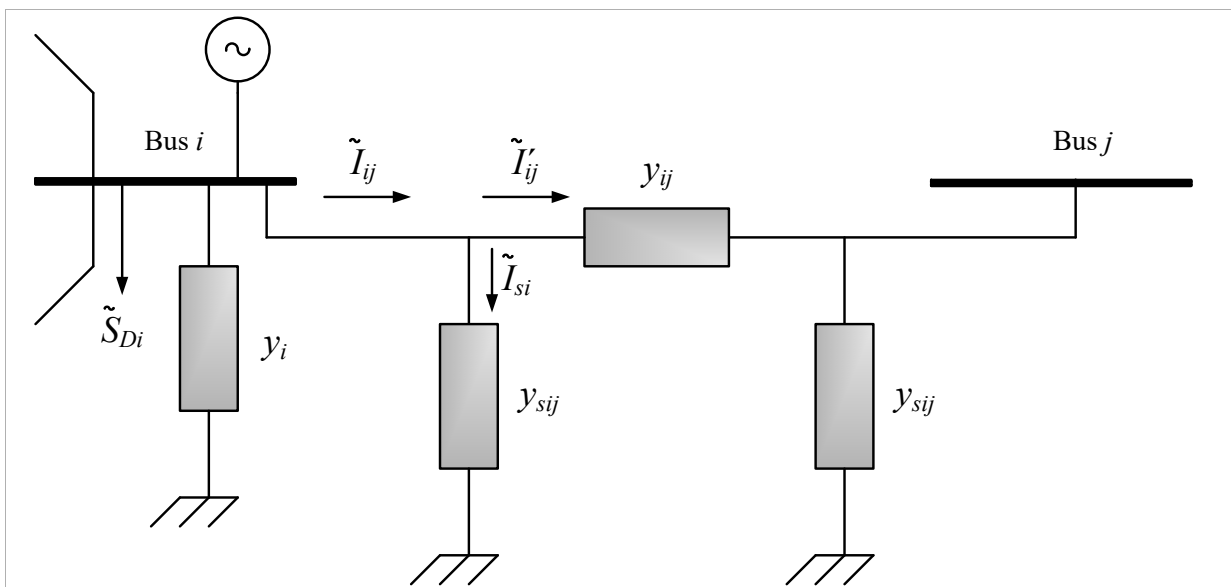


Figure 21:  $\pi$ -model of a power distribution line

Denoting with  $A(i)$  the set of buses which are directly linked to bus  $i$ , and with  $k$  a random bus belonging to  $A(i)$ , the expressions the power injection measurements are given below:

- Active power injection at bus  $i$  :

$$P_i = V_i^2 \sum_{k \in A(i)} (g_{ik} + g_{sk}) + V_i^2 g_i - V_i \sum_{k \in A(i)} V_k \alpha_{ik}$$

- Reactive power injection at bus  $i$  :

$$Q_i = -V_i^2 \sum_{k \in A(i)} (b_{ik} + b_{sik}) - V_i^2 b_i - V_i \sum_{k \in A(i)} V_k \beta_{ik}$$

$$\text{where } \alpha_{ik} = g_{ik} \cos(\delta_i - \delta_k) + b_{ik} \sin(\delta_i - \delta_k)$$

$$\text{and } \beta_{ik} = g_{ik} \sin(\delta_i - \delta_k) - b_{ik} \cos(\delta_i - \delta_k).$$

The expressions for power flow measurements through branch  $i - j$  are:

- Active power flow from bus  $i$  to bus  $j$  :

$$P_{ij} = V_i^2 (g_{ij} + g_{sij}) - V_i V_j \alpha_{ij}$$

- Reactive power flow from bus  $i$  to bus  $j$  :

$$Q_{ij} = -V_i^2 (b_{ij} + b_{sij}) - V_i V_j \beta_{ij}$$

The structure of the measurement Jacobian matrix  $\mathbf{H}(\mathbf{x})$  is as follows:

$$\mathbf{H}(\mathbf{x}) = \begin{pmatrix} \frac{\partial \mathbf{P}_{inj}}{\partial \boldsymbol{\delta}} & \frac{\partial \mathbf{P}_{inj}}{\partial \mathbf{V}} \\ \frac{\partial \mathbf{P}_{fl}}{\partial \boldsymbol{\delta}} & \frac{\partial \mathbf{P}_{fl}}{\partial \mathbf{V}} \\ \frac{\partial \mathbf{Q}_{inj}}{\partial \boldsymbol{\delta}} & \frac{\partial \mathbf{Q}_{inj}}{\partial \mathbf{V}} \\ \frac{\partial \mathbf{Q}_{fl}}{\partial \boldsymbol{\delta}} & \frac{\partial \mathbf{Q}_{fl}}{\partial \mathbf{V}} \\ \mathbf{0} & \frac{\partial \mathbf{V}_m}{\partial \mathbf{V}} \end{pmatrix}$$

where  $\mathbf{P}_{inj}$  and  $\mathbf{Q}_{inj}$  are the vectors of active and reactive power injection measurements,  $\mathbf{P}_{fl}$  and  $\mathbf{Q}_{fl}$  are the vectors of active and reactive power flow measurements, and  $\mathbf{V}_m$  is the vector of voltage magnitude measurements.

The expressions for partial derivatives of the measurements  $P_i$ ,  $Q_i$ ,  $P_{ij}$ ,  $Q_{ij}$  and  $V_i$  with regard to the voltage magnitude  $V_l$  and phase angle  $\delta_l$  of a randomly chosen bus  $l$  of the network are given below:

- Elements corresponding to  $P_i$  :

$$\frac{\partial P_i}{\partial \delta_l} = \begin{cases} V_i \sum_{k \in A(i)} V_k \beta_{ik}, l = i \\ -V_i V_l \beta_{il}, l \in A(i) \\ 0, l \neq i \wedge l \notin A(i) \end{cases}$$

$$\frac{\partial P_i}{\partial V_l} = \begin{cases} 2V_i \sum_{k \in A(i)} (g_{ik} + g_{sk}) + 2V_i g_i - \sum_{k \in A(i)} V_k \alpha_{ik}, l = i \\ -V_l \alpha_{il}, l \in A(i) \\ 0, l \neq i \wedge l \notin A(i) \end{cases}$$

- Elements corresponding to  $Q_i$  :

$$\frac{\partial Q_i}{\partial \delta_l} = \begin{cases} -V_i \sum_{k \in A(i)} V_k \alpha_{ik}, l = i \\ V_l V_l \alpha_{il}, l \in A(i) \\ 0, l \neq i \wedge l \notin A(i) \end{cases}$$

$$\frac{\partial P_i}{\partial V_l} = \begin{cases} -2V_i \sum_{k \in A(i)} (b_{ik} + b_{sk}) - 2V_i b_i - \sum_{k \in A(i)} V_k \beta_{ik}, l = i \\ -V_l \beta_{il}, l \in A(i) \\ 0, l \neq i \wedge l \notin A(i) \end{cases}$$

- Elements corresponding to  $P_{ij}$  :

$$\frac{\partial P_{ij}}{\partial \delta_l} = \begin{cases} V_l V_j \beta_{lj}, l = i \\ -V_l V_j \beta_{lj}, l = j \\ 0, l \neq i, j \end{cases}$$

$$\frac{\partial P_{ij}}{\partial V_l} = \begin{cases} -V_j \alpha_{ij} + 2V_i (g_{ij} + g_{sj}), l = i \\ -V_l \alpha_{il}, l = j \\ 0, l \neq i, j \end{cases}$$

- Elements corresponding to  $Q_{ij}$  :

$$\frac{\partial Q_{ij}}{\partial \delta_l} = \begin{cases} -V_l V_j \alpha_{lj}, l = i \\ V_l V_j \alpha_{lj}, l = j \\ 0, l \neq i, j \end{cases}$$

$$\frac{\partial Q_{ij}}{\partial V_l} = \begin{cases} -V_j \beta_{ij} - 2V_i (b_{ij} + b_{sj}), l = i \\ -V_i \beta_{ij}, l = j \\ 0, l \neq i, j \end{cases}$$

- Elements corresponding to  $V_i$  :

$$\frac{\partial V_i}{\partial V_l} = \begin{cases} 1, l = i \\ 0, l \neq i \end{cases} \text{ and } \frac{\partial V_i}{\partial \delta_l} = 0, \forall l$$

## B.2 Functions and partial derivatives of measurements from PMUs

In case that a PMU is installed at bus  $i$ , the phase angle  $\delta_i$  as well as a number of current phasors via incident branches, are also measured. The expressions for current phasor through branch  $i - j$  in rectangular coordinates, are provided below:

$$I_{ij}^{\%} = I_{ij,r} + jI_{ij,i}$$

$$I_{ij,r} = \left\{ V_i \left[ (g_{ij} + g_{sj}) \cos \delta_i - (b_{ij} + b_{sj}) \sin \delta_i \right] - V_j \left[ g_{ij} \cos \delta_j - b_{ij} \sin \delta_j \right] \right\}$$

$$I_{ij,i} = \left\{ V_i \left[ (b_{ij} + b_{sj}) \cos \delta_i + (g_{ij} + g_{sj}) \sin \delta_i \right] - V_j \left[ b_{ij} \cos \delta_j + g_{ij} \sin \delta_j \right] \right\}$$

The partial derivatives for the aforementioned measurements with regard to with regard to the voltage magnitude  $V_l$  and phase angle  $\delta_l$  of a random bus  $l$  of the network are expressed as follows:

$$\frac{\partial \delta_i}{\partial V_l} = 0, \forall l \text{ and } \frac{\partial \delta_i}{\partial \delta_l} = \begin{cases} 1, l = i \\ 0, l \neq i \end{cases}$$

$$\frac{\partial I_{ij,r}}{\partial \delta_l} = \begin{cases} -V_i \left[ (g_{ij} + g_{sj}) \sin \delta_i + (b_{ij} + b_{sj}) \cos \delta_i \right], l = i \\ V_j \left[ g_{ij} \sin \delta_j + b_{ij} \cos \delta_j \right], l = j \\ 0, l \neq i, j \end{cases}$$

$$\frac{\partial I_{ij,i}}{\partial \delta_i} = \begin{cases} V_i [(g_{ij} + g_{sij}) \cos \delta_i - (b_{ij} + b_{sij}) \sin \delta_i], l = i \\ -V_j [g_{ij} \cos \delta_j - b_{ij} \sin \delta_j], l = j \\ 0, l \neq i, j \end{cases}$$

$$\frac{\partial I_{ij,r}}{\partial V_i} = \begin{cases} [(g_{ij} + g_{sij}) \cos \delta_i - (b_{ij} + b_{sij}) \sin \delta_i], l = i \\ -[g_{ij} \cos \delta_j - b_{ij} \sin \delta_j], l = j \\ 0, l \neq i, j \end{cases}$$

$$\frac{\partial I_{ij,i}}{\partial V_i} = \begin{cases} [(b_{ij} + b_{sij}) \cos \delta_i + (g_{ij} + g_{sij}) \sin \delta_i], l = i \\ -[b_{ij} \cos \delta_j + g_{ij} \sin \delta_j], l = j \\ 0, l \neq i, j \end{cases}$$